PARTITION THEORY

by

Yanal Oueis

A Dissertation

Submitted to the Faculty of Purdue University

In Partial Fulfillment of the Requirements for the degree of

Doctor of Philosophy

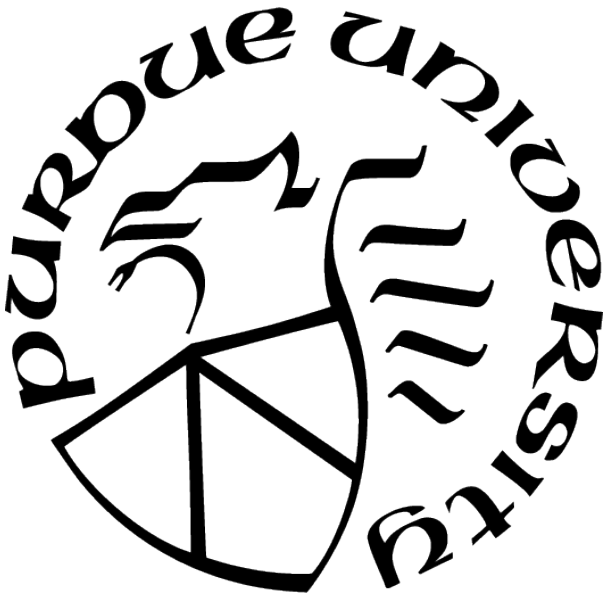

Department of Chemistry

West Lafayette, Indiana

May 2021

THE PURDUE UNIVERSITY GRADUATE SCHOOL
STATEMENT OF COMMITTEE APPROVAL

Dr. Adam Wasserman, Chair

Department of Chemistry

Dr. Lyudmila Slipchenko

Department of Chemistry

Dr. Gaurav Chopra

Department of Chemistry

Dr. Sabre Kais

Department of Chemistry

Approved by:

Dr. Christine Hrycyna

To ***

TABLE OF CONTENTS

LIST OF TABLES

LIST OF FIGURES

ABBREVIATIONS

DFT	Density-Functional Theory
HB	Hydrogen Bond
HK	Hohenberg-Kohn
HOMO	Highest Occupied Molecular Orbital
KS	Kohn-Sham
LUMO	Lowest Unoccupied Molecular Orbital
NAKE	Nonadditive Non-interacting Kinetic Energy
P-DFT	Partition Density-Functional Theory
PPLB	Perdew, Parr, Levy, and Balduz
PT	Partition Theory
XC	Exchange-Correlation

ABSTRACT

Partition Theory (PT) is a quantum chemistry method for simplifying a molecular calculation by breaking it down into fragment calculations. This "fragmentation" can lead to more efficient and/or more accurate results. The work in this thesis concerns studying fundamental aspects of PT and exact properties of energy functionals used in PT. We hope that these properties can be used for the development of feasible approximations to PT functionals.

We implemented PT so that it can be solved numerically exactly for model systems in 1-D. We used this implementation to study exact properties of the partition potential (a fictitious one-body potential used in PT to recover inter-fragment interactions). Our implementation can be used to study non-interacting and interacting electrons in 1D. We extended PT to systems supporting continuous electronic states (e.g., metals and metal surfaces) and demonstrated this method using a model system in 1D. We derived an exact virial relation for fragment energies and tested it on simple diatomic molecules in 3D. Finally, we studied properties of the partition potentials obtained through numerical inversions of formic acid dimer systems in 3D.

1. INTRODUCTION

Partition Theory is a particular type of *quantum-embedding* methods for electronic-structure calculations. In a quantum-embedding calculation, the full quantum system (e.g. a molecule) is divided into fragments for which properties can be obtained with a higher accuracy and/or at a lower computational cost. The properties of the full system are then computed from the properties of the fragments corrected for the inter-fragment interactions. Partition Theory uses electronic density as the main variable and is constructed analogously to the Kohn-Sham Density-Functional Theory.

This work is organized as follows. In Chapter 2, we review the formalism of the Density-Functional Theory. This chapter provides background information important for introducing PT later. In Chapter 3, we introduce PT and derive the equations that are used for fragment calculations within PT. In PT, the sum of fragment energies is minimized under the constraint that fragment electronic densities sum to the total density of the full system. We introduce the *partition potential*, an embedding potential that guarantees that the density constraint is satisfied at each point in space. In Chapter 4, we illustrate how PT works using exactly solvable models in 1-D. We also demonstrate several exact properties of the partition potential. In Chapter 5, we extend PT to systems supporting a continuum of electronic states. We demonstrate our extension on a model system designed to mimic metal-atom interactions. In Chapter 6, we derive a virial relationship for fragments within PT. Verification of the new relationship is done using a set of atomic dimers. In Chapter 7, we compute the partition potential for four different conformations of the formic acid dimer. We demonstrate that partition potential has no transferable features corresponding to particular types of hydrogen bonds.

Unless otherwise specified, we use Hartree atomic units throughout this work (reduced Planck constant, elementary charge, and electron mass are all equal to unity).

2. DENSITY-FUNCTIONAL THEORY

The solution of the non-relativistic Schrödinger equation for N electrons is a wavefunction depending on $3N$ spatial and N spin coordinates. Density-Functional Theory (DFT) replaces the many-body wavefunction with a one-body electron density function as its main variable. Within this reformulation of the electronic-structure problem, the equations are computationally easier to work with. However, the form of the energy operator is no longer readily available. In DFT, one does not seek to approximate electronic wavefunctions more accurately. Instead, the goal is to find a more accurate functional dependence of the energy as a functional of density.

In this chapter, we will review the Hohenberg-Kohn theorem, which laid the rigorous foundation of DFT. We will also review the formalism of the Kohn-Sham DFT, the most popular practical approach to DFT calculations.

2.1 Preliminaries: Many-Electron Problem in Quantum Chemistry

Finding solutions to the time-independent Schrödinger equation

$$\hat{H}\Psi = E\Psi \tag{2.1}$$

for electrons in the electrostatic field of "fixed" nuclei is the main interest of this work. The fixed-nuclei approximation (commonly referred to as the Born-Oppenheimer approximation) is central to the field of quantum chemistry [1]. Qualitatively, this approximation is justified by the fact that electrons are much lighter than nuclei and therefore move much faster. Quantitative aspects of this approximation have been recently discussed by Gross et al. [2] The form of the electronic hamiltonian $\hat{H}$ in the Eq. 2.1 is:

$$\hat{H} = \hat{T} + \hat{V}_{\text{ee}} + \hat{V}_{\text{ext}} \ . \tag{2.2}$$

The kinetic operator $\hat{T}$ is given by:

$$\hat{T} = -\frac{1}{2}\sum_{\mathrm{i}}^{N} \nabla_{\mathrm{i}}^2 \ , \tag{2.3}$$

where the summation is over N electronic spatial coordinates $\mathbf{r}_{\mathrm{i}}$. The electron-electron interaction operator is the sum of Coulomb operators between two electrons over all electron pairs:

$$\hat{V}_{\mathrm{ee}} = \frac{1}{2}\sum_{\mathrm{i}}^{N}\sum_{\mathrm{j}\neq\mathrm{i}}^{N} \frac{1}{|\mathbf{r}_{\mathrm{i}} - \mathbf{r}_{\mathrm{j}}|} \ . \tag{2.4}$$

The interaction energy of electrons with the external electrostatic field is described by the operator

$$\hat{V}_{\mathrm{ext}} = \sum_{\mathrm{i}}^{N} v_{\mathrm{ext}}(\mathbf{r}_{\mathrm{i}}) \ , \tag{2.5}$$

where $v_{\mathrm{ext}}(\mathbf{r}_{\mathrm{i}})$ is the interaction energy of an electron with nuclei of charge Z_A centered at $\mathbf{R}_A$:

$$v_{\mathrm{ext}}(\mathbf{r}_{\mathrm{i}}) = \sum_{A} \frac{-Z_A}{|\mathbf{r}_{\mathrm{i}} - \mathbf{R}_A|} \ . \tag{2.6}$$

In non-relativistic quantum mechanics, spin is introduced in an *ad hoc* fashion [3]. It is postulated that the electronic wavefunction must be antisymmetric with respect to the interchange of particle indices (i.e. $\Psi(\ldots,\mathbf{x}_{\mathrm{i}},\ldots,\mathbf{x}_{\mathrm{j}},\ldots) = -\Psi(\ldots,\mathbf{x}_{\mathrm{j}},\ldots,\mathbf{x}_{\mathrm{i}},\ldots)$, where $\mathbf{x}_{\mathrm{i}} = (\mathbf{r}_{\mathrm{i}}, s_{\mathrm{i}})$ is the particle coordinate combining both spatial and spin coordinates)[1]. In the absence of magnetic interactions, the electronic wavefunction should also be an eigenfunction of the total spin $\hat{S}^2$ operator.

In practical calculations, the antisymmetry condition is handled by forcing the wavefunction to have the form of the *Slater determinant* [1],

$$\Psi(\mathbf{x}_1, \mathbf{x}_2, \ldots, \mathbf{x}_N) \approx \begin{vmatrix} \chi_1(\mathbf{x}_1) & \chi_2(\mathbf{x}_1) & \ldots & \chi_N(\mathbf{x}_1) \\ \chi_1(\mathbf{x}_2) & \chi_2(\mathbf{x}_2) & \ldots & \chi_N(\mathbf{x}_2) \\ \vdots & \vdots & & \vdots \\ \chi_1(\mathbf{x}_N) & \chi_2(\mathbf{x}_N) & \ldots & \chi_N(\mathbf{x}_N) \end{vmatrix} = |\chi_1, \chi_2, \ldots, \chi_N\rangle \ . \tag{2.7}$$

[1]↑Discrete spin coordinate s_{i} can take the value of either $\uparrow$ or $\downarrow$ and satisfies $\alpha(\uparrow) = \beta(\downarrow) = 1$ and $\alpha(\downarrow) = \beta(\uparrow) = 0$, where α and β are eigenfunctions of the spin $\hat{S}_z$ operator.

Here, $\chi(\mathbf{x})$ is the *spin orbital*,

$$\chi(\mathbf{x}) = \begin{cases} \psi(\mathbf{r})\alpha(s) \\ \\ \psi(\mathbf{r})\beta(s) \end{cases} . \tag{2.8}$$

Alternatively, the spatial part can be solved independently and then combined with the eigenvalues of the N-spin $\hat{S}_{z,\text{total}}$ operator [3], [4]:

$$\Psi(\mathbf{x}_1, \mathbf{x}_2, \ldots, \mathbf{x}_N) = \sum \psi_{s_1,s_2,\ldots,s_N}(\mathbf{r}_1, \mathbf{r}_2, \ldots, \mathbf{r}_N) \, |s_1, s_2, \ldots, s_N\rangle \ ,$$

where the sum is over all $|s_1, s_2, \ldots, s_N\rangle$ spin states and $\psi_{s_1,s_2,\ldots,s_N}(\mathbf{r}_1, \mathbf{r}_2, \ldots, \mathbf{r}_N)$ are the degenerate eigenstates of the spatial hamiltonian.

The main DFT variables, electronic density $n(\mathbf{r})$ and spin-up (and -down) densities $n_s(\mathbf{r})$ are defined through[2]:

$$n(\mathbf{r}) = \sum_{s=\uparrow,\downarrow} n_s(\mathbf{r}) = \sum_{s=\uparrow,\downarrow} N \int d\mathbf{x}_2 \ldots d\mathbf{x}_N \ |\Psi(\mathbf{x}, \mathbf{x}_2, \ldots, \mathbf{x}_N)|^2 \ . \tag{2.9}$$

The possibility to use $n(\mathbf{r})$ instead of the wavefunction as the main variable in quantum mechanical calculations with hamiltonians of the form of Eq. 2.2 was proven by the *Hohenberg-Kohn theorem* [5].

2.2 Hohenberg-Kohn Theorem

From Eqs. 2.3—2.5, it should be clear that for fixed N the system is completely determined by the location of its nuclei (i.e. by the Eq. 2.6). In principle, if we know N and $v_{\text{ext}}(\mathbf{r})$ we can solve Eq. 2.2 to obtain the ground state wavefunction $\Psi_0(\mathbf{x}, \mathbf{x}_2, \ldots, \mathbf{x}_N)$ and all other properties of the system (including its electronic density). The Hohenberg-Kohn Theorem [5] establishes that the ground state density $n_0(\mathbf{r})$ can be used in place of $v_{\text{ext}}(\mathbf{r})$.

[2]↑We use the shortcut notation $\int d\mathbf{x} = \sum_s \int d^3\mathbf{r}$.

We will take a look at the elegant proof of the Hohenberg-Kohn theorem given by Levy [6]. We start by introducing the *universal density functional* that returns the sum of the kinetic and the electron-electron interaction energies for a given density $n(\mathbf{r})$:

$$F[n] = \min_{\Psi \to n} \langle \Psi | \hat{T} + \hat{V}_{\text{ee}} | \Psi \rangle \ , \tag{2.10}$$

where the minimization is over all antisymmetric wavefunctions $\Psi(\mathbf{x}, \mathbf{x}_2, \ldots, \mathbf{x}_N)$ that integrate to density $n(\mathbf{r})$ through Eq. 2.9. Levy established the variational principle for DFT by proving that for any $n(\mathbf{r})$[3]:

$$F[n] + \int d^3\mathbf{r} \ v_{\text{ext}}(\mathbf{r}) n(\mathbf{r}) \geq E_0 \ , \tag{2.11}$$

where $E_0 = \langle \Psi_0 | \hat{H} | \Psi_0 \rangle$. Levy also demonstrated that

$$F[n_0] = \langle \Psi_0 | \hat{T} + \hat{V}_{\text{ee}} | \Psi_0 \rangle \ , \tag{2.12}$$

providing an alternative definition of the ground state wavefunction $\Psi_0(\mathbf{x}, \mathbf{x}_2, \ldots, \mathbf{x}_N)$: the ground state wavefunction is the wavefunction that minimizes the expectation value of $\hat{T} + \hat{V}_{\text{ee}}$ and integrates to the ground state density. Starting with $n_0(\mathbf{r})$, we, in principle, can find $\Psi_0(\mathbf{x}, \mathbf{x}_2, \ldots, \mathbf{x}_N)$ using this definition. We can then use this $\Psi_0(\mathbf{x}, \mathbf{x}_2, \ldots, \mathbf{x}_N)$ to reconstruct the external potential according to:

$$\sum_{\text{i}}^{N} v_{\text{ext}}(\mathbf{r}_{\text{i}}) = -\frac{\hat{T}\Psi_0}{\Psi_0} - \hat{V}_{\text{ee}} + E_0 \ , \tag{2.13}$$

where we used Eqs. 2.2—2.5 and the fact that:

$$\int d^3\mathbf{r} \ n(\mathbf{r}) = N \ . \tag{2.14}$$

Eqs. 2.10—2.13 illustrate that for a given $n_0(\mathbf{r})$ we can find a unique corresponding $v_{\text{ext}}(\mathbf{r})$ and that $n(\mathbf{r})$ alone can, in principle, be used to describe the electronic structure of molecules.

[3]↑Note that $\langle \Psi | \hat{V}_{\text{ext}} | \Psi \rangle = \int d^3\mathbf{r} \ v_{\text{ext}}(\mathbf{r}) n(\mathbf{r})$.

2.3 Kohn-Sham DFT

Reformulating the electronic structure problem in terms of $n(\mathbf{r})$— a function of only 3 spatial coordinates— simplifies how the equations are handled computationally. However, it comes with a drawback that the analytical form of $F[n]$ is not known for systems with more than 2 electrons. It also turns out that approximating $F[n]$ directly as a functional of $n(\mathbf{r})$ is problematic. The biggest error comes from approximating the kinetic energy functional $T[n]$ [7]. To solve this problem, Kohn and Sham [8] suggested that $T[n]$ can be well approximated by the kinetic energy of non-interacting electrons (i.e., electrons with $\hat{V}_{\text{ee}} = 0$ that satisfy the antisymmetry relation) with the density $n(\mathbf{r})$. This approach leads to the formulation of the *Kohn-Sham equations*, a set of Schrödinger-like equations for orbitals of the non-interacting electrons with the same ground state density $n_0(\mathbf{r})$ as the real interacting system.

2.3.1 Kohn-Sham Equations

In Kohn-Sham DFT (KS-DFT [8]), we map the problem of interacting electrons to a system of non-interacting electrons in a fictitious external one-body potential, called the Kohn-Sham potential or $v_{\text{KS}}(\mathbf{r})$. The Kohn-Sham potential is chosen such that the non-interacting system has the same ground state density as the interacting system. The energy of this system is given as:

$$E_{\text{KS}}[n] = T_{\text{S}}[n] + \int d^3\mathbf{r}\ v_{\text{KS}}(\mathbf{r})n(\mathbf{r})\ , \tag{2.15}$$

where $T_{\text{S}}[n]$ is the kinetic energy of the non-interacting electrons. Note that for a given $n_0(\mathbf{r})$, $v_{\text{KS}}(\mathbf{r})$ is uniquely defined. The minimization of Eq. 2.15 with respect ot $n(\mathbf{r})$ leads to:

$$0 = \frac{\delta T_{\text{S}}[n]}{\delta n(\mathbf{r})} + v_{\text{KS}}(\mathbf{r})\ . \tag{2.16}$$

From Eq. 2.10, $T_{\text{S}}[n]$ is:

$$T_{\text{S}}[n] = \min_{\Psi \to n_0} \langle \Psi | \hat{T} | \Psi \rangle\ . \tag{2.17}$$

The minimizing wavefunction in Eq. 2.17 is (for a closed-shell system) a Slater determinant

$$\Phi_0(\mathbf{x}_1, \mathbf{x}_2, \ldots, \mathbf{x}_N) = \left|\phi_1\alpha, \phi_1\beta, \ldots, \phi_{N/2}\alpha, \phi_{N/2}\beta\right\rangle \ , \tag{2.18}$$

where orbitals are the eigenfunctions of

$$[-\frac{1}{2}\nabla^2 + v_{\mathrm{KS}}(\mathbf{r})]\phi_{\mathrm{i}}(\mathbf{r}) = \varepsilon_{\mathrm{i}}\phi_{\mathrm{i}}(\mathbf{r}) \ , \tag{2.19}$$

and $n_0(\mathbf{r})$ is given by:

$$n_0(\mathbf{r}) = 2\sum_{\mathrm{i}}^{N/2} |\phi_{\mathrm{i}}(\mathbf{r})|^2 \ . \tag{2.20}$$

We can now write the following decomposition of the energy functional of the *interacting* system:

$$E[n] = T_{\mathrm{S}}[n] + E_{\mathrm{H}}[n] + \int d^3\mathbf{r}\ v_{\mathrm{ext}}(\mathbf{r})n(\mathbf{r}) + E_{\mathrm{XC}}[n] \ , \tag{2.21}$$

where the the classical electrostatic (*Hartree*) energy is:

$$E_{\mathrm{H}}[n] = \frac{1}{2}\int d^3\mathbf{r}d^3\mathbf{r}'\ \frac{n(\mathbf{r})n(\mathbf{r}')}{|\mathbf{r}-\mathbf{r}'|} \ . \tag{2.22}$$

It turns out that $E_{\mathrm{H}}[n]$ for most systems accounts for a large part of the electron-electron interaction energy. The exchange-correlation (XC) energy is then a small "leftover" piece accounting for all quantum effects:

$$E_{\mathrm{XC}}[n] = (T[n] - T_{\mathrm{S}}[n]) + (\ \langle\Psi|\hat{V}_{\mathrm{ee}}|\Psi\rangle - E_{\mathrm{H}}[n]) \ . \tag{2.23}$$

Taking the derivative of Eq. 2.21 with respect to $n(\mathbf{r})$ gives:

$$0 = \frac{\delta T_{\mathrm{S}}[n]}{\delta n(\mathbf{r})} + \int d^3\mathbf{r}'\ \frac{n(\mathbf{r}')}{|\mathbf{r}-\mathbf{r}'|} + v_{\mathrm{ext}}(\mathbf{r}) + \frac{\delta E_{\mathrm{XC}}[n]}{\delta n(\mathbf{r})} \ , \tag{2.24}$$

where we define the *Hartree potential*:

$$v_{\mathrm{H}}[n](\mathbf{r}) = \frac{\delta E_{\mathrm{H}}[n]}{\delta n(\mathbf{r})} = \int d^3\mathbf{r}'\ \frac{n(\mathbf{r}')}{|\mathbf{r}-\mathbf{r}'|} \ , \tag{2.25}$$

and the *exchange-correlation potential*:

$$v_{\mathrm{XC}}[n](\mathbf{r}) = \frac{\delta E_{\mathrm{XC}}[n]}{\delta n(\mathbf{r})} \ . \tag{2.26}$$

Since the definition of $T_{\mathrm{S}}[n]$ is the same in Eq. 2.16 and in Eq. 2.24, we identify:

$$v_{\mathrm{KS}}[n](\mathbf{r}) = v_{\mathrm{H}}(\mathbf{r}) + v_{\mathrm{ext}}(\mathbf{r}) + v_{\mathrm{XC}}[n](\mathbf{r}) \ . \tag{2.27}$$

The ground state density $n_0(\mathbf{r})$ for the real interacting system can be found by solving

$$[-\frac{1}{2}\nabla^2 + v_{\mathrm{H}}(\mathbf{r}) + v_{\mathrm{ext}}(\mathbf{r}) + v_{\mathrm{XC}}[n](\mathbf{r})]\phi_{\mathrm{i}}(\mathbf{r}) = \varepsilon_{\mathrm{i}}\phi_{\mathrm{i}}(\mathbf{r})$$

using some *approximate exchange-correlation functional*. We note that $v_{\mathrm{KS}}[n](\mathbf{r})$ implicitly depends on orbitals $\phi_{\mathrm{i}}(\mathbf{r})$ through density. Therefore, KS equations must be solved self-consistently.

2.3.2 Approximate Exchange-Correlation Functionals

Along their famous equations, Kohn and Sham [8] also introduced the first modern XC approximation, called the *local-density approximation* or LDA. In LDA, the XC energy has the form:

$$E_{\mathrm{XC}}[n] = \int d^3\mathbf{r}\ \epsilon_{\mathrm{XC}}[n](\mathbf{r})n(\mathbf{r}), \tag{2.28}$$

where $\epsilon_{\mathrm{XC}}[n](\mathbf{r})$ is the energy per particle for the uniform electron gas. LDA is commonly used even today. In fact, the function form of the *exchange energy* $E_{\mathrm{X}}[n]$, defined through

$$\begin{aligned} E_{\mathrm{XC}}[n] &= E_{\mathrm{C}}[n] + E_{\mathrm{X}}[n] = \\ &(\langle\Phi|\hat{H}|\Phi\rangle - T_{\mathrm{S}}[n] - E_{\mathrm{H}}[n] - V_{\mathrm{ext}}[n]) + (\langle\Psi|\hat{H}|\Psi\rangle - \langle\Phi|\hat{H}|\Phi\rangle) \ , \end{aligned} \tag{2.29}$$

is known exactly for the uniform electron gas. The *correlation energy* $E_{\mathrm{C}}[n]$ can be determined through parameterization of the highly accurate calculations of the uniform electron gas [9]. In Eq. 2.29, the term $V_{\mathrm{ext}}[n]$ is simply:

$$V_{\mathrm{ext}}[n] = \int d^3\mathbf{r}\ v_{\mathrm{ext}}(\mathbf{r})n(\mathbf{r})\ . \tag{2.30}$$

More sophisticated XC functionals exist [10]. *Generalized Gradient Approximation* functionals (or GGA) [11]–[13] that use the gradient of the density to capture some non-homogeneity of electronic density and *meta-GGA* [14] that use the Laplacian of the density are among the most successful modern functionals [9]. Parametrized hybrid functionals [15]–[17] that include a fraction of the exact exchange (from Hartree-Fock theory) also became very popular for chemical applications [9].

2.3.3 Spin-unrestricted KS-DFT

It is straightforward to generalize KS-DFT to the spin-unrestricted case. We choose our reference system of non-interacting electrons in a way that spin-up and spin-down densities of the non-interacting system and of the real system are the same [18] (in contrast to "regular" KS-DFT, where only the total densities are equal). Mathematically, it is accomplished by introducing a magnetic component to $v_{\mathrm{KS}}(\mathbf{r})$ that interacts only with the spin [18], [19]:

$$v_{\mathrm{KS}}(\mathbf{r}) = v_{\mathrm{KS,electrostatic}}(\mathbf{r}) + v_{\mathrm{KS,spin}}(\mathbf{r}) \begin{pmatrix} 1 & 0 \\ 0 & -1 \end{pmatrix}\ . \tag{2.31}$$

KS spin orbitals can now be found from:

$$[-\frac{1}{2}\nabla^2 + v_{\mathrm{KS},s}(\mathbf{r})]\phi_{\mathrm{i},s}(\mathbf{r}) = \varepsilon_{\mathrm{i}}\phi_{\mathrm{i},s}(\mathbf{r})\ , \tag{2.32}$$

where s is either $\uparrow$ or $\downarrow$ and:

$$v_{\mathrm{KS},\uparrow/\downarrow}(\mathbf{r}) = v_{\mathrm{KS,electrostatic}}(\mathbf{r}) \pm v_{\mathrm{KS,spin}}(\mathbf{r}) = v_{\mathrm{H}}[n](\mathbf{r}) + v_{\mathrm{ext}}(\mathbf{r}) + v_{\mathrm{XC}\uparrow/\downarrow}[n](\mathbf{r})\ , \tag{2.33}$$

with:

$$v_{\mathrm{XC},\uparrow/\downarrow}[n](\mathbf{r}) = \frac{\delta E_{\mathrm{XC}}[n_\uparrow, n_\downarrow]}{\delta n_{\uparrow/\downarrow}(\mathbf{r})} \ . \tag{2.34}$$

The KS wavefunction is still a Slater determinant of the form:

$$\Phi_0(\mathbf{x}_1, \mathbf{x}_2, \ldots, \mathbf{x}_N) = \left|\phi_1^\alpha \alpha, \phi_1^\beta \beta, \phi_2^\alpha \alpha, \phi_2^\beta \beta, \ldots\right\rangle \ . \tag{2.35}$$

We note that $\Phi_0(\mathbf{x}_1, \mathbf{x}_2, \ldots, \mathbf{x}_N)$ is not an eigenfunction of the total spin $\hat{S}^2$ operator if $\phi_{\mathrm{i}}^\alpha \neq \phi_{\mathrm{i}}^\beta$ for all doubly-occupied indices. It turns out that most modern functional approximations as well as the computational software packages work within the spin KS-DFT formalism [9].

2.4 DFT for non-integer electrons

Our discussion so far has been limited to the case of integer electron numbers. However, non-integer number of electrons can arise in an open system as, for example, a time average [20]. For the case of non-integer electron number $N = M + \omega$ $(0 \leq \ \omega \leq 0)$, Perdew, Parr, Levy, and Balduz (PPLB [20]) showed using the grand canonical ensemble theory that the energy of the open system is given by:

$$E_0(N) = (1-\omega)E_0(M) + \omega E_0(M+1), \tag{2.36}$$

and the density is given by:

$$n_{0,N}(\mathbf{r}) = (1-\omega)n_{0,M}(\mathbf{r}) + \omega n_{0,M+1}(\mathbf{r}). \tag{2.37}$$

The chemical potential of the open system at zero temperature is [20], [21]:

$$\mu = \frac{\delta E[n]}{\delta n(\mathbf{r})} = E_0(M+1) - E_0(M) \ . \tag{2.38}$$

We should note that for $\omega = 0$, μ in Eq. 2.38 is undefined (i.e., μ is different depending on the side the derivative is taken on). Eqs. 2.36—2.38 are exact as long as $E_0(N)$ is a convex function of integer N values (which is empirically the case for all known Coulomb

systems [22]). Recently, the same results were derived by Ayers et al. [23] without evoking ensembles (only using exact known properties of the energy functional). Gál and Geerlings [19] generalized Eqs. 2.36—2.38 for spin-DFT.

2.5 Connection to the Partition Theory

The idea of mapping an interacting system to a non-interacting system is central to the Partition Theory (PT) where we deal with non-interacting molecular fragments "mimicking" the real interacting molecule. The goal of this section is to highlight the relation between PT and DFT with as few technicalities as possible. For this reason, we will restrict ourselves to the system of two fragments (A and B) each containing an integer number of electrons (N_A and N_B respectively). The extension to a more general case with an arbitrary number of open systems that can exchange electrons among each other will follow in the subsequent chapter.

We imagine that fragments A and B are not interacting with each other. The electrons within each fragment are interacting and indistinguishable, but we *can* distinguish A-electrons from B-electrons. Fragments are defined through the position of their atoms:

$$\hat{V}_\mathrm{J} = \sum_\mathrm{i}^{N_\mathrm{J}} v_\mathrm{J}(\mathbf{r}_\mathrm{i}) \ , \tag{2.39}$$

where J is either A or B. We also imagine that the fragments are embedded in the same external one-body potential $v_\mathrm{P}(\mathbf{r})$. In PT, $v_\mathrm{P}(\mathbf{r})$ (or the partition potential) will play the role of restoring the interaction energy between A and B while enforcing that the electronic densities of A and B sum to the density of AB. The operator of $v_\mathrm{P}(\mathbf{r})$ acting on the fragment J can be written simply as:

$$\hat{V}_\mathrm{P,J} = \sum_\mathrm{i}^{N_\mathrm{J}} v_\mathrm{P}(\mathbf{r}_\mathrm{i}) \ , \tag{2.40}$$

By analogy to Sec. 2.2 and to Ref. [6], we introduce the following functional:

$$Q[n_\mathrm{A}, n_\mathrm{B}] = \min_{\Psi_\mathrm{A}\to n_\mathrm{A}} \langle \Psi_\mathrm{A}|\hat{F}_\mathrm{A}|\Psi_\mathrm{A}\rangle + \min_{\Psi_\mathrm{B}\to n_\mathrm{B}} \langle \Psi_\mathrm{B}|\hat{F}_\mathrm{B}|\Psi_\mathrm{B}\rangle \ , \tag{2.41}$$

where the operator $\hat{F}_{\rm J}$ is defined through Eqs. 2.3 and 2.4 at $N_{\rm J}$ electrons:

$$\hat{F}_{\rm J} = \hat{T}_{\rm J} + \hat{V}_{\rm ee,J} \ . \tag{2.42}$$

Let us now look at the quantity

$$\mathcal{E}[n_{\rm A}, n_{\rm B}] = Q[n_{\rm A}, n_{\rm B}] + \int d^3\mathbf{r}\ v_{\rm A}(\mathbf{r}) n_{\rm A}(\mathbf{r}) + \int d^3\mathbf{r}\ v_{\rm B}(\mathbf{r}) n_{\rm B}(\mathbf{r}) + \int d^3\mathbf{r}\ v_{\rm P}(\mathbf{r}) n(\mathbf{r}) \ , \tag{2.43}$$

where $n(\mathbf{r}) = n_{\rm A}(\mathbf{r}) + n_{\rm B}(\mathbf{r})$. Clearly, the expression on the right-hand side can be written as:

$$\langle \Psi_{\rm A}[n_{\rm A}] | \tilde{H}_{\rm A} | \Psi_{\rm A}[n_{\rm A}] \rangle + \langle \Psi_{\rm B}[n_{\rm B}] | \tilde{H}_{\rm B} | \Psi_{\rm B}[n_{\rm B}] \rangle \ ,$$

where $\Psi_{\rm A}[n_{\rm A}]$ and $\Psi_{\rm B}[n_{\rm B}]$ are the wavefunctions that satisfy the minimization on the right-hand side of Eq. 2.41 and $\tilde{H}_{\rm J} = \hat{F}_{\rm J} + \hat{V}_{\rm ext,J} + \hat{V}_{\rm P,J}$. Since $\tilde{H}_{\rm J}$ only acts on J-electrons:

$$\mathcal{E}[n_{\rm A}, n_{\rm B}] = \langle \Psi_{\rm A}[n_{\rm A}] | \langle \Psi_{\rm B}[n_{\rm B}] | \tilde{H}_{\rm A} + \tilde{H}_{\rm B} | \Psi_{\rm A}[n_{\rm A}] \rangle | \Psi_{\rm B}[n_{\rm B}] \rangle \geq \tilde{E}_0 = \left\langle \tilde{\Psi}_{\rm AB,0} \right| \tilde{H}_{\rm AB} \left| \tilde{\Psi}_{\rm AB,0} \right\rangle \ . \tag{2.44}$$

Here, $\tilde{H}_{\rm AB} = \tilde{H}_{\rm A} + \tilde{H}_{\rm B}$ and the inequality is simply due to the variational principle. Note that any wavefunction in the product space can be expanded as $|\Phi_{\rm AB}\rangle = \sum_{\rm i,j} c_{\rm ij} |\Psi_{\rm A,i}\rangle |\Psi_{\rm B,j}\rangle$, where $|\Psi_{\rm J,i}\rangle$ is an eigenstate of $\tilde{H}_{\rm J}$. For the ground state $|\Psi_{\rm AB,0}\rangle$, only the terms where both $|\Psi_{\rm A,i}\rangle$ and $|\Psi_{\rm B,j}\rangle$ are the ground state eigenfunctions (of $\tilde{H}_{\rm A}$ and $\tilde{H}_{\rm B}$ respectively) can enter the expansion. It, therefore, becomes clear that[4]:

$$\tilde{E}_0 = \langle \Psi_{\rm A,0} | \langle \Psi_{\rm B,0} | \tilde{H}_{\rm A} + \tilde{H}_{\rm B} | \Psi_{\rm A,0} \rangle | \Psi_{\rm B,0} \rangle \ . \tag{2.45}$$

Now, let us chose $n_{\rm A,0}$ and $n_{\rm B,0}$ to be the ground state densities of $\tilde{H}_{\rm A}$ and $\tilde{H}_{\rm B}$ respectively. Again, we get from the variational principle:

$$\mathcal{E}[n_{\rm A,0}, n_{\rm B,0}] = \langle \Psi_{\rm A}[n_{\rm A,0}] | \langle \Psi_{\rm B}[n_{\rm B,0}] | \tilde{H}_{\rm A} + \tilde{H}_{\rm B} | \Psi_{\rm A}[n_{\rm A,0}] \rangle | \Psi_{\rm B}[n_{\rm B,0}] \rangle \geq \tilde{E}_0 \ . \tag{2.46}$$

[4]↑In the case of a degenerate ground state of A (and/or B), Eq. 2.45 holds for a particular orthogonal degenerate ground eigenstate $|\Psi_{\rm A,0}\rangle$ (and/or $|\Psi_{\rm B,0}\rangle$).

Substituting the expression for $\tilde{E}_0$ from Eq. 2.45 into 2.46 yields:

$$\langle\Psi_{\mathrm{A}}[n_{\mathrm{A},0}]|\hat{F}_{\mathrm{A}}|\Psi_{\mathrm{A}}[n_{\mathrm{A},0}]\rangle + \langle\Psi_{\mathrm{B}}[n_{\mathrm{B},0}]|\hat{F}_{\mathrm{B}}|\Psi_{\mathrm{B}}[n_{\mathrm{B},0}]\rangle \geq \langle\Psi_{\mathrm{A},0}|\hat{F}_{\mathrm{A}}|\Psi_{\mathrm{A},0}\rangle + \langle\Psi_{\mathrm{B},0}|\hat{F}_{\mathrm{B}}|\Psi_{\mathrm{B},0}\rangle \ . \tag{2.47}$$

However, from the definition of $Q[n_{\mathrm{A}}, n_{\mathrm{B}}]$, $\langle\Psi_{\mathrm{J}}[n_{\mathrm{J},0}]|\hat{F}_{\mathrm{J}}|\Psi_{\mathrm{J}}[n_{\mathrm{J},0}]\rangle \leq \langle\Psi_{\mathrm{J},0}|\hat{F}_{\mathrm{J}}|\Psi_{\mathrm{J},0}\rangle$. Therefore, Eq. 2.47 holds if and only if:

$$\langle\Psi_{\mathrm{A}}[n_{\mathrm{A},0}]|\hat{F}_{\mathrm{A}}|\Psi_{\mathrm{A}}[n_{\mathrm{A},0}]\rangle + \langle\Psi_{\mathrm{B}}[n_{\mathrm{B},0}]|\hat{F}_{\mathrm{B}}|\Psi_{\mathrm{B}}[n_{\mathrm{B},0}]\rangle = \langle\Psi_{\mathrm{A},0}|\hat{F}_{\mathrm{A}}|\Psi_{\mathrm{A},0}\rangle + \langle\Psi_{\mathrm{B},0}|\hat{F}_{\mathrm{B}}|\Psi_{\mathrm{B},0}\rangle \ . \tag{2.48}$$

From Eq. 2.48, we can conclude the following. Given the ground state densities of $\tilde{H}_{\mathrm{A}}$ and $\tilde{H}_{\mathrm{B}}$, we can find $|\Psi_{\mathrm{A}}[n_{\mathrm{A},0}]\rangle$ and $|\Psi_{\mathrm{B}}[n_{\mathrm{B},0}]\rangle$ through two minimizations on the right-hand side of Eq. 2.41 (even without knowing $v_{\mathrm{A}}(\mathbf{r})$ and/or $v_{\mathrm{B}}(\mathbf{r})$). We can then use $|\Psi_{\mathrm{A}}[n_{\mathrm{A},0}]\rangle$ and $|\Psi_{\mathrm{B}}[n_{\mathrm{B},0}]\rangle$ to construct $\left|\tilde{\Psi}_{\mathrm{AB},0}\right\rangle = |\Psi_{\mathrm{A}}[n_{\mathrm{A},0}]\rangle\,|\Psi_{\mathrm{B}}[n_{\mathrm{B},0}]\rangle$. Finally, we can use $\left|\tilde{\Psi}_{\mathrm{AB},0}\right\rangle$ to recover (up to a constant)

$$\sum_{\mathrm{J=A,B}} \sum_{\mathrm{i}}^{N_{\mathrm{J}}} v_{\mathrm{P}}(\mathbf{r}_{\mathrm{i}}) + v_{\mathrm{J}}(\mathbf{r}_{\mathrm{i}})$$

analogously to Eq. 2.13. Therefore, for a particular decomposition of AB (i.e., for fixed $v_{\mathrm{A}}(\mathbf{r})$ and $v_{\mathrm{B}}(\mathbf{r})$), we can find a unique $v_{\mathrm{P}}(\mathbf{r})$ from $n_{\mathrm{A},0}(\mathbf{r})$ and $n_{\mathrm{B},0}(\mathbf{r})$. Observe that Eqs. 2.44 and 2.48 establish that, in principle, there exists a universal functional $Q[n_{\mathrm{A}}, n_{\mathrm{B}}]$ that has the ground state energy as its lower bound and when minimized solves the problem of two independent fragments embedded in the same external potential.

Keeping in mind the properties of $Q[n_{\mathrm{A}}, n_{\mathrm{B}}]$ from Eqs. 2.44 and 2.48, let us now assume that the potential $v_{\mathrm{P}}(\mathbf{r})$ is a special potential that guarantees that the density of our fictitious system of non-interacting fragments is the same as the density of the interacting system AB[5]. We can choose to write the energy of the interacting system AB as:

$$E_{\mathrm{AB},0} = E_{\mathrm{f}} + E_{\mathrm{P}} \ , \tag{2.49}$$

[5]↑Note that such $v_{\mathrm{P}}(\mathbf{r})$ may not exist for some AB systems.

where:

$$E_{\mathrm{f}} = Q[n_{\mathrm{A},0}, n_{\mathrm{B},0}] + \int d^3\mathbf{r}\ v_{\mathrm{A}}(\mathbf{r}) n_{\mathrm{A},0}(\mathbf{r}) + \int d^3\mathbf{r}\ v_{\mathrm{B}}(\mathbf{r}) n_{\mathrm{B},0}(\mathbf{r})\ , \tag{2.50}$$

and E_{P} is just the "remaining" energy that accounts for the interactions between A and B. By construction, $E_{\mathrm{f}}[n_{\mathrm{AB}}]$ of the interacting system is equal to that of the fictitious system at the stationary point (i.e., at $n_{\mathrm{AB}}(\mathbf{r}) = n_{\mathrm{AB},0}(\mathbf{r})$). In addition, we established that $v_{\mathrm{P}}(\mathbf{r})$ is unique for given $n_{\mathrm{A},0}(\mathbf{r})$ and $n_{\mathrm{A},0}(\mathbf{r})$. Therefore, we can identify an important relationship between $E_{\mathrm{P}}[n_{\mathrm{AB}}]$ and $v_{\mathrm{P}}(\mathbf{r})$:

$$\frac{\delta E_{\mathrm{P}}[n_{\mathrm{AB}}]}{\delta n_{\mathrm{AB}}} = v_{\mathrm{P}}(\mathbf{r})\ . \tag{2.51}$$

It is useful to further decompose $E_p[n_{\mathrm{AB}}]$ into *non-additive electron-nuclear* and *non-additive electron-electron* energy contributions:

$$E_{\mathrm{P}}[n_{\mathrm{AB}}] = E_{\mathrm{ee}}^{\mathrm{nad}}[n_{\mathrm{A}}, n_{\mathrm{B}}] + V_{\mathrm{ext}}^{\mathrm{nad}}[n_{\mathrm{A}}, n_{\mathrm{B}}]\ . \tag{2.52}$$

The functional form of the the electron-nuclear non-additive energy can be derived trivially:

$$V_{\mathrm{ext}}^{\mathrm{nad}}[n_{\mathrm{A}}, n_{\mathrm{B}}] = \int d^3\mathbf{r}\ v_{\mathrm{B}}(\mathbf{r}) n_{\mathrm{A}}(\mathbf{r}) + \int d^3\mathbf{r}\ v_{\mathrm{A}}(\mathbf{r}) n_{\mathrm{B}}(\mathbf{r})\ . \tag{2.53}$$

The functional form of

$$E_{\mathrm{ee}}^{\mathrm{nad}}[n_{\mathrm{A}}, n_{\mathrm{B}}] = F[n_{\mathrm{A}} + n_{\mathrm{B}}] - Q[n_{\mathrm{A}}, n_{\mathrm{B}}] \tag{2.54}$$

is generally not known and needs to be approximated in practice. We emphasise that the universality of $Q[n_{\mathrm{A}}, n_{\mathrm{B}}]$ illustrated above is essential for the task of developing widely applicable approximations to $Q[n_{\mathrm{A}}, n_{\mathrm{B}}]$.

3. PARTITION THEORY

This section contains work from the article entitled "Exact partition potential for model systems of interacting electrons in 1-D" written by the author and Adam Wasserman published in the European Physical Journal of B [24].

In Sec. 2.5, we considered a simple two-fragment partition problem and established the following about the Partition Theory (PT). In PT, we imagine a fictitious system of non-interacting fragments embedded in a global potential (i.e., same for all fragments). The fragments are constrained to have densities that sum to the total molecular density while minimizing the sum of fragment energies (more on this quantity later). The uniqueness of the fragment densities is ensured by the global embedding potential, according to the theorem of ref. [25]. In this chapter, we will take a closer look at PT and will re-derive its formalism for a general case of arbitrary number of open fragments that can exchange electrons among each other.

3.1 Partition Theory

To formally introduce the PT, we partition the external potential $v(\mathbf{r})$ into fragments labeled by the index α:

$$v(\mathbf{r}) = \sum_{\alpha} v_\alpha(\mathbf{r}) \ . \tag{3.1}$$

PT is based on the following decomposition of the molecular ground state energy[1]:

$$E_v[n_0] = \min_{n\to N} [\min_{\{n_\alpha\}\to n} [E_{\rm f}[\{n_\alpha\}]] + E_{\rm P}[n]] \ , \tag{3.2}$$

where $E_{\rm f}[\{n_\alpha\}]$ is the sum of fragment energies and $E_{\rm P}[n]$ is the partition energy. In eq. 3.2, the outer minimization is over all densities that integrate to N electrons. Each of the fragment contributions to $E_{\rm f}$ is defined to have the PPLB functional form:

$$E_{\rm f}[\{n_\alpha\}] = \sum_{\alpha} \{(1-\omega_\alpha)E_{v_\alpha}[n_{p_\alpha}] + \omega_\alpha E_{v_\alpha}[n_{p_\alpha+1}]\} \ , \tag{3.3}$$

[1]↑Note that we now label energy functionals with their corresponding external potential in the subscript (e.g., v or v_α).

where p_α and ω_α are the integer and fractional parts of N_α (number of electrons in fragment α). The inner minimization in 3.2 is over all p_α, ω_α, $n_{p_\alpha}(\mathbf{r})$, and $n_{p_\alpha+1}(\mathbf{r})$ that produce the density $n_\mathrm{f}(\mathbf{r}) = n_0(\mathbf{r})$ according to (See. Eq. 2.37):

$$n_\mathrm{f}(\mathbf{r}) = \sum_\alpha \left\{(1-\omega_\alpha)n_{p_\alpha}(\mathbf{r}) + \omega_\alpha n_{p_\alpha+1}(\mathbf{r})\right\} . \tag{3.4}$$

To avoid finite-difference derivatives, it is common to fix the integer part of the occupation numbers and use $\{n_\alpha\}$ to denote the set of all ω_α's, $n_{p_\alpha}(\mathbf{r})$'s, and $n_{p_\alpha+1}(\mathbf{r})$'s. We also follow this convention in this text. Therefore, all our derivatives with respect to ω_α, $n_{p_\alpha}(\mathbf{r})$, or $n_{p_\alpha+1}(\mathbf{r})$ are not the "formal" derivatives but rather constrained derivatives that keep the integer part of the corresponding fragment α constant.

The inner minimization in eq. 3.2 is done by the method of Lagrange multipliers. The equivalent unconstrained extremization is done for the following functional:

$$G[\{n_\alpha\}, v_\mathrm{P}(\mathbf{r})] = E_\mathrm{f}[\{n_\alpha\}] + \int d\mathbf{r} v_\mathrm{P}(\mathbf{r})[n_\mathrm{f}(\mathbf{r}) - n_0] , \tag{3.5}$$

where the *partition potential*, $v_\mathrm{P}(\mathbf{r})$, has been introduced as the Lagrange multiplier that forces condition 3.4 to be satisfied at each point in space. Eq. 3.5 also brings out the physical meaning of the fragment densities

$$n_\alpha(\mathbf{r}) = (1-\omega_\alpha)n_{p_\alpha}(\mathbf{r}) + \omega_\alpha n_{p_\alpha+1}(\mathbf{r}) . \tag{3.6}$$

They are the ensemble ground state densities of N_α electrons in the potential $(v_\alpha(\mathbf{r}) + v_\mathrm{P}(\mathbf{r}))$. The partition potential $v_\mathrm{P}(\mathbf{r})$ is the above-mentioned global embedding potential that guarantees the uniqueness of the n_α's. [25] Note that $E_{v_\alpha}[n_{p_\alpha}]$ in eq. 3.3 is *not* the correct ground state energy corresponding to $n_{p_\alpha}(\mathbf{r})$, but $E_{v_\alpha+v_\mathrm{P}}[n_{p_\alpha}]$ is.

3.1.1 Chemical Potential

Stationarity of $G[\{n_\alpha\}, v_{\rm P}(\mathbf{r})]$ with respect to ω_α implies: [25]

$$\mu_\alpha^{\rm PT} = \mu_\beta^{\rm PT} \ , \tag{3.7}$$

for any two fragments α and β, where the α-chemical potential of PT is defined as

$$\begin{aligned} \mu_\alpha^{\rm PT} =& (E_{v_\alpha}[n_{p_\alpha+1}] + \int d\mathbf{r} v_{\rm P}(\mathbf{r}) n_{p_\alpha+1}(\mathbf{r})) - \\ & (E_{v_\alpha}[n_{p_\alpha}] + \int d\mathbf{r} v_{\rm P}(\mathbf{r}) n_{p_\alpha}(\mathbf{r})) \ . \end{aligned} \tag{3.8}$$

Note that similarly to Eq. 2.38, $\mu_\alpha^{\rm PT}$ is undefined when N_α is integer. Therefore, stationarity of $G[\{n_\alpha\}, v_{\rm P}(\mathbf{r})]$ may correspond not only to Eq. 3.7 but also to $\mu_\alpha^{\rm PT}$ being undefined for one or more fragments.

3.1.2 Decomposition of $v_{\rm P}(\mathbf{r})$

Following the standard KS decomposition of Eq. 2.21, the partition energy of eq. 3.2 can be written as:

$$\begin{aligned} E_{\rm P}[n] =& T_{\rm S}^{\rm nad}[\{n_\alpha\}] + E_{\rm ext}^{\rm nad}[\{n_\alpha\}] + E_{\rm H}^{\rm nad}[\{n_\alpha\}] + \\ & E_{\rm XC}^{\rm nad}[\{n_\alpha\}] \ , \end{aligned} \tag{3.9}$$

The superscript "nad" in Eq. 3.9 indicates that each of these functionals is a non-additive contribution defined (for an arbitrary functional Π) as: $\Pi^{\rm nad}[\{n_\alpha\}] = \Pi[n] - \sum_\alpha \{(1-\omega_\alpha)\Pi_\alpha[n_{p_\alpha}] + \omega_\alpha \Pi_\alpha[n_{p_\alpha+1}]\}$.

The relationship between $E_{\rm P}[\{n_\alpha\}]$ and $v_{\rm P}(\mathbf{r})$ was derived by Nafziger and Wasserman [26]:

$$\begin{aligned} v_{\rm P}(\mathbf{r}) = \int d\mathbf{r} \sum_\alpha \{ & \frac{\delta E_{\rm P}}{\delta n_{p_\alpha}(\mathbf{r}')} \frac{\delta n_{p_\alpha}(\mathbf{r}')}{\delta n_{\rm f}(\mathbf{r})} + \\ & \frac{\delta E_{\rm P}}{\delta n_{p_\alpha+1}(\mathbf{r}')} \frac{\delta n_{p_\alpha+1}(\mathbf{r}')}{\delta n_{\rm f}(\mathbf{r})} \}. \end{aligned} \tag{3.10}$$

Observe that Eq. 3.10 can be derived from Eq. 2.51 using the chain rule for the functional derivative on the right-hand side. Substituting 3.9 into 3.10 leads to a useful decomposition of $v_{\mathrm{P}}(\mathbf{r})$ into contributions from kinetic, external, Hartree, and exchange-correlation parts.

3.1.3 Spin in PT

Analogously to KS-DFT, we can extend PT to the spin-unrestricted case. We chose our reference system in such a way that spin-up and spin-down densities of the non-interacting fragments and of the full system are the same. These constraints can be enforced by introducing two separate partition potentials: $v_{\mathrm{P},\uparrow}(\mathbf{r})$ and $v_{\mathrm{P},\downarrow}(\mathbf{r})$.

In the case of spin-unrestricted PT, optimization with respect to the number of electrons in fragments is problematic as the convexity with respect to both M and M_{S}[2] is no longer guaranteed (in contrast to Eq. 2.36, where the convexity with respect to M only is required). In practice (see Chap. 7 of this manuscript), we fix occupations and spin states of fragments to the ones of the isolated fragments.

3.2 Partition-DFT

It is worth pointing out that fragment calculations in PT can be performed at any level of theory. In fact, we can apply different methods to different fragments (see, e.g., Chap. 5 of this manuscript). However, KS-DFT provides the most direct way to take advantage of Eq. 3.9 that is important for practical application of PT. When fragment calculation are performed with DFT, we will refer to the method as the Partition-DFT or P-DFT.

Fragment calculations in P-DFT can be performed by solving effective KS equations of the form:

$$[-\frac{1}{2}\nabla^2 + v_{\mathrm{H}}[n_\alpha](\mathbf{r}) + v_\alpha(\mathbf{r}) + v_{\mathrm{XC}}[n_\alpha](\mathbf{r}) + v_{\mathrm{P}}[\{n_\alpha\}](\mathbf{r})]\phi_{\mathrm{i}}(\mathbf{r}) = \varepsilon_{\mathrm{i}}\phi_{\mathrm{i}}(\mathbf{r}) \ , \tag{3.11}$$

making P-DFT straightforward to implement within quantum chemistry computational packages that already work with DFT.

[2]↑Here, M_{S} is the difference between the integer number of up and down electrons.

4. EXACT PARTITION POTENTIAL FOR MODEL SYSTEMS OF INTERACTING ELECTRONS IN 1D

This section contains work from the article entitled "Exact partition potential for model systems of interacting electrons in 1-D" written by the author and Adam Wasserman published in the European Physical Journal of B [24].

In this chapter, we will demonstrate how PT works on simple systems designed to model diatomic molecules. We will find the numerically exact partition potential for 1-D systems of two interacting electrons in 1-D. At integer fragment occupations, the kinetic contribution to the partition potential develops sharp features in the internuclear region that nearly cancel corresponding features of exchange-correlation. They occur at locations that coincide with those of well-known features of the underlying molecular Kohn-Sham potential. For non-integer fragment occupations, we demonstrate that the fragment Kohn-Sham gaps determine the kinetic part of the partition potential. Our results highlight the importance of non-additive noninteracting kinetic and exchange-correlation energy approximations in density-embedding methods at large internuclear separations and the importance of nonadditive noninteracting kinetic energy approximations at all separations.

4.1 Model System and Numerical Methods

The properties of each fragment as well as the entire system are computed on a fine real grid. Density-to-potential inversion techniques are used to solve the PT problem (*i.e.* the problem of finding $v_{\mathrm{P}}(\mathbf{r})$ for a given density and choice of partitioning). A more detailed discussion of the numerical methods is presented below.

4.1.1 Model Hamiltonians

Our model of a 1-D dimer has two interacting valence electrons. The soft-coulomb (SC) potential is used to model charge-charge interactions. The electronic Hamiltonian is:

$$\mathcal{H} = \sum_{\mathrm{i}=1,2} \left\{ -\frac{1}{2}\nabla_{x_\mathrm{i}}^2 - \frac{1}{\sqrt{1.0 + (x_\mathrm{i} - R_\mathrm{H})^2}} - \frac{Z_\mathrm{X}}{\sqrt{1.0 + (x_\mathrm{i} - R_\mathrm{X})^2}} \right\} + \frac{\lambda}{\sqrt{1.0 + (x_1 - x_2)^2}} \ , \tag{4.1}$$

where x_i is the coordinate of the i^{th} electron, R_X is the position of the nucleus X (X stands for either H or He), Z_X is the nuclear charge and λ is the parameter that switches the electron-electron interaction on ($\lambda = 1$) or off ($\lambda = 0$). We use the softening parameter value of 1.0 and a simulation box of 25 a.u. The case of LiH is discussed separately in Eq. 4.11.

With the nuclear-nuclear interaction given by:

$$V_\mathrm{nn} = \frac{Z_\mathrm{X}}{\sqrt{3.0 + (R_\mathrm{X} - R_\mathrm{H})^2}} \ , \tag{4.2}$$

the equilibrium bond-length is $R_0 = 1.6$ a.u. for H_2 and $R_0 = 2.1$ a.u. for HeH^+.

The fragment Hamiltonians have the form:

$$\mathcal{H}_{p_\alpha+1} = \sum_{\mathrm{i}=1,2} \left\{ -\frac{1}{2}\nabla_{x_\mathrm{i}}^2 - \frac{Z_\mathrm{X}}{\sqrt{1.0 + (x_\mathrm{i} - R_\mathrm{X})^2}} + v_\mathrm{P}(x_\mathrm{i}) \right\} + \frac{\lambda}{\sqrt{1.0 + (x_1 - x_2)^2}} \tag{4.3}$$

and

$$\mathcal{H}_{p_\alpha} = -\frac{1}{2}\nabla_x^2 - \frac{Z_\mathrm{X}}{\sqrt{1.0 + (x - R_\mathrm{X})^2}} + v_\mathrm{P}(x) \ . \tag{4.4}$$

4.1.2 Decomposition of $v_{\mathrm{P}}(x)$

With the strategy introduced by eqs. 3.9 and 3.10, we rewrite $v_{\mathrm{P}}(x)$ as:

$$v_{\mathrm{P}}(x) = v_{\mathrm{P,kin}}(x) + v_{\mathrm{P,ext}}(x) + v_{\mathrm{P,H}}(x) + v_{\mathrm{P,XC}}(x) \ , \tag{4.5}$$

where the components correspond to those of E_{P} in Eq. 3.9. To calculate each component, we note:

$$\frac{\delta T_{\mathrm{S}}^{\mathrm{nad}}[n_{p_\alpha}]}{\delta n_{p_\alpha}(x)} = (1-\omega_\alpha)(v_{\mathrm{KS}}[n_{p_\alpha}](x) - v_{\mathrm{KS}}[n_0](x)), \tag{4.6a}$$

$$\frac{\delta E_{\alpha}^{\mathrm{nad}}[n_{p_\alpha}]}{\delta n_{p_\alpha}(x)} = (1-\omega_\alpha)(v(x) - v_\alpha(x)), \tag{4.6b}$$

$$\frac{\delta E_{\mathrm{H}}^{\mathrm{nad}}[n_{p_\alpha}]}{\delta n_{p_\alpha}(x)} = (1-\omega_\alpha)\int dx_1 \frac{n_0(x_1) - n_{p_\alpha}(x_1)}{\sqrt{1.0 + (x_1 - x)^2}}, \tag{4.6c}$$

$$\frac{\delta E_{\mathrm{XC}}^{\mathrm{nad}}[n_{p_\alpha}]}{\delta n_{p_\alpha}(x)} = (1-\omega_\alpha)(v_{\mathrm{XC}}[n_0](x) - v_{\mathrm{XC}}[n_{p_\alpha}](x)). \tag{4.6d}$$

The equivalent derivatives with respect to the $n_{p_\alpha+1}$ are omitted for brevity. The functional derivatives in eqs. 4.6 can be readily calculated and used further to obtain $v_{\mathrm{P,kin}}(x)$, $v_{\mathrm{P,ext}}(x)$ and $v_{\mathrm{P,H}}(x)$. The remaining $v_{\mathrm{P,XC}}(x)$ is calculated as a difference between the full $v_{\mathrm{P}}(x)$ and the first three components. For the functional derivative $\delta n_{p_\alpha}(x')/\delta n_f(x)$ in Eq. 3.10, we use the local approximation: [27]

$$\frac{\delta n_{p_\alpha}(x')}{\delta n_0(x)} \approx \mathcal{Q}_{p_\alpha}(x, x') \equiv \frac{n_{p_\alpha}(x')}{n_0(x)}\delta(x - x') \ , \tag{4.7}$$

resulting in the following equations for the components:

$$
\begin{aligned}
v_{\mathrm{P,kin}}(x) =& \sum_{\alpha}\{\omega_{\alpha}\mathcal{Q}_{p_{\alpha}+1}(x,x)v_{\mathrm{KS}}^{(-)}[n_{p_{\alpha}+1}](x)+ \\
& (1-\omega_{\alpha})\mathcal{Q}_{p_{\alpha}}(x,x)v_{\mathrm{KS}}^{(-)}[n_{p_{\alpha}}](x)\}- \\
& v_{\mathrm{KS}}^{(-)}[n_0](x),
\end{aligned} \tag{4.8a}
$$

$$
v_{\mathrm{P,ext}}(x) = \sum_{\alpha}\{(v(x)-v_{\alpha}(x))\frac{n_{\alpha}(x)}{n_0(x)}\}, \tag{4.8b}
$$

$$
\begin{aligned}
v_{\mathrm{P,H}}(x) =& \sum_{\alpha}\Bigg\{\omega_{\alpha}\mathcal{Q}_{p_{\alpha}+1}(x,x) \\
& \cdot\int dx_1 \frac{n_0(x_1)-n_{p_{\alpha}+1}(x_1)}{\sqrt{1.0+(x_1-x)^2}}+ \\
& (1-\omega_{\alpha})\mathcal{Q}_{p_{\alpha}}(x,x)\int dx_1 \frac{n_0(x_1)-n_{p_{\alpha}}(x_1)}{\sqrt{1.0+(x_1-x)^2}}\Bigg\},
\end{aligned} \tag{4.8c}
$$

$$
\begin{aligned}
v_{\mathrm{P,XC}}(x) =& v_{\mathrm{XC}}^{(-)}[n_0](x)- \\
& \sum_{\alpha}\{\omega_{\alpha}\mathcal{Q}_{p_{\alpha}+1}(x,x)v_{\mathrm{XC}}^{(-)}[n_{p_{\alpha}+1}](x)+ \\
& (1-\omega_{\alpha})\mathcal{Q}_{p_{\alpha}}(x,x)v_{\mathrm{XC}}^{(-)}[n_{p_{\alpha}}](x)\},
\end{aligned} \tag{4.8d}
$$

where the superscript "$(-)$" indicates that the x-independent constant in $v_{\mathrm{KS}}(x)$ at integer electron number is calculated at the limit from below. Since this approximation satisfies the sum rule, $\sum_{\alpha}\{\mathcal{Q}_{p_{\alpha}}+\mathcal{Q}_{p_{\alpha}+1}\}=\delta(x-x')$, the sum of $v_{\mathrm{P}}(x)$ components yields the *exact* $v_{\mathrm{P}}(x)$. [27] Although this local approximation was shown to be reliable for various systems [26], it can still affect the individual components. Finally, we note that since $v_{\mathrm{KS}}^{(-)}[n_{p_{\alpha}}](x) = v_{\alpha}(x)+v_{\mathrm{H}}[n_{p_{\alpha}}](x)+v_{\mathrm{XC}}^{(-)}[n_{p_{\alpha}}](x)+v_{\mathrm{P}}(x)$, eqs. 4.8 can be derived simply by construction.

4.1.3 Numerical methods

Exact diagonalization: Hamiltonians 4.1, 4.3 and 4.4 are all diagonalized on a real grid using the sixth order central finite difference method for the $\nabla_{x_i}^2$ operator. [28] We note that both 4.1 and 4.3 are symmetric under the particle index interchange and all the eigenstates are either symmetric or antisymmetric. Spatially symmetric solutions correspond to the spin zero state while the antisymmetric spatial solutions correspond to triplet spin states. It

therefore becomes clear that we simply need to search for the lowest eigenstate of 4.3 or 4.4. [29], [30] We then use a Matlab built-in *eigs* function to solve for the lowest eigen-pair of the resulting Hamiltonian matrices (size N^2-by-N^2, where N is the number of grid points).

Density-to-potential inversions: To obtain the exact $v_{\mathrm{P}}(x)$, we need to perform a numerical inversion. The following outlines the inversion algorithm employed to find $v_{\mathrm{P}}(x)$ for a particular partitioning at a fixed set of fragment occupation numbers:

0. Start with an initial guess for $v_{\mathrm{P}}(x)$.

1. Use eqs. 3.4, 4.3 and 4.4 to compute the sum of fragment densities in the presence of $v_{\mathrm{P}}(x)$.

2. Calculate the difference between the total molecular density and the sum from 1.

3. Based on the value from 2, decide whether the sum of the fragment densities is sufficiently close to the total molecular density. If it is, the optimization is done; otherwise go to 4.

4. Update $v_{\mathrm{P}}(x)$. Go to step 1.

We note that the algorithm assumes that the total molecular density can be pre-computed. For the convergence criterion in step 3 we use the value of the following functional at step k:

$$\theta^{(k)}[n_{\mathrm{f}}^{(k)}] = \frac{1}{2^2}\int dx[n_{\mathrm{f}}^{(k)}(x) - n_0(x)]^2 \ , \tag{4.9}$$

where the factor 2 in the denominator appears because we have two electrons. For the update in step 4, we utilize the Broyden's method. [31] After the algorithm is converged, we methodically vary the occupation numbers to eventually scan the entire set and find the minimum. The initial guess of $v_{\mathrm{P}}(x) = 0$ in step 0 and the convergence thresholds of 10^{-14} in step 3 are sufficient for obtaining accurate energies. To obtain accurate and smooth potentials, we apply the following procedure. After the initial optimization to $\theta^{(k)} \sim 10^{-14}$, we compute $v_{\mathrm{P,kin}}^{(k)}(x)$, $v_{\mathrm{P,ext}}^{(k)}(x)$, $v_{\mathrm{P,H}}^{(k)}(x)$ and $v_{\mathrm{P,XC}}^{(k)}(x)$ using eqs. 4.8. In particular, we use the exact molecular density to compute derivatives of Eq. 4.6 and the current $n_{\mathrm{f}}^{(k)}(x)$ to compute the factors of Eq. 4.7. We then use the computed potetials to find

$\bar{v}_{\mathrm{P,kin}}(x) = v_{\mathrm{P}}^{(k)}(x) - v_{\mathrm{P,ext}}^{(k)}(x) - v_{\mathrm{P,H}}^{(k)}(x) - v_{\mathrm{P,XC}}^{(k)}(x)$ and $\bar{v}_{\mathrm{P,XC}}(x) = v_{\mathrm{P}}^{(k)}(x) - v_{\mathrm{P,ext}}^{(k)}(x) - v_{\mathrm{P,H}}^{(k)}(x) - v_{\mathrm{P,kin}}^{(k)}(x)$. Finally, we construct the new guess for $v_{\mathrm{P}}(x)$ by adding $\bar{v}_{\mathrm{P,kin}}(x)$, $\bar{v}_{\mathrm{P,XC}}(x)$, $v_{\mathrm{P,ext}}^{(k)}(x)$ and $v_{\mathrm{P,H}}^{(k)}(x)$. This new guess is run through a single cycle of the algorithm to return the improved results. This procedure does not significantly improve the energy results. However, it markedly improves the density convergence in the low-density regions and produces smooth potentials. Applying this procedure periodically within our algorithm can converge it to machine precision ($\max|n_{\mathrm{f}}^{(k)}(x) - n_0(x)| \sim 10^{-16}$). However, no appreciable changes in features of the potentials are observed after the threshold of $\theta \sim 10^{-14}$.

Since each fragment can only have up to 2 electrons, the KS potentials can be obtained analytically. The expressions for the inversions are trivial. [32]

4.2 Illustrative Results and Discussion

4.2.1 H_2 Model

We consider first a symmetric dimer model of H_2 at two different internuclear separations: the equilibrium bond length, $R_0 = 1.60$ a.u., and the large separation, $R = 10.0$ a.u. The optimal occupations for this model is clearly $N_{\mathrm{H,left}} = 1.0$ and $N_{\mathrm{H,right}} = 1.0$. We analyze features of $v_{\mathrm{P}}(x)$ and how they are affected by the electron-electron interaction. Our results highlight the importance of approximating $v_{\mathrm{P,kin}}(x)$ and $v_{\mathrm{P,XC}}(x)$ accurately in density embedding calculations, as previously pointed out by several computational studies using approximate $T_{\mathrm{S}}^{\mathrm{nad}}[n_{p_\alpha}]$ [33]–[36] For the noninteracting system, we show that $v_{\mathrm{P}}(x)$ is dominated by $v_{\mathrm{P,ext}}(x)$ at $R_0 = 1.60$ and by $v_{\mathrm{P,kin}}(x)$ $R_0 = 10.0$.

In Fig. 4.1, we plot the PT deformations of the fragment densities ($\delta n_\alpha(x) = n_\alpha(x) - n_\alpha^0(x)$, where $n_\alpha^0(x)$ is the density of an isolated fragment) and partition potentials corresponding to these two cases. At $R = 10.0$, both densities are slightly shifted away from the interatomic region. In contrast, at the equilibrium separation, the densities are shifted towards the bonding region. Furthermore, the interatomic interactions are markedly weaker at the larger separation. This is reflected in the density deformations and $v_{\mathrm{P}}(x)$ features that are roughly two orders of magnitude smaller than those at the equilibrium bond distance.

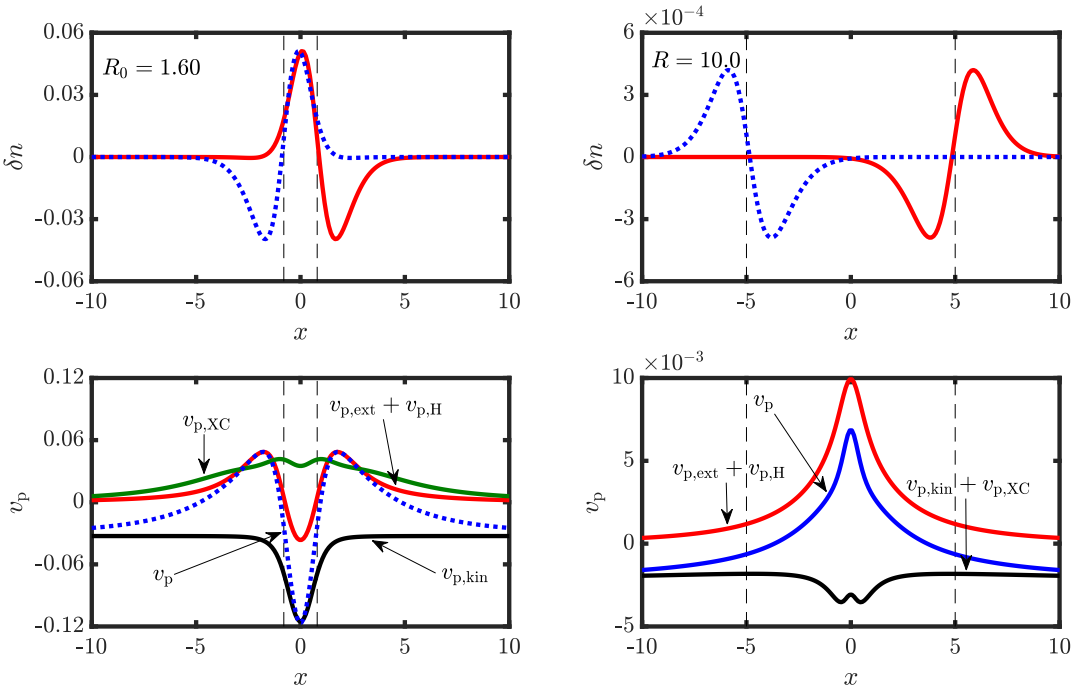

Figure 4.1. 1-D H_2 model at $R_0 = 1.60$ a.u. (left) and $R = 10.0$ a.u. (right). Top: deformations of the fragment densities $\delta n_\alpha(x) = n_\alpha(x) - n^0_\alpha(x)$, where $n^0_\alpha(x)$ is the density of an isolated fragment. Bottom: partition potential $v_{\mathrm{P}}(x)$ and its components defined through Eq. 4.5. Vertical dashed lines indicate the position of nuclei. The electron-electron interaction parameter $\lambda = 1$.

In the bottom panels of Fig. 4.1, we analyze the origin of these features through the decomposition of Eq. 4.5. We combine $v_{\mathrm{P,ext}}(x)$ and $v_{\mathrm{P,H}}(x)$ because $v_{\mathrm{P,ext}}(x)$ has a deep well and $v_{\mathrm{P,H}}(x)$ has a high peak in the internuclear region. However, their sum is on the order of the features in $v_{\mathrm{P}}(x)$. Adding the external and Hartree components can be further justified by the fact that in practical calculations both can be computed exactly, but $v_{\mathrm{P,kin}}(x)$ and $v_{\mathrm{P,XC}}(x)$ require approximations. In the plot for $R = 10.0$, we also combine $v_{\mathrm{P,kin}}(x)$ and $v_{\mathrm{P,XC}}(x)$, as they are analyzed separately later in the paper. At the equilibrium, the depth of the well in $v_{\mathrm{P}}(x)$ is determined by the $v_{\mathrm{P,kin}}(x)$ and the $v_{\mathrm{P,ext}}(x) + v_{\mathrm{P,H}}(x)$ terms. The position of the peaks is also determined by the $v_{\mathrm{P,ext}}(x) + v_{\mathrm{P,H}}(x)$ contribution. We note that the effect of the non-additive XC term is small relative to the other components. At $R = 10.0$, the peak in the middle comes from $v_{\mathrm{P,ext}}(x) + v_{\mathrm{P,H}}(x)$. The contribution from

$v_{\mathrm{P,kin}}(x)$ is almost completely cancelled by $v_{\mathrm{P,XC}}(x)$, but fine features persist even when the threshold $\theta^{(k)}$ is decreased to 10^{-23}.

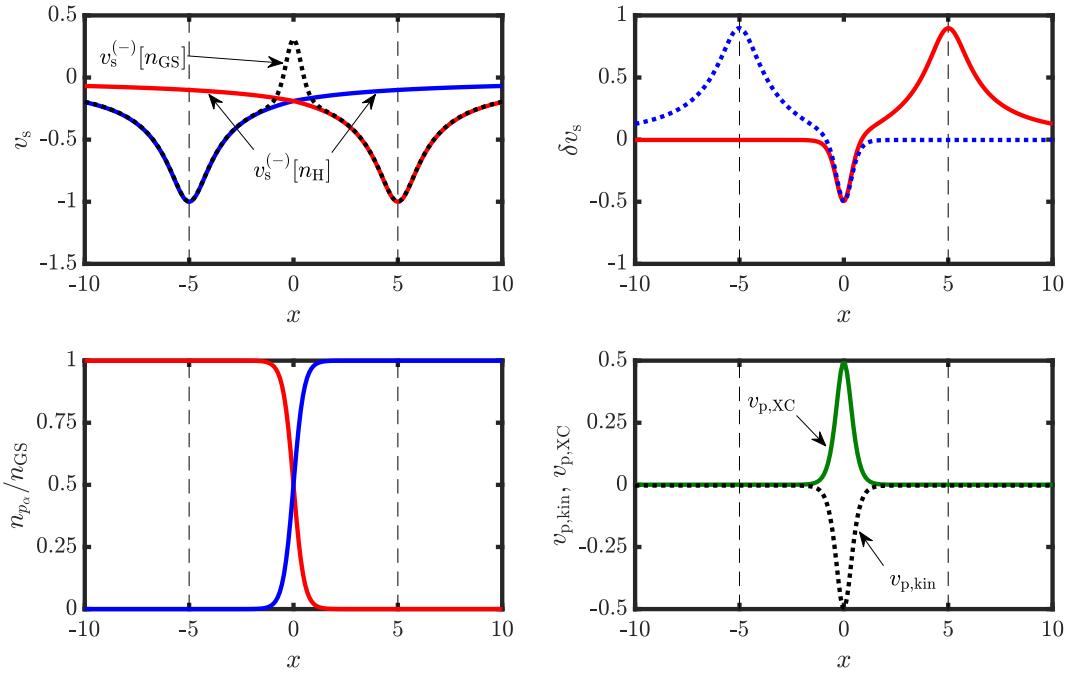

Figure 4.2. The relationship between features of $v_{\mathrm{P,kin}}(x)$ and the peak of molecular $v_{\mathrm{KS}}(x)$ for H_2 model at $\lambda = 1$ and $R = 10.0$. Top left: molecular KS potential $v_{\mathrm{KS}}^{(-)}[n_0](x)$ and fragment KS potentials $v_{\mathrm{KS}}^{(-)}[n_{\mathrm{H}}](x)$. Top right: the differences between the molecular and fragment potentials. Bottom left: $n_{p_\alpha}(x)/n_0(x)$ terms. Bottom right: kinetic and XC contributions to the partition potential. Vertical dashed lines indicate the position of nuclei.

It may appear that the contributions from $v_{\mathrm{P,kin}}(x)$ and $v_{\mathrm{P,XC}}(x)$ at large separation are unimportant as they cancel each other. However, the bottom right panel in Fig. 4.2 shows that these features have high magnitude. Since in practice $v_{\mathrm{P,kin}}(x)$ and $v_{\mathrm{P,XC}}(x)$ are approximated separately, the accuracy of the total $v_{\mathrm{P}}(x)$ can be highly sensitive to the errors in these approximations.

In addition, Fig. 4.2 shows the formation of $v_{\mathrm{P,kin}}(x)$ according to Eq. 4.8a. Top left panel shows $v_{\mathrm{KS}}^{(-)}[n_0](x)$ along with $v_{\mathrm{KS}}^{(-)}[n_{\mathrm{H}}](x)$'s. We observe that $v_{\mathrm{KS}}^{(-)}[n_{\mathrm{H}}](x)$ matches closely

with $v_{\rm KS}^{(-)}[n_0](x)$ in the nuclear regions. The difference between the fragment and molecular KS potentials $\delta v_{\rm KS}(x)$, plotted at the top right, has the flat region around their nucleus. The differences are weighted by the corresponding $n_{p_\alpha}(x)/n_0(x)$ terms and summed, producing the total $v_{\rm P,kin}(x)$. We note that $v_{\rm P,kin}(x)$ has a well from the peak in $v_{\rm KS}^{(-)}[n_0](x)$. The peak in $v_{\rm P,XC}(x)$ has the *same* origin [37]–[40] and it nearly cancels the well in $v_{\rm P,kin}(x)$. This cancelation is not exact and the fine features in $v_{\rm P,kin}(x) + v_{\rm P,XC}(x)$ can still be observed.

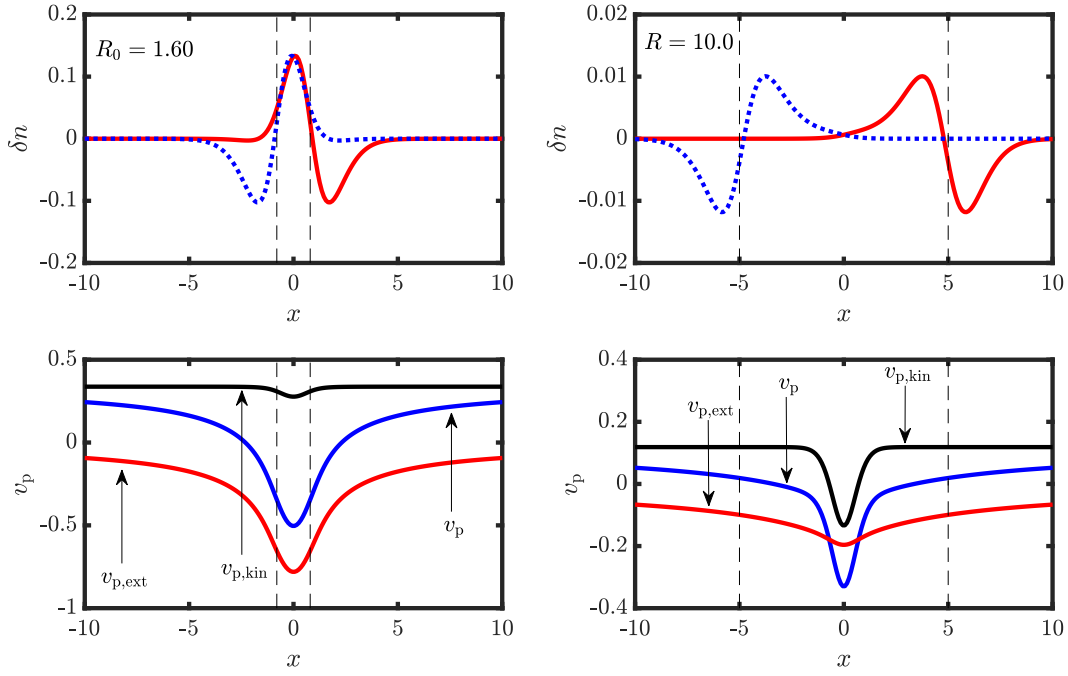

Figure 4.3. Same as Fig. 4.1, but for $\lambda = 0$

We turn off the electron-electron interaction in the system by setting $\lambda = 0$. The results are shown in Fig. 4.3. Our method recovers the trivial result that $v_{\rm p,H}(x)$ and $v_{\rm p,XC}(x)$ are zero. At both separations, $v_{\rm P}(x)$ has a single well. At equilibrium, this well is dominated by $v_{\rm P,ext}(x)$. In contrast, at $R = 10.0$, the well is predominantly determined by $v_{\rm P,kin}(x)$. The $v_{\rm P}(x)$ plots are consistent with previously reported ones for noninteracting systems, [41], [42]

but the present work shows that the well in $v_{\mathrm{P}}(x)$ is dominated by different components at *different* internuclear distances.

4.2.2 HeH Ion Model

We study the features of $v_{\mathrm{P}}(x)$ in the simplest heteronuclear molecular ion HeH^+ at equilibrium separation. This model has non-integer optimal occupations. We use this fact to analyze the relationship between the kinetic component of $v_{\mathrm{P}}(x)$ and the KS gap of PT fragments.

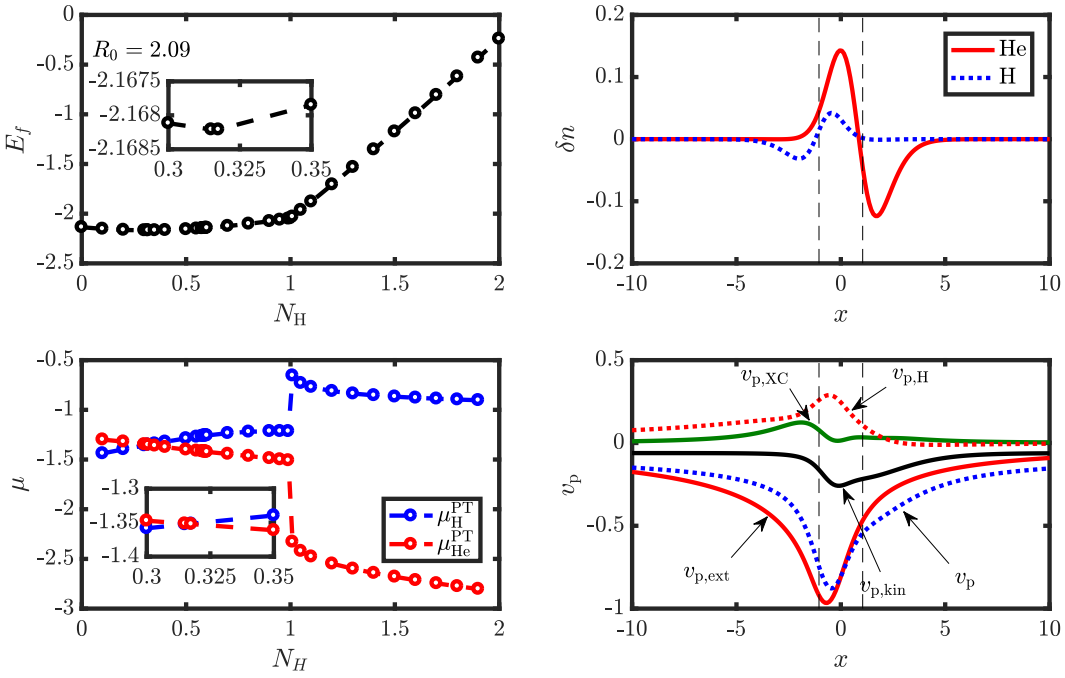

Figure 4.4. Summary of the PT results for the model system of HeH^+ at equilibrium separation and $\lambda = 1$. Left: fragment energies (top) and PT chemical potentials (bottom) at varying occupations on H atom. Right: density deformations relative relative to the isolated fragments with the optimal electron occupations (top) and corresponding partition potential along its components (bottom). Vertical dashed lines indicate the position of nuclei (H is on the left).

The left two panels of Fig. 4.4 show the behavior of $E_{\rm f}[\{n_\alpha\}]$ as a function of the number of electrons on the hydrogen atom, at the equilibrium bond distance of 2.09 *a.u.* The curvature of the energy plot is an important consequence of accounting for the finite-distance interfragment interactions (in contrast, the plot of energy versus the number of electrons in DFT consists of straight-line segments). This curvature does not smoothen the graph at integer occupations, where it still has a cusp. The graph has a minimum when $N_{\rm H} \approx 0.3175$. At this occupation, we also observe the chemical potential equalization of the fragments. A rigorous definition of fragments allows the discussion of the nature of a chemical bond and the optimal occupations suggest the amount of the ionic character a bond has. The connection between 1-D models and real bonds is, of course, not obvious. More generally, the physical interpretation of PT fragment properties is still an open question.

The top right panel of Fig. 4.4 shows the density deformations relative to the isolated fragments with the optimal electron occupations. We observe that both He and H densities are shifted towards the interatomic region. The partition potential that facilitates this shift is plotted at the bottom right of Fig. 4.4, along with its components. Although its overall shape is similar to H_2 at equilibrium bond distance, $v_{\rm P}(x)$ of HeH^+ is dominated by $v_{\rm P,ext}(x)$. Naively, this can be attributed to the fact that HeH^+ is an ion and the electron-nuclear interactions are the dominant ones.

The non-integer occupation numbers allow to establish the relationship between $v_{\rm P,kin}(x)$ and the fragment KS gaps $\Delta^\alpha = {\rm I}^\alpha - {\rm A}^\alpha$, where ${\rm I}^\alpha$ is the ionization potential and ${\rm A}^\alpha$ is the electron affinity of a fragment in the presence of $v_{\rm P}(x)$. If we assume the near-linearity of the fragment KS potentials, [43] Eq. 4.8a can be approximated as $v_{\rm P,kin}(x) \approx v^{\rm nl}_{\rm P,kin}(x)$, where:

$$v^{\rm nl}_{\rm P,kin}(x) = \sum_\alpha \Bigg\{ \frac{n_\alpha(x)}{n_0(x)} v_{\rm KS}[n_\alpha](x) - (1-\omega_\alpha)\Delta^\alpha \mathcal{Q}_{p_\alpha}(x,x) \Bigg\} - v^{(-)}_{\rm KS}[n_0](x) \ . \tag{4.10}$$

Fig. 4.5 indicates that this approximation is in excellent agreement with the exact $v_{\rm P,kin}(x)$. The right panel in Fig. 4.5 compares the molecular KS potential to the weighted sum of the fragment KS potentials, $\sum_\alpha n_\alpha[n_\alpha](x)/n_0(x) v_{\rm KS}(x)$ from Eq. 4.10. We can see that

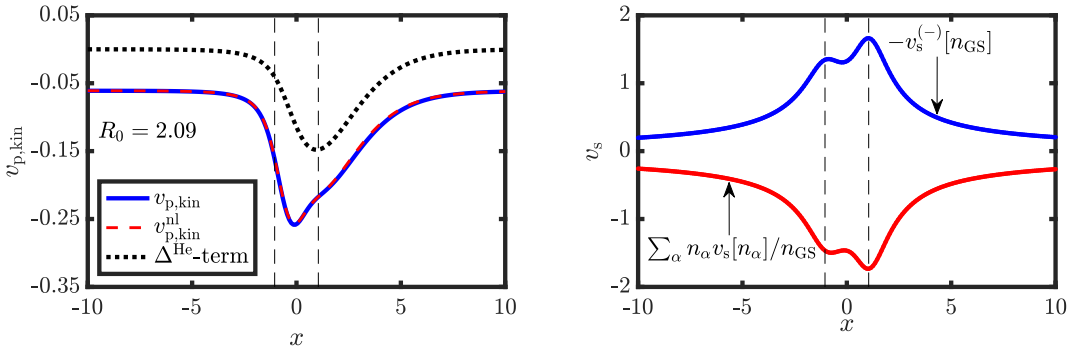

Figure 4.5. The relationship between $v_{\mathrm{P,kin}}$ and Δ^{He} defined through Eq. 4.10. Δ^{He}-term stands for $-(1-\omega_{\mathrm{He}})\Delta^{\mathrm{He}}\mathcal{Q}_{p_{\mathrm{He}}}(x,x)$. Vertical dashed lines indicate the position of nuclei (H is on the left).

these two contributions almost entirely cancel out and $v_{\mathrm{P,kin}}(x)$ is largely determined by the $(1-\omega_{\mathrm{He}})\Delta^{\mathrm{He}}\mathcal{Q}_{p_{\mathrm{He}}}(x,x)$ term (note that there is no contribution from Δ^{H} because $p_{\mathrm{H}}=0$). Additional calculations on model systems suggest that the fragment KS term closely mimics $-v_{\mathrm{KS}}^{(-)}[n_0](x)$ in the high density regions, but it misses its low density peak-and-step features.

4.2.3 LiH Model

We consider a heteroatomic dimer model of lithium hydride that separates into neutral fragments. In this model, the core electrons are not treated explicitly but their effects are simulated by adjusting the parameters of the external potential function. The modified electronic Hamiltonian of Eq. 4.1 is:

$$\mathcal{H} = \sum_{\mathrm{i}=1,2}\left\{-\frac{1}{2}\nabla_{x_{\mathrm{i}}}^2 - \frac{1}{\sqrt{2.25+(x_{\mathrm{i}}-R_{\mathrm{Li}})^2}} - \frac{Z_{\mathrm{X}}}{\sqrt{0.6+(x_{\mathrm{i}}-R_{\mathrm{H}})^2}}\right\} + \frac{1}{\sqrt{0.7+(x_1-x_2)^2}}\,, \tag{4.11}$$

where the SC parameters for Li, H and electron-electron interactions (2.25, 0.70 and 0.60 respectively) are chosen following the same considerations as in ref. [39]. These parameters produce the correct ionization potential difference between isolated Li and H atoms. The

individual ionization potentials produced by this model are higher than the real ones, making the densities less diffuse and allowing us to use a simulation box of 25 a.u.

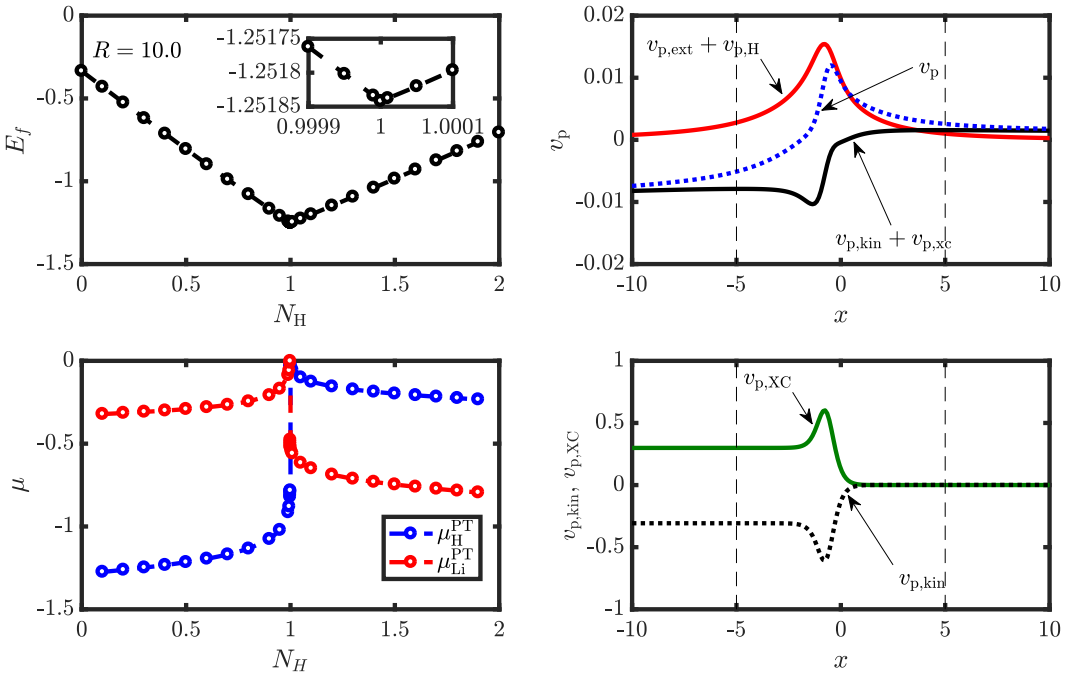

Figure 4.6. Summary of the PT results for the model system of LiH, defined through Eq. 4.11 at $R = 10.0$. Left: fragment energies (top) and PT chemical potentials (bottom) at varying occupations on H atom. Right: partition potential and its components (top); kinetic and XC contributions to $v_{\mathrm{P}}(x)$ (bottom). Vertical dashed lines indicate the position of nuclei (H is on the left)

The results for LiH are summarized in Fig. 4.6. The left two graphs show the fragment energies and chemical potentials at varying occupation numbers. E_{f} is minimized when N_{H} (and obviously N_{Li}) is equal to 1. This point is a cusp in E_{f} as expected from Eq. 3.3. $R = 10.0$ *a.u.* can be taken as the large separation limit in our model and it shows that the bond breaking is homolytic. Although not obvious from the plot, the graph of E_{f} is curved, similar to the one for HeH^+ in Fig. 4.4. The chemical potentials exhibit a step-like feature into integer occupations, which prevent the condition of Eq. 3.8 to be satisfied. The right

two graphs show $v_{\mathrm{P}}(x)$ and its decomposition. Similarly to the case of H_2, $v_{\mathrm{P}}(x)$ has a peak in the internuclear region, dominated by the $v_{\mathrm{P,ext}}(x)+v_{\mathrm{P,H}}(x)$ term. Moreover, the $v_{\mathrm{P,kin}}(x)$ and $v_{\mathrm{P,XC}}(x)$ almost completely cancel out. Analogously to the case of H_2, their features are connected to the features of the molecular KS potential. [37]–[40] In addition to the peak, in this case, $v_{\mathrm{P,kin}}(x)$ and $v_{\mathrm{P,XC}}(x)$ also display a step. The steps almost entirely cancel out. The remaining small peak we observe in the top right panel of Fig. 4.6 is likely due to the long range nature of SC potentials.

4.2.4 A Closer Look at Spin in PT

We study the equalization of spin densities in the model of He_2^+ with three interacting electrons. The system is described with a modified hamiltonian of Eq. 4.1:

$$\mathcal{H} = \sum_{\mathrm{i}=1,2,3} \left\{ -\frac{1}{2}\nabla_{x_\mathrm{i}}^2 - \frac{2}{\sqrt{1.0+(x_\mathrm{i}-R_{\mathrm{He,left}})^2}} - \frac{2}{\sqrt{1.0+(x_\mathrm{i}-R_{\mathrm{He,right}})^2}} \right\} + \frac{1}{\sqrt{1.0+(x_1-x_2)^2}} + \frac{1}{\sqrt{1.0+(x_1-x_3)^2}} + \frac{1}{\sqrt{1.0+(x_2-x_3)^2}} \,. \tag{4.12}$$

For the case of 3 electrons, we no longer have a straightforward mapping between the ground state of the spatial hamiltonian 4.12 and the spatial part of the true ground state wavefunction of the system. We briefly discussed this issue in Sec. 2.1. A more detailed discussion can be found in the appendix.

It is worth pointing out that only the total density (but not *spin densities*) equalize in spin-unresolved PT. We illustrate this in Fig. 4.7 where we plot *spin densities*

$$n_{\mathrm{S}}(\mathbf{r}) = n_{\uparrow}(\mathbf{r}) - n_{\downarrow}(\mathbf{r}) \tag{4.13}$$

for the ground state of the full system $n_{\mathrm{S,0}}(x)$ (blue solid line) and for the sum of fragment densities at convergence $n_{\mathrm{S,f}}(x)$ (red dashed line). Notably, $n_{\mathrm{S,0}}(x)$ has regions of both positive and negative values. This important [44]–[46] feature of $n_{\mathrm{S,0}}(x)$ is completely "missed" by $n_{\mathrm{S,f}}(x)$. This behavior is, however, expected as we only constrain the total density in our calculations. Although, in principle, only the ground state density is required to get any

property of the system, in practice, functional dependence of many observables on density is not readily available (e.g., even the spin density $n_{\mathrm{S},0}(\mathbf{r})$ cannot be easily obtained from $n_0(\mathbf{r})$). It is, therefore, desirable to have a theory that reproduces both spin and total densities of the full system. In PT, this can be achieved by introducing a separate embedding potential for spin-up and spin-down electrons:

$$G[\{n_{\uparrow,\alpha}, n_{\downarrow,\alpha}\}, \{v_{\mathrm{P},\uparrow}, v_{\mathrm{P},\downarrow}\}] = E_{\mathrm{f}}[\{n_{\uparrow,\alpha}, n_{\downarrow,\alpha}\}] + \int d^3\mathbf{r}\; v_{\mathrm{P},\uparrow}[n_{\uparrow,\mathrm{f}}(\mathbf{r}) - n_{\uparrow,0}(\mathbf{r})] + \int d^3\mathbf{r}\; v_{\mathrm{P},\uparrow}[n_{\downarrow,\mathrm{f}}(\mathbf{r}) - n_{\downarrow,0}(\mathbf{r})]\ . \tag{4.14}$$

This is analogous to our treatment of spin in KS-DFT: PT reference system is now a fictitious system of non-interacting fragments in the external field with a magnetic component that interacts only with spin.

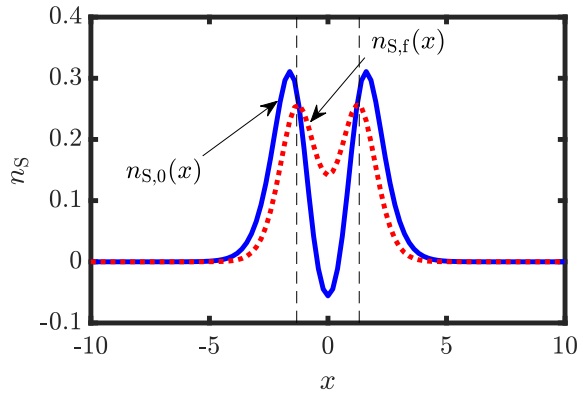

Figure 4.7. Spin densities (defined through Eq. 4.13) for the He_2^+ model. Blue solid line: spin density of the full system $n_{\mathrm{S},0}(x)$. Red dashed line: spin density of the sum of the fragments $n_{\mathrm{S,f}}(x)$.

Fragment energy in the case of spin-resolved PT does not have a simple formula similar to Eq. 3.3 that comes directly from the PPLB energy Eq. 2.36. Recall that Eq. 2.36 holds due to convexity of energy with respect to the electron number N. Gál and Geerlings [19]

investigated the generalization of the PPLB Eq. 2.36 to the spin-resolved case. For the case of an integer number of electrons ($N = M$) and a non-integer *spin-difference* number

$$N_{\mathrm{S}} = N_{\uparrow} - N_{\downarrow} = (M_{\uparrow} - M_{\downarrow}) + (\omega_{\uparrow} - \omega_{\downarrow}) = M_{\mathrm{S}} + \omega_{\mathrm{S}} \tag{4.15}$$

(with the integer part M_s and the fractional part ω_s of N_s)[1], they derived:

$$E_0(M, N_{\mathrm{S}} = M_{\mathrm{S}} \pm \omega_{\mathrm{S}}) = (1 - \frac{\omega_{\mathrm{S}}}{2})E(M, M_{\mathrm{S}}) + \frac{\omega_{\mathrm{S}}}{2}E(M, M_{\mathrm{S}} \pm 2) \ , \tag{4.16}$$

with $0 \leq \omega_{\mathrm{S}} \leq 2$. It is critical to mention that in Eq. 4.16, $E(M, M_{\mathrm{S}})$ (or $E(M, M_{\mathrm{S}} \pm 2)$) is the lowest energy at the given M_{S} (i.e., $E_{0,\mathrm{S}}(M, M_{\mathrm{S}})$ or $E_{0,\mathrm{S}}(M, M_{\mathrm{S}} \pm 2)$) if $E_{0,\mathrm{S}}(M, M_{\mathrm{S}})$ (or $E_{0,\mathrm{S}}(M, M_{\mathrm{S}} \pm 2)$) is convex. Otherwise, $E_{0,\mathrm{S}}(M, M_{\mathrm{S}}) > E(M, M_{\mathrm{S}})$ (or $E_{0,\mathrm{S}}(M, M_{\mathrm{S}} \pm 2) > E(M, M_{\mathrm{S}} \pm 2)$). The convexity with respect to M_{S} is clearly not commonplace. One obvious system where the M_{S} convexity does not hold is the Nitrogen atom [22], [47]. It is known that the ground state of the Nitrogen atom has $M_{\mathrm{S}} = \pm 3$ (i.e., all three valence p-electrons are either spin-up or spin-down). Therefore, any $E(N = 7, N_{\mathrm{S}} \in (-3, 3))$ for Nitrogen is a superposition of just $E(N = 7, N_{\mathrm{S}} = -3)$ and $E(N = 7, N_{\mathrm{S}} = -3)$ terms.

The systems with non-integer N and non-zero magnetic field (as we have in the spin-resolved PT) are even more problematic as the simultaneous convexity with respect to N and N_{S} is now required to have the "PPLB-like" equation for $E_{\mathrm{f}}[\{n_{\uparrow,\alpha}, n_{\downarrow,\alpha}\}]$. The constrained minimization over all $E_{0,\mathrm{S}}(M, M_{\mathrm{S}})$ is clearly required, but computationally is not feasible. How can this issue be resolved in practice?

We suggest that Eq. 4.14 is minimized for a fixed functional form of $E_{\mathrm{f}}[\{n_{\uparrow,\alpha}, n_{\downarrow,\alpha}\}]$. In the He_2^+ model, we can set

$$E_{\mathrm{f}}[\{n_{\uparrow,\alpha}, n_{\downarrow,\alpha}\}] = E_{\mathrm{left}}(N_{\uparrow} = 1, N_{\downarrow} = 1) + E_{\mathrm{right}}(N_{\uparrow} = 1, N_{\downarrow} = 0) \tag{4.17}$$

[1]↑Note that we use the lowercase "s" to represent the spin state (↑ or ↓) and the capital "S" to represent quantities depending on the difference of spin-up and spin-down electrons.

by putting 2 electrons in the left fragment and 1 electron in the right fragment. Alternatively, we can chose a more "intuitive" form:

$$E_{\rm f}[\{n_{\uparrow,\alpha}, n_{\downarrow,\alpha}\}] = \sum_{\alpha} 0.5E_{v_\alpha}(N_\uparrow = 1, N_\downarrow = 1) + 0.5E_{v_\alpha}(N_\uparrow = 1, N_\downarrow = 0) \ , \tag{4.18}$$

where we have 1.5 electrons (1 spin-up electron and 0.5 spin-down electron) in each fragment. Even though such fixed forms of $E_{\rm f}[\{n_{\uparrow,\alpha}, n_{\downarrow,\alpha}\}]$ may be consistent with the equations of Gál and Geerlings [19] for isolated fragments, they will not necessarily be correct in presence of $v_{\rm P}(\mathbf{r})$. This approach also comes with a drawback that a rigorous definition of the fragment chemical potential is no longer possible.

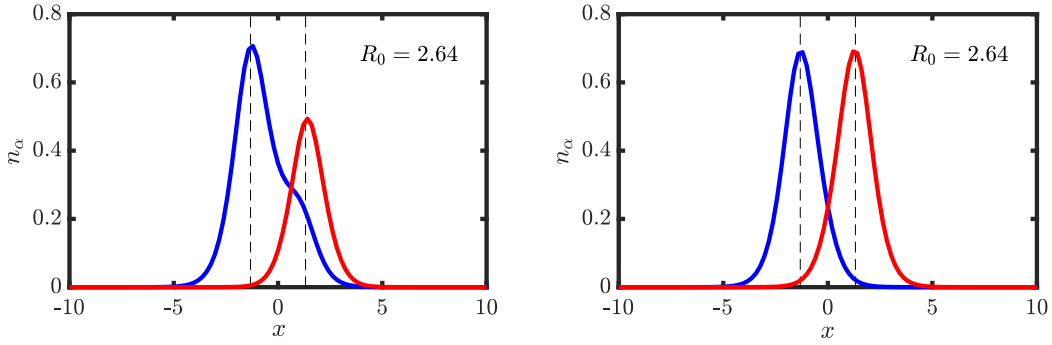

Figure 4.8. Fragment densities for the He_2^+ model at $R_0 = 2.64$. Left panel: functional form of $E_{\rm f}[\{n_{\uparrow,\alpha}, n_{\downarrow,\alpha}\}]$ is defined through Eq. 4.17. Right panel: functional form of $E_{\rm f}[\{n_{\uparrow,\alpha}, n_{\downarrow,\alpha}\}]$ is defined through Eq. 4.18.

In Fig. 4.8, we plot the PT densities corresponding to the fragment occupations chosen above. In both cases, calculations successfully converged at a rate similar to the one of the spin-unresolved calculation. Notably, the fragment energy in the spin-*unresolved* case is the lowest among the 3 calculations we performed.

In Fig. 4.8, we observe that the density of the left Helium fragment is delocalized in the case of integer occupations on the fragments (left panel). Although the case of 1D He_2^+ is extreme, this "leaking" of density into the spatial regions of other fragments can be problematic with real 3D calculations where the localization is important for accuracy

and efficiency of fragment calculations. We believe that the "correct" choice of the form of $E_{\mathrm{f}}[\{n_{\uparrow,\alpha}, n_{\downarrow,\alpha}\}]$ in practice will depend on a particular functional approximation to $E_{\mathrm{P}}[n]$, and this issue should be taken into consideration when these approximations are developed.

4.3 Concluding Remarks

In spite of the simplicity of this model, we expect the same features discovered here to be present in real molecules. Explicit treatment of core electrons and 3D-Coulomb interactions would be of course needed to verify this.

Finally, the decomposition of $v_{\mathrm{P}}(x)$ through Eq. 4.5 provides a useful way for identifying the origin of important features of $v_{\mathrm{P}}(x)$ and linking them to the approximations used in practical density-embedding calculations. We plan to investigate in future work the extent to which approximate XC and non-additive kinetic energy functionals reproduce the features of $v_{\mathrm{P}}(x)$ observed here.

5. DENSITY EMBEDDING WITH CONSTRAINED CHEMICAL POTENTIAL

This section contains work from the article entitled "Partition potential for hydrogen-bonding in formic acid dimers" written by the author, Kelsie Niffenegger, Jonathan Nafziger, and Adam Wasserman published in the Molecual Physics [48].

To this point, we have only discussed systems with finite number of electrons. In this chapter, we will formulate a chemical-potential constrained density embedding method for systems where different fragments can have either continuum or discrete electronic states. We will illustrate the method with the simplest model system designed to mimic an atom near a metal surface. It is trivial to separate the full system into two fragments (metal and atom) only when the distance between them is infinite. In this case, a *range* of metallic chemical potentials, μ, will lead to an identical number of electrons, N, on the atom. Our density embedding method can be used to define fragments even at *finite* separations. We show that using these definitions for fragments, the typical $N(\mu)$ staircase function is partially smoothed out due to the finite-distance interactions, resembling finite-temperature effects. Fractional occupations on the atom occur only for sharply-defined μ's. Because calculating fractional charges is important in various fields, from electrolysis to catalysis, solar cells and organic electronics, we anticipate several potential uses of the proposed approach.

In Sec. 5.1, we review how PPLB equations (see Sec. 2.4) can be use to describe atom-metal interactions. We describe *our* method in Sec. 5.2 and illustrate it through explicit numerical computation in Sec. 5.3. We end with a brief summary and outlook in Sec. 5.4.

5.1 PPLB Equations for Atom-Metal Interactions

According to PPLB theorem (see Sec. 2.4 and Eqs. 2.36—2.38), the ground-state energy of an N-electron system ($E(N)$, N can be a non-integer number) is a piecewise-continuous linear function of N. At strictly zero temperature, an atom or molecule that is in equilibrium

with a *far-away* metal reservoir, will be neutral in the ground state for any chemical potential μ in the range

$$-I < \mu < -A \ , \tag{5.1}$$

where I is the ionization potential and A the (positive) electron affinity of the neutral atom. For chemical potentials lower than $-I$, the atom transfers one electron to the reservoir. For chemical potentials higher than $-A$, the atom receives one electron from the reservoir. The number of electrons in the atom is thus a staircase function of the chemical potential (black dot-dash line in Fig. 5.1), which is clearly only sharply defined for non-integer numbers. The range of μ that is consistent with the integer m is the fundamental energy gap of the atom, $E_{\rm g} = I - A$, which is thus given by the total discontinuity in the derivative of $E(N)$ with respect to N at $N = M$. All properties of the system involving derivatives of the energy with respect to N are similarly undefined at the integers at zero temperature.

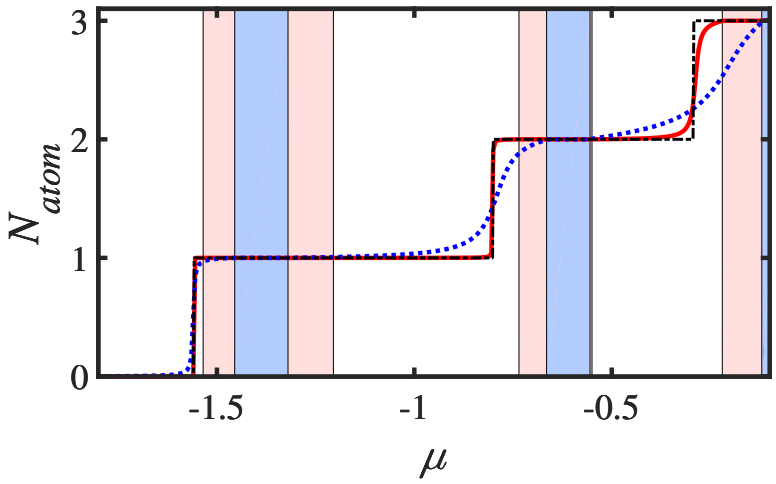

Figure 5.1. The atomic fragment occupation number $N_{\rm atom}$ as a function of the system chemical potential, μ, for $R = 3$ (dotted blue line), $R = 5$ (solid red line), and $R > 10$ (dot-dash black line). The step-like behavior that occurs at large separations smooths out as we bring the fragments closer together. The light blue and salmon-shaded regions highlight μ values for which $N_{\rm atom}$ is exactly integer at $R = 3$ and $R = 5$ respectively.

A smoothening of the discontinuities at integer numbers of electrons and a range of μ that is narrower than $I - A$ can be found by applying techniques of the grand-canonical ensemble at finite temperature [21]. The main result of the work in this chapter is that sharper values of μ can be found even at zero temperature by considering *finite distances* from the metal reservoir. To show this, an unambiguous definition is needed for the charge of the atom when it is located at an interacting distance from the metal. We provide such definition by requiring that the chemical potential of the two fragments (metal and atom) be equal while satisfying the standard constraint of density-embedding methods, i.e. that the sum of the two fragment densities be equal to the total electronic density. With this definition of fragments, the regions of strictly integer numbers of electrons on the atom are narrower than $I - A$ when the atom is at an interacting distance from the reservoir (red and blue lines in Fig. 5.1). Outside of the shaded regions in Fig. 5.1, the atom acquires a fractional number of electrons. At large separations between the atom and the metal, our model recovers the PPLB results. At shorter separations, the regions of integer occupations shrink but do *not* collapse to a single point. Due to the finite-distance interactions, the effective values of I and A are different from those of the isolated atom. As a result, the narrowing of the integer windows is not symmetric with respect to $(I + A)/2$ and is markedly different near different integer occupations.

5.2 Chemical-potential constrained Partition-DFT

Consider a system of electrons in an external potential $v(\mathbf{r})$ that can be written as:

$$v(\mathbf{r}) = v_{\text{atom}}(\mathbf{r}) + v_{\text{metal}}(\mathbf{r}) \quad , \tag{5.2}$$

where $v_{\text{metal}}(\mathbf{r})$ describes a background periodic or semi-periodic metallic potential supporting a continuum of electronic levels occupied up to a Fermi energy, ϵ_F, and $v_{\text{atom}}(\mathbf{r})$ is a localized potential such as the Coulomb or screened-Coulomb potential of an atom. The partition of Eq.(5.2) is useful when one wants to describe an atomic defect in a solid or an atom adsorbed on a metal surface.

The task of finding the number of electrons on the atom, $N_{\rm atom}$, is trivial only when $v_{\rm atom}(\mathbf{r})$ is non-zero far from all regions where $v_{\rm metal}(\mathbf{r})$ is non-zero, in which case one recovers the black staircase function of Fig.1 with $\mu = \epsilon_F$. The total density $n(\mathbf{r})$ for the combined system of atom and metal can be partitioned as $n_{\rm atom}(\mathbf{r}) + n_{\rm metal}(\mathbf{r})$ in many different ways. Partition Density Functional Theory (P-DFT, [26], [49], [50]) provides an elegant, unambiguous method for performing such a partition when the number of electrons is finite and the external potential for each fragment vanishes in all directions as $|\mathbf{r}| \to \infty$. Fragments in P-DFT are isolated from each other and are in contact with a far-away electronic reservoir through which they can exchange electrons. The interaction energy between the fragments is recovered by means of a unique global embedding potential, referred to here as the reactivity potential, $v_{\rm R}(\mathbf{r})$ (to distinguish it from the partition potential we defined for finite systems). The prescription to determine $N_{\rm atom}$ becomes simple: Minimize the sum of the fragment energies (i.e. atom and metal) subject to the constraint that the fragment densities sum to to the correct total density, and then calculate the number of electrons in the atom as $N_{\rm atom} = \int n_{\rm atom}(\mathbf{r}) d\mathbf{r}$. This number is in general not an integer because each P-DFT fragment energy is given by the ensemble expression of Eq.(2.36), where the non-integer ω is one of the parameters to be optimized during the energy minimization.

In the case of the potential of Eq.(5.2), however, $v_{\rm metal}(\mathbf{r})$ does not vanish as $|\mathbf{r}| \to \infty$ in all directions, and one of the fragment energies is infinite. The approach of P-DFT is thus not directly applicable.

In lieu of an energy minimization, we propose here to impose a chemical-potential equalization constraint, shown to be equivalent to energy-minimization for the case of finite systems [25]. The prescription is just as simple: Find the fragment densities that equalize the chemical potentials of the fragments and the chemical potential of the combined system:

$$\mu_{\rm atom} = \mu_{\rm metal} = \mu \quad , \tag{5.3}$$

while adding to the correct total density. The resulting density of the atom is an ensemble ground-state density of $v_{\rm atom}(\mathbf{r})$ modified by the addition of $v_{\rm R}(\mathbf{r})$. The latter piece is identical for both atomic and metallic fragments.

When N_{atom} is an integer, μ_{atom} is defined only within a range, so Eq. 5.3 is applicable only for *non*-integer values of N_{atom}. For integer occupations, the condition of Eq. 5.3 is modified taking into account Eq. 5.1:

$$-I_{\text{atom}} < \mu_{\text{metal}} = \mu < -A_{\text{atom}} \quad , \tag{5.4}$$

where I_{atom} and A_{atom} are computed *in the presence of* $v_{\text{R}}(\mathbf{r})$. We consider our method converged if either N_{atom} is non-integer and condition 5.3 is satisfied *or* if N_{atom} is integer and condition 5.4 is satisfied. In the following section, we successfully apply this method to a model system that mimics an atom-metal interface in 1-D; however, the rigorous derivation of the conditions for the existence of a unique reactivity potential for systems with semi-infinite fragments is still not established.

5.3 Simple Illustration

We choose the simplest non-trivial system that exhibits the features we need: One semi-infinite fragment (the 'metal') and one finite fragment with a small number of bound states (the 'atom'). The total number of electrons is infinite, but the electrons are non-interacting and restricted to move in only one dimension.

5.3.1 Model System

The metal is represented by a potential that goes to a negative constant $-V_0$ as $x \to -\infty$:

$$v_{\text{metal}}(x) = \frac{-V_0}{1 + \mathrm{e}^{s(x-R)}} \quad , \tag{5.5}$$

and is populated with non-interacting 'spinless electrons' up to the Fermi level ϵ_F, with $-V_0 < \epsilon_F < 0$. In Eq. 5.5, R is the separation between the metal surface and the center of the atomic potential, and s is a parameter that determines the steepness of the step. The form of the potential allows it to be smooth enough to be used with finite-difference methods

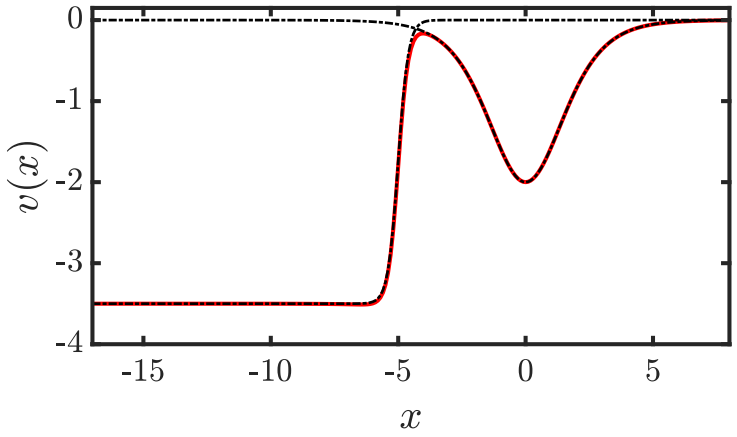

Figure 5.2. The potentials v_{metal} and v_{atom} (dashed black lines) along with the total external potential v (solid red line) for the parameters $R = 5$, $\gamma = 0.5$, $Z = 2$, and $V_0 = 3.5$.

on a spatial grid while preserving a steep step-like feature. The atom is represented by a finite potential with a finite number of bound states:

$$v_{\text{atom}}(x) = -Z\cosh^{-2}(\gamma x) \quad , \tag{5.6}$$

where Z and γ are parameters that control the depth and width of the well. We use $V_0 = 3.5$, $Z = 2$, and $\gamma = 0.5$ throughout the paper. The total external potential is then just the sum of v_{metal} and v_{atom} according to Eq.(5.2), as shown in Fig. 5.2.

The full system of metal plus atom produces a continuum of states. All calculations are done at zero temperature so $\mu = \epsilon_F$. The reactivity potential $v_{\text{R}}(x)$ ensures fragment densities sum to the total density of the system. The densities of the total system and of the metal fragment are calculated using the Green's function approach [51], [52]. The total system density $n(x)$ for a large separation $R = 15$ is shown in Fig. 5.3. We can see that as the chemical potential of the system increases through the energy levels of the isolated atomic potential, the density near the atom increases in large jumps every time the chemical potential reaches a bound state. The atomic densities have the ensemble form [20]:

$$n_{\text{atom}}(x) = \omega n_{p+1}(x) + (1-\omega)n_p(x) \quad , \tag{5.7}$$

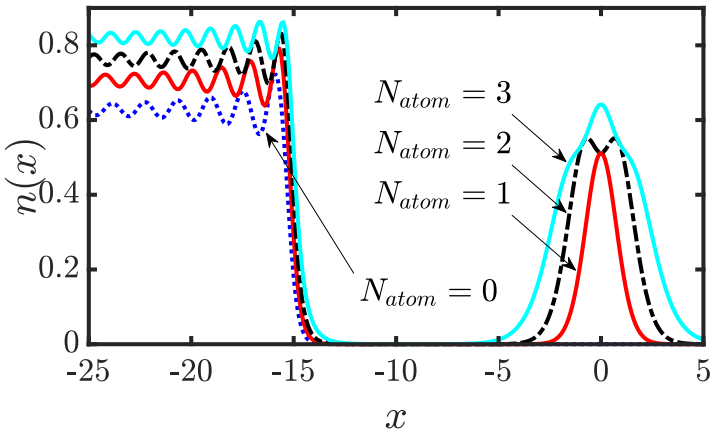

Figure 5.3. Total system densities, $n(x)$, for four choices of μ which give $N_{\text{atom}} = 0, 1, 2$, and 3 using a separation $R = 15$.

where p is the lower bounding integer of N_{atom}, $0 \leq \omega < 1$, and $N_{\text{atom}} = p + \omega$. Calculations of the atomic densities at integer occupations are trivial.

5.3.2 Search for Chemical-potential Equalization

To obtain a single point on the N_{atom} versus μ plot in Fig. 5.1, we perform a numerical algorithm for a set value of μ. This algorithm consists of an 'inner' inversion that computes the reactivity potential at the current guess of N_{atom} and an 'outer' loop that updates N_{atom} until one of the chemical-potential equalization conditions, Eq. 5.3 or Eq. 5.4, is satisfied. Our inversion method requires the precomputed total density $n(x)$ for each μ. We set μ_{metal} equal to μ and do not vary it throughout the inversion procedure.

We choose $v^{(0)}_{\text{R,Guess}}(x) = 0$ as our initial guess for $v_{\text{R}}(x)$. To calculate the initial guess for N_{atom}, we start by calculating the isolated atomic density, $n^{(0)}_{\text{atom}}(x)$. We separate $n^{(0)}_{\text{atom}}(x)$ into contributions from the density of the highest occupied atomic orbital (HOMO) and the density due to the core electrons, $n^{(0)}_{\text{atom}}(x) = n^{(0)}_{\text{core}}(x) + n^{(0)}_{\text{HOMO}}(x)$. The number of states included in the core region, N_{core}, is equal to the number of eigenvalues of the isolated atom which are below μ.

At each iteration $k \geq 0$ of the 'outer' loop, we use the current values $N^{(k)}_{\text{atom}}$ and $v^{(k)}_{\text{R,Guess}}(x)$ to compute the $v^{(k)}_{\text{R}}(x)$ that minimizes the difference between $n(x)$ and $n^{(k)}_{\text{f}}(x) = n^{(k)}_{\text{metal}}(x) +$

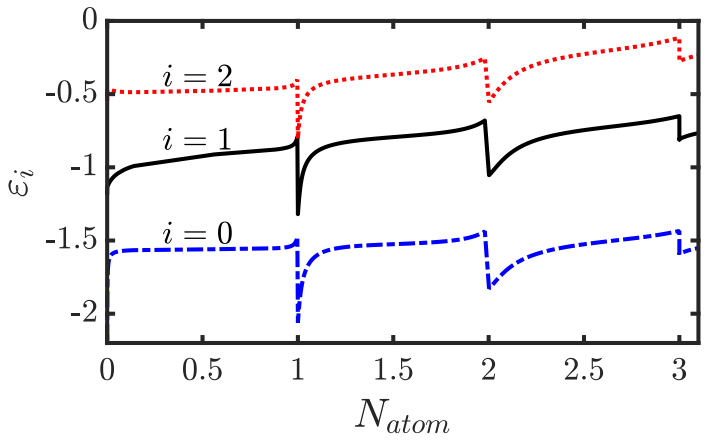

Figure 5.4. The atomic fragment eigenvalues ε_{i} as the fragment occupation number N_{atom} passes through the integer occupation of one for $R = 3$.

$n^{(k)}_{\mathrm{atom}}(x)$ to numerical precision (i.e. $v^{(k)}_{\mathrm{R,Guess}}(x)$ is used as an initial guess to find $v^{(k)}_{\mathrm{R}}(x)$ at fixed $N^{(k)}_{\mathrm{atom}}$ and μ_{metal}). The resulting fragment densities are used to calculate the fragment responses $\chi^{(k)}_{\alpha}(x, x')$ that are then used to update $v^{(k)}_{\mathrm{R,Guess}}(x)$.

If $N^{(k)}_{\mathrm{atom}}$ is not an integer, then $\mu^{(k)}_{\mathrm{atom}}$ equals the HOMO energy $\varepsilon^{(k)}_{\mathrm{HOMO}}$ in the presence of $v^{(k)}_{\mathrm{R}}(x)$, and Eq. 5.3 is used to check if the algorithm has converged. On the other hand, if $N^{(k)}_{\mathrm{atom}}$ is an integer, the convergence criteria of Eq. 5.4 is employed, with $-I_{\mathrm{atom}} = \varepsilon^{(k)}_{\mathrm{HOMO}}$ and $-A_{\mathrm{atom}} = \varepsilon^{(k)}_{\mathrm{LUMO}}$, where $\varepsilon^{(k)}_{\mathrm{LUMO}}$ is the energy of lowest unoccupied atomic orbital in the presence of $v^{(k)}_{\mathrm{R}}(x)$.

If neither of the conditions is met, one continues by calculating $N^{(k+1)}_{\mathrm{atom}}$ and repeating the above procedure.

5.3.3 Chemical Potentials, Energies and Densities

The origin of the discontinuities of the chemical potential can be understood in terms of the atomic orbitals ε_{i} (in the presence of $v_{\mathrm{R}}(x)$). Near integer occupations, the energy of the HOMO shifts up from the left and the energy of the LUMO shifts down from the right, as seen in Fig. 5.4. Even for separations as small as $R = 3$, levels do not equalize.

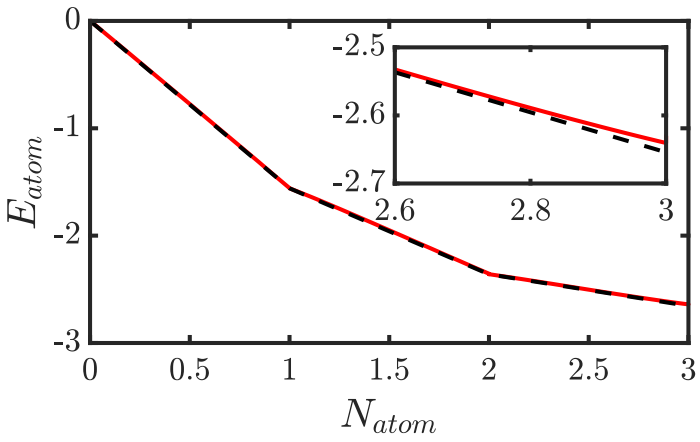

Figure 5.5. The atomic fragment energy $E_{\rm atom}$ as a function of the fragment occupation number $N_{\rm atom}$ for $R = 3$ (solid red line) and $R = \infty$ (dashed black line).

The effect of the finite-distance interactions on the energy of the atom can be seen in Fig. 5.5. The energy of the atom is defined as the sum of occupied orbitals *minus* the energy contribution from the reactivity potential:

$$E_{\rm atom} \equiv \sum_{\rm i=1}^{p_{\rm atom}} \varepsilon^{\rm i}_{\rm atom} + w\varepsilon^{\rm LUMO}_{\rm atom} - \int dx v_{\rm R}(x) n_{\rm atom}(x) \quad . \tag{5.8}$$

In Fig. 5.5, the dashed line shows the energy at large separation, $R = 15$. It consists of *straight* line segments [20], [53], [54]. At short distances (e.g. $R = 3$, solid red in Fig. 5.5) the line segments have a slight curvature. As shown in the inset plot of Fig. 5.5, the curvature is more noticeable for $N_{\rm atom}$ in the range of 2 to 3, where $E_{\rm atom}$ values are more evenly spaced. This curvature is the consequence of the inter-fragment interactions, but it does not smoothen the cusps at integer occupations.

The atomic fragment density at large values of R jumps abruptly when going through integer occupations, as can been seen in the top ($N_{\rm atom} = 1$) and middle ($N_{\rm atom} = 2$) panels of Fig. 5.6. For each value of $N_{\rm atom}$, increasing the Fermi energy of the system changes almost exclusively $n_{\rm metal}(x)$. As these changes occur, we observe an increase in the value of the metal density accompanied by a decrease in the period of density (Friedel) oscillations. The bottom panel of Fig. 5.6 shows the representative behavior of fragment densities at small

separations. Densities corresponding to non-integer values of N_{atom} begin to appear. We note that, in this regime, the density of the metal fragment appears unchanged for different values of μ_{metal}. The density response of the system to infinitesimal changes of μ is thus largely localized to either atom or metal fragments.

In the case of finite systems, the sum of fragment energies typically displays cusps at integer occupations and/or local minima at fractional occupations [42]. When searching for the lowest value of this summed energy, fragments may acquire either integer numbers when the infimum is a cusp (exactly an integer), or fractional numbers when it is not. Here, we are not directly minimizing energies but attempting to equalize chemical potentials. The blue and salmon-colored bands in Fig.4 indicate those regions where chemical-potential equalization could not be achieved. The fact that those regions join smoothly with the 'near-integer' regions where chemical potentials were successfully equalized indicates that any difference due to numerical precision between 'exact' and 'near' integers is unimportant in practice.

Finally, the smoothening of the N vs. μ staircase in Fig.1 suggests a possible analogy between finite distances and finite temperatures. In Fig. 5.7, we compare our calculated N_{atom} to the average number of particles $\bar{n}$ from a Fermi-Dirac (FD) distribution:

$$\bar{n} = \frac{1}{\mathrm{e}^{(\varepsilon_{\mathrm{i}}^{(0)} - \mu)/kT} + 1} \tag{5.9}$$

where k is Boltzmann's constant and T is the temperature. It is apparent from the figures that the analogy is not exact. The FD distribution at specified (unphysical) temperatures can capture some of the behavior of $N_{\text{atom}}(\mu)$ around the step between integer numbers or the upper region of the curve as it flattens near the integer. It cannot capture both at once, or correctly follow the behavior of the lower region as it rises from the lower integer.

5.4 Conclusions and Outlook

An essential feature of charge-transfer physics at metallic interfaces is that the metal has a continuum of electronic states whereas an atom or molecule, when isolated, supports only a discrete set of states. When the atom or molecule is adsorbed on the metallic surface,

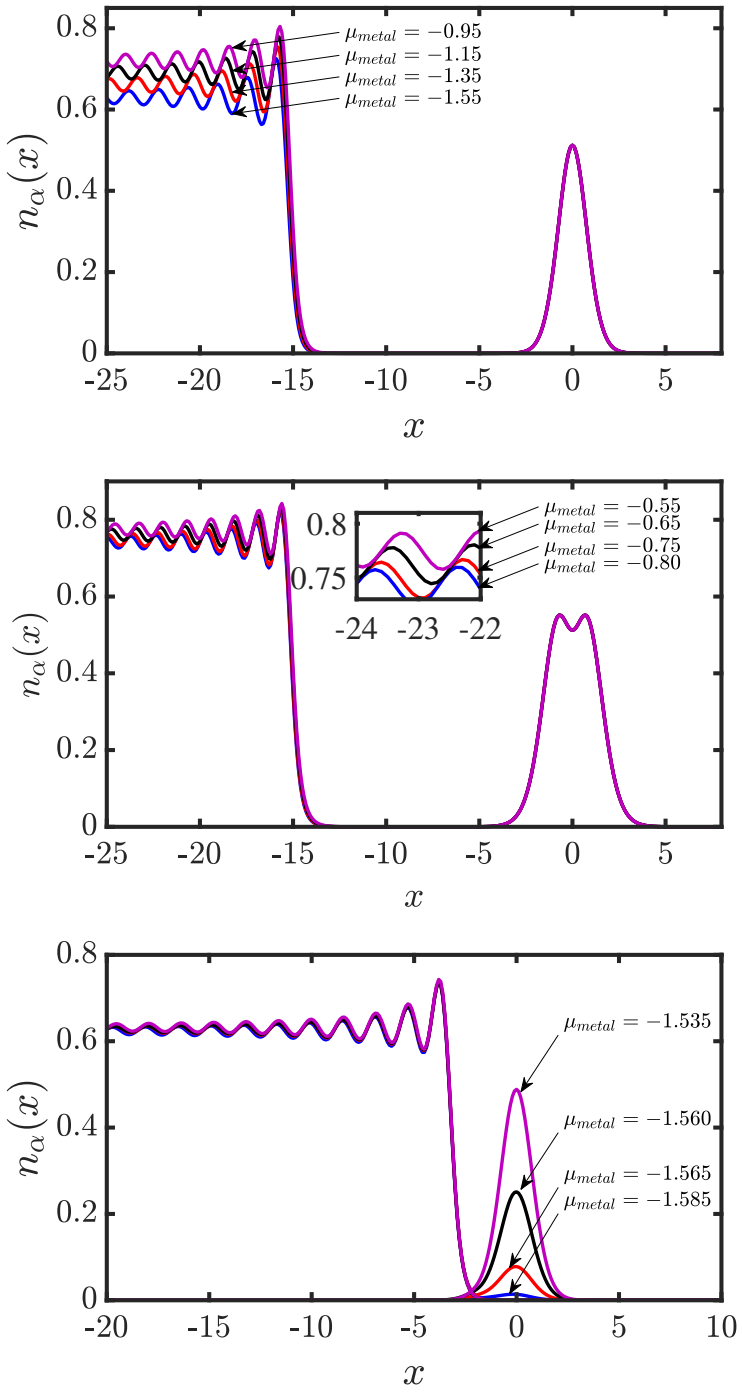

Figure 5.6. Fragment densities $n_\alpha(x)$ at various values of R and μ_{metal}. Top: $R = 15$ and values of μ_{metal} corresponding to $N_{\text{atom}} = 1$: -1.55 (blue), -1.35 (red), -1.15 (black), and -0.95 (violet). Middle: $R = 15$ and values of μ_{metal} corresponding to $N_{\text{atom}} = 2$: -0.8 (blue), -0.75 (red), -0.65 (black), and -0.55 (violet). Bottom: $R = 3$ and values of μ_{metal} producing values of N_{atom} between 0 and 1: -1.585 (blue), -1.565 (red), -1.56 (black), and -1.535 (violet).

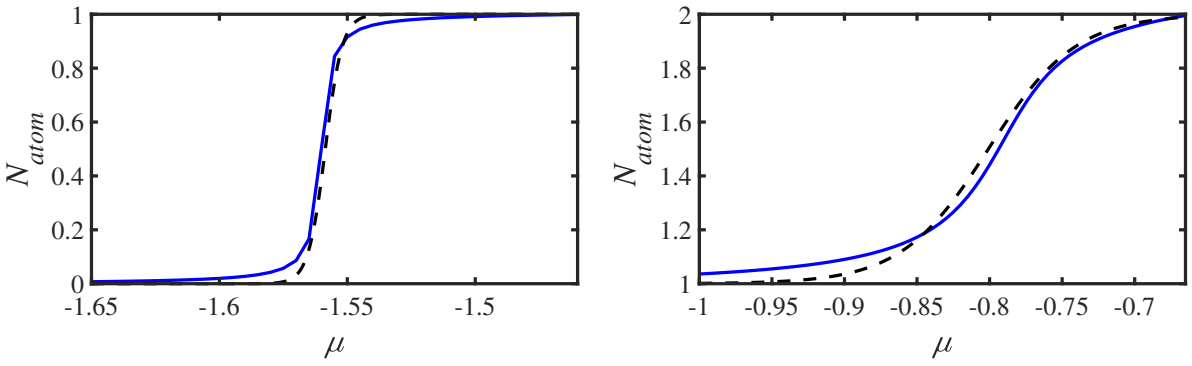

Figure 5.7. The atomic fragment occupation numbers N_{atom} (solid blue line) compared to the Fermi-Dirac $\bar{n}$ (dashed black line). Top: $T = 1050\ K$ and $\varepsilon_0^{(0)} = -1.5586$. Bottom: $T = 9500\ K$ and $\varepsilon_1^{(0)} = -0.8008$.

the coupling between continuum (metallic) and discrete (molecular) levels poses a challenge for embedding methods. It is this challenge that we have addressed here. In the extension of Frozen-density embedding [55] to fragments with non-integer particle numbers [56], the total energy is minimized under the constraint that each fragment density integrates to a pre-established fractional value. In this method, each fragment has a different chemical potential along with a different embedding potential, and the fractional charges on the fragments are not an output but an input for the calculations. As an alternative, we propose *chemical-potential equalization* as the main criterion for determining fractional charges in density embedding. By imposing a chemical-potential equalization constraint, we have shown that the chemical potential of an integer-electron system can be smaller than $I - A$ when the system (here, an atom) is at interacting distances from a metallic reservoir of electrons. A continuous change in a *global* molecular property, μ, distorts the density of one fragment (either metal or atom) markedly more than the density of the other fragment. The typical N_{atom} vs. μ staircase function is smoothed-out as a result of the finite-distance interactions between the 'atom' and the 'metal'. Further work will examine the extent to which these results are generalizable: Do they apply to 3D, Coulomb-interacting systems? If so, is there any physical meaning that can be attached to the resulting reactivity potentials?

Our method should prove useful for calculations on semi-infinite systems and allow treatment of different fragments with different computational techniques. For example, an atomic

or a molecular fragment can be treated with an accurate wave-function method and the semi-infinite metal fragment can be treated with a more innate Green's function method. The method provides a convenient way to account for the finite-distance interactions near the metal surface. Furthermore, because calculating fractional charges is important in various fields, from electrolysis [6], [57] to catalysis [58], solar cells and organic electronics [59], [60], we an

6. VIRIAL RELATIONS IN DENSITY EMBEDDING

This section contains work from the article entitled "Virial relations in density embedding" written by the author, Kaili Jiang, Martín A. Mosquera, and Adam Wasserman published in the International Journal of Quantum Chemistry [61].

The accuracy of charge-transfer excitation energies, solvatochromic shifts and other environmental effects calculated via various density embedding techniques depend critically on the approximations employed for the non-additive non-interacting kinetic energy functional, $T_{\rm S}^{\rm nad}[n]$ [33]. Approximating this functional remains an important challenge in electronic structure theory. To assist in the development and testing of approximations for $T_{\rm S}^{\rm nad}[n]$, we derive two virial relations for fragments in molecules. These establish separate connections between the non-additive kinetic energies of the non-interacting and interacting systems of electrons, and quantities such as the electron-nuclear attraction forces, the partition energy and potential, and the Kohn-Sham potentials of the system and its parts. We numerically verify both relations on diatomic molecules.

6.1 Introduction and Notation

In our analysis to this point, we have only looked at partition potentials obtained through exact numerical inversions. A functional approximation to $v_{\rm P}(\mathbf{r})$ is needed in order for PT to be practical and to be able to compete with KS-DFT and other embedding methods. Approximations for the nonadditive non-interacting kinetic energy $T_{\rm S}^{\rm nad}$ (NAKE) are central to the development of accurate $v_{\rm P}(\mathbf{r})$ functionals. The development of accurate approximations of the full $T_{\rm s}[n]$ for orbital-free DFT is a notoriously difficult problem [62], explaining why most DFT calculations today still rely on the Kohn-Sham (KS) [8] or generalized-KS [63] schemes. However, approximating the NAKE is a different challenge than approximating the full $T_{\rm s}[n]$. Cancellation of errors can sometimes lead to acceptable NAKEs [64] but not much is known about such errors or how to control them. Deriving exact conditions for the NAKE would be helpful to guide the construction of improved approximations for it [65]. We derive here two virial relations that may be useful toward that goal.

The quantum virial theorem provides relationships between the kinetic energy and the potential energy of electronic systems. In Kohn-Sham DFT [8], virial relations have been proven [66]–[68] that establish the connections between the kinetic and potential energies of both, the real system of interacting electrons and the auxiliary system of non-interacting electrons. Establishing analogous virial relations in embedding methods is challenging when the fragment densities are not v-representable [69], [70], as discussed in ref.[71] and in ref.[72] in the context of the early embedding method of ref.[73]. However, the fragment densities of P-DFT *are* physical ground-state v-representable densities for which virial relations apply just as they would for any physical system in isolation. Furthermore, due to the globality of the partition potential in P-DFT [26], [49], [50], terms can be grouped together leading to particularly simple virial expressions, as we show here.

Using the index "α" to label the fragments, the kinetic energy of fragment α is $K_\alpha[n_\alpha]$. Following Eq. 3.9, the non-additive kinetic energy is defined as:

$$K^{\rm nad}[\{n_\alpha\}] \equiv K[n] - \sum_\alpha K_\alpha[n_\alpha] \ , \tag{6.1}$$

where $K[n]$ is the total kinetic energy for density $n(\mathbf{r})$. Equation 6.1 is the most direct method to calculate $K^{\rm nad}$. We will be contrasting Equation 6.1 later on with a virial expression, Equation 6.11. Similarly, the NAKE is defined by

$$T_{\rm s}^{\rm nad}[\{n_\alpha\}] \equiv T_{\rm s}[n] - \sum_\alpha T_{\rm s}[n_\alpha] \ , \tag{6.2}$$

With the virial theorem, we can derive exact relations between $T_s^{\rm nad}[n]$ and the densities and potentials that can be obtained through P-DFT calculations. These relations can be used as exact constraints in constructing approximations to $T_s^{\rm nad}[n]$.

6.2 Virial Relations

We now derive two virial relations for fragments in molecules. For a many-electron system of ground state $|\Psi_0\rangle$ and density $n_0(\mathbf{r}) = \langle\Psi_0|\hat{n}(\mathbf{r})|\Psi_0\rangle$[1] governed by the hamiltonian of Eq. 2.2, the virial theorem can be expressed as [66]:

$$2K[n] + V_{\text{ee}}[n] = \int d^3r n(\mathbf{r})\mathbf{r}\cdot\nabla v(\mathbf{r}) \ , \tag{6.3}$$

where $K[n] = \langle\Psi[n]|\hat{T}|\Psi[n]\rangle$ and $V_{\text{ee}} = \langle\Psi[n]|\hat{V}_{\text{ee}}|\Psi[n]\rangle$ are the total kinetic and electron repulsion energies. Similarly, for the KS system of non-interacting electrons with kinetic energy T_s,

$$2T_{\text{s}}[n] = \int d^3r n(\mathbf{r})\mathbf{r}\cdot\nabla v_{\text{KS}}[n](\mathbf{r}) \ , \tag{6.4}$$

Equation 6.4 is applicable not only to the exact XC functional, but also to approximate XC functionals at self-consistency.

Although P-DFT makes use of a grand-canonical ensemble formalism to describe fragments with fractional numbers of electrons, we restrict the present analysis for simplicity to cases where the fragments, labeled by index α, have integer numbers of electrons N_α (the one exception in the examples that follow is H_2^+, where each atomic fragment is assigned a charge of 0.5). The total number of electrons in the molecule, N, is given by the sum of the N_α, and all single-particle operators are similarly additive. In particular, the external potential $v(\mathbf{r}) = \sum_\alpha v_\alpha(\mathbf{r})$, kinetic operator $\hat{T} = \sum_\alpha \hat{T}_\alpha$ and density operator $\hat{n}(\mathbf{r}) = \sum_\alpha \hat{n}_\alpha(\mathbf{r})$ are all additive. However, $\hat{V}_{\text{ee}} \neq \sum_\alpha \hat{V}_{\text{ee},\alpha}$ as all electrons interact with one another.

We establishes that in PT, there is only one embedding potential $v_p(\mathbf{r})$ such that the many-electron Schrödinger equations

$$\left[\hat{H}_\alpha + \int d^3r v_{\text{p}}(\mathbf{r})\hat{n}_\alpha(\mathbf{r})\right]|\psi_\alpha\rangle = E_\alpha|\psi_\alpha\rangle \ , \tag{6.5}$$

[1]↑In this chapter, we drop the subscript "0" for simplicity of notation.

lead to fragment densities $n_\alpha(\mathbf{r}) = \langle\psi_\alpha|\hat{n}_\alpha(\mathbf{r})|\psi_\alpha\rangle$ with the additive property:

$$\sum_\alpha n_\alpha(\mathbf{r}) = n(\mathbf{r}) \ , \tag{6.6}$$

In Equation 6.5, we explicitly wrote the fragment hamiltonian with ground state $|\psi_\alpha\rangle$ as $\hat{H}_\alpha = \hat{T}_\alpha + \hat{V}_{\mathrm{ee},\alpha} + \int d^3r v_\alpha(\mathbf{r})\hat{n}_\alpha(\mathbf{r})$. Because the $n_\alpha(\mathbf{r})$ are true ground-state densities for N_α electrons in $v_\alpha(\mathbf{r}) + v_p(\mathbf{r})$, virial relations analogous to Equations 6.3 and 6.4 hold for the fragments:

$$2K_\alpha + V_{\mathrm{ee},\alpha} = \int d^3r n_\alpha(\mathbf{r})\mathbf{r}\cdot\nabla[v_\alpha(\mathbf{r}) + v_{\mathrm{p}}(\mathbf{r})] \ , \tag{6.7}$$

where $K_\alpha = K[n_\alpha] = \langle\psi_\alpha[n_\alpha]|\hat{T}_\alpha|\psi_\alpha[n_\alpha]\rangle$, $V_{\mathrm{ee},\alpha} = V_{\mathrm{ee}}[n_\alpha] = \langle\psi_\alpha[n_\alpha]|\hat{V}_{\mathrm{ee},\alpha}|\psi_\alpha[n_\alpha]\rangle$, and

$$2T_{\mathrm{s},\alpha} = \int d^3r n_\alpha(\mathbf{r})\mathbf{r}\cdot\nabla v_{\mathrm{s},\alpha}[n_\alpha](\mathbf{r}) \ . \tag{6.8}$$

Note that $v_{\mathrm{s},\alpha}(\mathbf{r}) = v_\alpha(\mathbf{r}) + v_{\mathrm{H},\alpha}(\mathbf{r}) + v_{\mathrm{XC},\alpha}(\mathbf{r}) + v_{\mathrm{p}}(\mathbf{r})$. Next, subtract Equation 6.8 from Equation 6.7 to get

$$T_{\mathrm{c},\alpha} = -E_{\mathrm{XC},\alpha} - \int d^3r n_\alpha(\mathbf{r})\mathbf{r}\cdot\nabla v_{\mathrm{XC},\alpha}(\mathbf{r}) \ , \tag{6.9}$$

where $T_{\mathrm{c},\alpha} = K_\alpha - T_{\mathrm{s},\alpha}$ is the correlation kinetic energy of fragment α.[66]

Summing up Equation 6.7 over all fragments, we obtain

$$\begin{aligned} 2K_{\mathrm{f}}\ [\{n_\alpha\}]\ &+V_{\mathrm{ee,f}}[\{n_\alpha\}] = \\ &\sum_\alpha \int d^3r n_\alpha(\mathbf{r})\mathbf{r}\cdot\nabla[v_\alpha(\mathbf{r}) + v_{\mathrm{p}}(\mathbf{r})] \ , \end{aligned} \tag{6.10}$$

where $K_{\mathrm{f}}[\{n_\alpha\}] \equiv \sum_\alpha K_\alpha$ and $V_{\mathrm{ee,f}}[\{n_\alpha\}] \equiv \sum_\alpha V_{\mathrm{ee},\alpha}$. Finally, combining Equation 6.3 with Equation 6.10 and rearranging terms:

$$\begin{aligned} K^{\mathrm{nad}}[\{n_\alpha\}] \ &= \ V_{\mathrm{ext}}^{\mathrm{nad}}[\{n_\alpha\}] + \int d^3r \sum_\alpha n_\alpha(\mathbf{r})\mathbf{r}\cdot\nabla v_{\mathrm{ext},\alpha}^{\mathrm{nad}}(\mathbf{r}) \\ &\quad -E_{\mathrm{p}}[n] - \int d^3r n(\mathbf{r})\mathbf{r}\cdot\nabla v_{\mathrm{p}}(\mathbf{r}) \ , \end{aligned} \tag{6.11}$$

where 6.11, $V_{\rm ext}^{\rm nad}[\{n_\alpha\}] = \int d^3r\,\{n(\mathbf{r})v(\mathbf{r}) - \sum_\alpha n_\alpha(\mathbf{r})v_\alpha(\mathbf{r})\}$ is the non-additive external energy, and $v_{{\rm ext},\alpha}^{\rm nad}(\mathbf{r}) \equiv \delta V_{\rm ext}^{\rm nad}/\delta n_\alpha(\mathbf{r}) = v(\mathbf{r}) - v_\alpha(\mathbf{r})$.

Equation 6.11 provides a way to calculate the non-additive KE in terms of quantities that can all be obtained through embedding (P-DFT) calculations.

Alternatively, subtracting Equation 6.8 from Equation 6.4, we find:

$$T_{\rm s}^{\rm nad}[\{n_\alpha\}] = \frac{1}{2}\int d^3r\{\sum_\alpha n_\alpha(\mathbf{r})\mathbf{r}\cdot\nabla[v_{\rm s}(\mathbf{r}) - v_{{\rm s},\alpha}(\mathbf{r})]\}\ , \tag{6.12}$$

providing, together with Equation 6.11, a route to the calculation of the non-additive correlation kinetic energy, as

$$T_{\rm c}^{\rm nad}[\{n_\alpha\}] = K^{\rm nad}[\{n_\alpha\}] - T_{\rm s}^{\rm nad}[\{n_\alpha\}]\ . \tag{6.13}$$

6.3 Numerical Verification and Discussion

In Tables 6.1 and 6.2, we provide numerical verification of Equations 6.11 and 6.12 on diatomic molecules (i.e. each molecule is partitioned into its two constituent atoms). All calculations are performed on a real-space code that solves the KS equations in prolate spheroidal coordinates [26]. P-DFT calculations were done with an algorithm that is numerically "exact" for a given approximation to the XC functional [33].

Table 6.1. Numerical verification of Equation 6.11. $K_{\rm I}^{\rm nad}$ is calculated through Equations 6.1, 6.13, and 6.12. $K_{\rm II}^{\rm nad}$ is calculated through Equation 6.11. The H_2^+ result in the top line is from exact one-electron calculations for which $K_{\rm I}^{\rm nad}$ is calculated directly from wavefunctions.

System	$K_{\rm I}^{\rm nad} \times 10^2$	$K_{\rm I}^{\rm nad}/K_{\rm II}^{\rm nad}$
H_2^+ (exact)	-8.522	0.99914
H_2^+	-8.259	0.99994
H_2	-12.571	0.99993
Li_2	1.716	1.01237
He_2	0.1107	1.00025
Ne_2	0.2999	1.00366
Ar_2	0.4424	1.00417

Table 6.2. Numerical verification of Equation 6.12. $T_{\mathrm{s,I}}^{\mathrm{nad}}$ is calculated through Equation 6.2, and $T_{\mathrm{s,II}}^{\mathrm{nad}}$ is calculated through Equation 6.12.

System	$T_{s,\mathrm{I}}^{\mathrm{nad}} \times 10^2$	$T_{s,\mathrm{I}}^{\mathrm{nad}}/T_{s,\mathrm{II}}^{\mathrm{nad}}$
H_2^+	-8.181	0.99997
H_2	-15.207	0.99997
Li_2	0.4917	1.0035
He_2	0.0993	1.00014
Ne_2	0.2750	1.00239
Ar_2	0.4050	1.00239

Table 6.3. Comparison in the NAKE of He_2 when approximated functionals are used. $T_{\mathrm{s,I}}^{\mathrm{nad}}$ is calculated directly from the approximated functionals. $T_{\mathrm{s,II}}^{\mathrm{nad}}$ is calculated using Equation 6.12, where the approximated NAKE functionals are used in calculating the partition potential.

Functional	$T_{s,\mathrm{I}}^{\mathrm{nad}} \times 10^3$	$T_{s,\mathrm{II}}^{\mathrm{nad}} \times 10^3$	$T_{s,\mathrm{I}}^{\mathrm{nad}}/T_{s,\mathrm{II}}^{\mathrm{nad}}$
TF[74], [75]	1.198	1.402	0.85419
vW[76]	-37.823	-37.824	0.99999
GEA2[77], [78]	-1.561	-1.146	1.36154
TW02[79]	1.136	1.444	0.78654
LC94[80]	0.565	0.812	0.69630
R-PBE[34]	0.995	1.196	0.83215

Table 6.1 shows a very close agreement between the non-additive kinetic energy calculated through Equation 6.1, denoted as $K_{\mathrm{I}}^{\mathrm{nad}}$, and calculated through the virial relation of Equation 6.11, denoted as $K_{\mathrm{II}}^{\mathrm{nad}}$. The main source of error comes from the calculation of the gradient of the potentials on the right-hand-side of Equation 6.11, as the densities have cusps and the potentials singularities at the nuclei. Similar agreement can be seen in Table 6.2 that compares $T_{s,\mathrm{I}}^{\mathrm{nad}}$ (Equation 6.2) and $T_{s,\mathrm{II}}^{\mathrm{nad}}$ (Equation 6.12).

The results in Tables 6.1 and 6.2 are a numerical verification of Equations 6.11 and 6.12. The virial relation is satisfied for each fragment *and* for the full molecule. The latter occurs because the algorithm of ref.[33] guarantees that the sum of fragment densities reproduces the full-molecular KS density.

Table 6.3 provides the ratio $T_{\mathrm{s,I}}^{\mathrm{nad}}/T_{\mathrm{s,II}}^{\mathrm{nad}}$ for He_2 when instead of using exact numerical inversions, as before, one uses an approximate density-functional for $T_{\mathrm{s}}^{\mathrm{nad}}$, as is typically done in subsystem-DFT calculations [81]. $T_{\mathrm{s,I}}^{\mathrm{nad}}$ is constructed from approximate $T_{\mathrm{s}}[n]$ functionals on the right-hand side of Equation 6.2. In Equation 6.12, $T_{\mathrm{s,II}}^{\mathrm{nad}}$ is calculated with the same $T_{\mathrm{s}}[n]$ approximation and the expression $v_{\mathrm{s}}(\mathbf{r}) - v_{\mathrm{s},\alpha}(\mathbf{r}) = \delta T_{\mathrm{s}}^{\mathrm{nad}}[n]/\delta n_{\alpha}(\mathbf{r})$ [33]. In contrast to the results of the exact inversion algorithm, Equations 6.11 and 6.12 are not trivially satisfied in the case of approximate density functionals. The full-molecular density $n(\mathbf{r})$, resulting from the sum of fragment densities in Equation 6.6, is now a self-consistent result and does not reproduce the full-molecular KS density.

For most approximate $T_{\mathrm{s}}^{\mathrm{nad}}$ functionals, the virial relation Equation 6.12 is not well preserved. Interestingly, the von Weisäcker (vW) functional yields an extremely accurate virial relation for He_2 even though the vW functional is only exact for the fragments. This indicates that the left-hand side and the right-hand side of Equation 6.4 are nearly equal for this approximate functional, implying that $T_{\mathrm{s}}^{\mathrm{vW}}[n^{\mathrm{vW,P-DFT}}] = T_{\mathrm{s}}[\tilde{n}]$, where $n^{\mathrm{vW,P-DFT}}$ is the He_2 density from a P-DFT calculation that uses the vW functional, and $\tilde{n}$ is the exact density corresponding to the KS potential $v_{\mathrm{s}}[n^{\mathrm{vW,P-DFT}}](\mathbf{r})$, where $v_{\mathrm{s}}[n^{\mathrm{vW,P-DFT}}](\mathbf{r})$ is calculated by plugging the density $n^{\mathrm{vW,P-DFT}}$ into the Hartree, XC and external potential functionals. The entire error here is fragment-density-driven [82], and it is clearly very small. However, our previous study [34] showed that vW NAKE performed poorly for systems of rare gas dimers, indicating that the performance of NAKE functionals should not be judged based on Equation 6.12 *alone*.

7. PARTITION POTENTIAL FOR HYDROGEN-BONDING IN FORMIC ACID DIMERS

This section contains work from the article entitled "Partition potential for hydrogen-bonding in formic acid dimers" written by the author, Sara Gómez, Albeiro Restrepo, and Adam Wasserman published in the International Journal of Quantum Chemistry [83].

Among the many types of intermolecular interactions, hydrogen-bonding is of particular interest because hydrogen bonds (HB's) are known to be responsible for stabilization of various chemical systems from the life-supporting properties of liquid water [84]–[87] to the tertiary structures of biomolecules in charge of storing and replicating genetic information. [88] Although the very nature of hydrogen bonding is not without controversy [89]–[92], several types of HB's are recognized in the literature. [47] Of particular interest to this work are the conventional *primary hydrogen bonds*, where a hydrogen atom sits between two electronegative atoms, and the non-conventional, *secondary hydrogen bonds*, where a proton is donated from a non-polar C–H bond.

Although P-DFT is particularly well suited to study molecular clusters, these systems are challenging because intermolecular interaction energies in clusters are significantly smaller than energies associated with formal bonds. Individual molecules in clusters retain their chemical identities to a large degree and require carefully constructed partition potentials to account for the comparatively weak interactions. Previously, P-DFT was successfully applied to water dimers, [93] where it was shown that the partition potential and P-DFT densities can be used to describe the mechanism of hydrogen-bond formation.

The question we address in this chapter is whether the partition potential has transferable features corresponding to particular types of HB's. Finding transferability would imply that the partition potential around a hydrogen bond in one molecule could be used as a starting point to calculate approximate interaction energies in other molecules with similar HB's, an appealing prospect for computational chemistry. The formic acid dimers are ideal systems to investigate this question because their four lowest-energy conformations have two types of primary HB's (C=O$\cdots$H–O and H–O$\cdots$H–O) and two types of secondary HB's (C=O$\cdots$H–C, H–O$\cdots$H–C). Is $v_{\mathrm{P}}(\mathbf{r})$ in the vicinity of a primary HB in one of these four dimers a good

approximation to $v_{\mathrm{P}}(\mathbf{r})$ for a primary HB in a different dimer? What about the same question for secondary HB's? Previous work on one-dimensional model systems [94] taught us that the transferability of P-DFT *densities* was about an order of magnitude higher than that of real-space partitioning schemes, so it is reasonable to expect transferable features in the underlying partition potentials. However, we find that the answer is *no* in both cases (primary and secondary), contrary to naive intuition. Conversely, monomer density deformations *do* have specific features that can be used to distinguish between different types of HB's.

7.1 Preliminaries and Methods

Despite being the smallest carboxylic acid, the conformational space for the formic acid dimers is notoriously rich, with a considerable number of structures already experimentally detected [95]. For our work, we selected four lowest energy motifs from this set (shown in Fig. 7.1). We optimized their geometries and confirmed the found stationary points are true minima by frequency calculations using the B3LYP XC functional and Dunning's aug-cc-pVTZ basis set. P-DFT calculations were performed over the resulting geometries. B3LYP and PW91 were used as XC functionals in the construction of the effective potentials. The partition potential was expanded using aug-cc-pVTZ basis set. PW91 has been shown to be useful for the evaluation of intermolecular interactions in hydrogen-bonded systems. In particular, the dimers of water and formic acid for which PW91 computed interaction energies showed only slight changes with respect to CCSD(T). [96] It has also been concluded that large basis sets for $v_{\mathrm{P}}(\mathbf{r})$ lead to accurate total densities. [93] All calculations were carried out using the NWChem package [97].

For P-DFT calculations, we choose two monomers as fragments and label them *left* (L) and *right* (R). The inversion algorithm for obtaining the partition potential is based on computing the fragment density response, $\chi_f(\mathbf{r},\mathbf{r}')$ at each step and updating $v_{\mathrm{P}}(\mathbf{r})$ through: [93], [98]

$$\delta v_{\mathrm{P}}(\mathbf{r}) = \int d\mathbf{r}' \chi_{\mathrm{f}}(\mathbf{r},\mathbf{r}')^{-1} \left(\sum_{\mathrm{i}} n_{\mathrm{i}}(\mathbf{r}') - n_{\mathrm{f}}(\mathbf{r}') \right) . \tag{7.1}$$

For our choice of fragmentation, $n_{\mathrm{f}}(\mathbf{r}) = n_{\mathrm{L}}(\mathbf{r}) + n_{\mathrm{R}}(\mathbf{r})$.

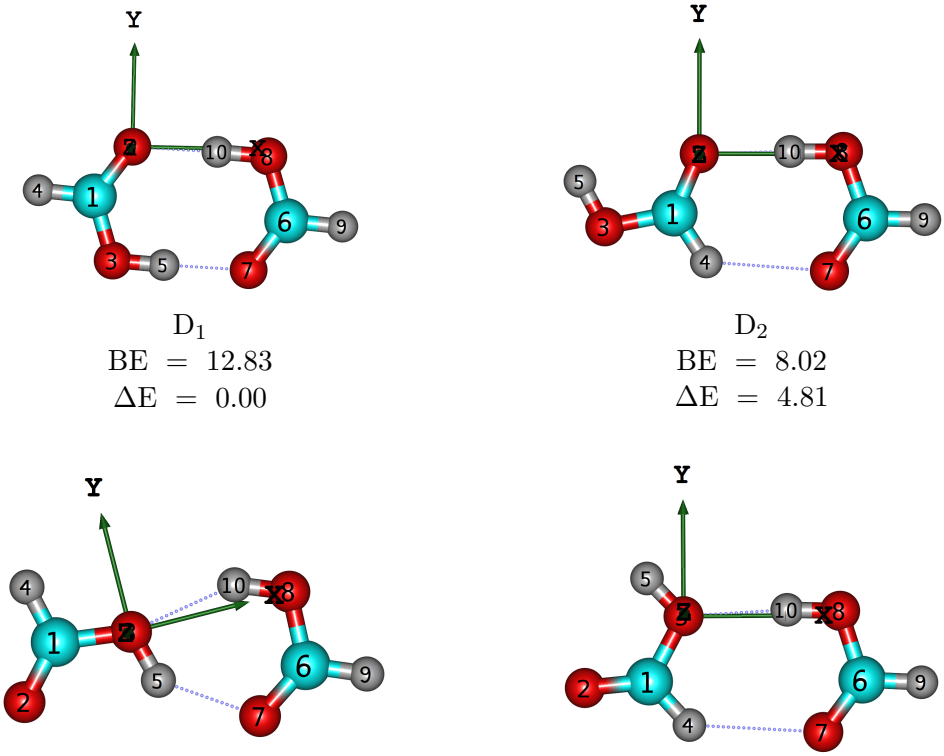

D_1
BE = 12.83
ΔE = 0.00

D_2
BE = 8.02
ΔE = 4.81

D_3
BE = 6.41
ΔE = 6.42

D_4
BE = 5.58
ΔE = 7.25

Figure 7.1. Lowest energy dimers of formic acid from the MP2/6–311++G(*d,p*) Potential Energy Surface. Both monomers are in the *anti* conformation. BE's are the CCSD(T)/6–311++G(*d,p*) binding energies calculated as the difference between the given dimer and the isolated fragments. Relative energies with respect to the global minimum are shown. All energies in kcal/mol and corrected for zero-point vibrational energies. The right monomer (R), which simultaneously acts as a donor and acceptor of hydrogen bonds, is shown in the same perspective in all cases. The origin of coordinates is placed at the oxygen atom in the left (L) monomer.

As discussed in Chapter 3, P-DFT is generally formulated for varying non-integer fragment occupations. In this work, however, we fix occupations to the ones of isolated fragments. This simplification increases the efficiency of the method as optimization with respect to occupation numbers is not needed. Previous work on simpler systems suggests that occupations usually lock to integers when fragments have similar electronic structures. Since we work with neutral dimers with small dipole moments, we choose neutral fragments and focus attention on monomer density deformations:

$$\Delta n_{\mathrm{i}}(\mathbf{r}) = n_{\mathrm{i}}(\mathbf{r}) - n_{\mathrm{i}}^{0}(\mathbf{r}) \ , \tag{7.2}$$

where $n_{\mathrm{i}}^{0}(\mathbf{r})$ is the density of an isolated i-fragment.

7.2 Results and Discussion

7.2.1 Energy Analysis

We begin by introducing the *preparation energy*, E_{prep}, which will be useful for describing fragment interactions within P-DFT formalism. The preparation energy is defined as the energy required to distort the density of isolated fragments to the P-DFT density of fragments within the dimer:

$$E_{\mathrm{prep}} = E_{\mathrm{f}}[n_{\mathrm{L}}(\mathbf{r}), n_{\mathrm{R}}(\mathbf{r})] - (E_{\mathrm{L}}[n_{\mathrm{L}}^{0}(\mathbf{r})] + E_{\mathrm{R}}[n_{\mathrm{R}}^{0}(\mathbf{r})]) \ , \tag{7.3}$$

We can also identify the preparation energy of a fragment i:

$$E_{\mathrm{prep}}^{\mathrm{i}} = E_{\mathrm{i}}[n_{\mathrm{i}}(\mathbf{r})] - E_{\mathrm{i}}[n_{\mathrm{i}}^{0}(\mathbf{r})] \ . \tag{7.4}$$

The partition energy energy ($E_{\mathrm{p}} = E_{\mathrm{Dimer}}[n_{\mathrm{L}}(\mathbf{r}), n_{\mathrm{R}}(\mathbf{r})] - E_{\mathrm{f}}[n_{\mathrm{L}}(\mathbf{r}), n_{\mathrm{R}}(\mathbf{r})]$, see Eq. 3.2) can then be viewed as the interaction energy among the "prepared" fragments. The binding energy, BE, is simply the sum of these two energy contributions:

$$\mathrm{BE} = E_{\mathrm{P}} + E_{\mathrm{prep}} = E_{\mathrm{Dimer}}[n_{\mathrm{L}}(\mathbf{r}), n_{\mathrm{R}}(\mathbf{r})] - (E_{\mathrm{L}}[n_{\mathrm{L}}^{0}(\mathbf{r})] + E_{\mathrm{R}}[n_{\mathrm{R}}^{0}(\mathbf{r})]) \ . \tag{7.5}$$

Since all four dimers have their atoms lie on a plane, it is most convenient to visualize the densities and potentials at values of **r** belonging to this plane.

Table 7.1 lists relevant quantities extracted from the P-DFT calculations using both B3LYP and PW91 functionals. The experimental BE for D_1 is -59.5 ± 0.5 kJ/mol (2.27×10^{-2} a.u.) [99]. The BE's computed with eq. 7.5 yield 2.90×10^{-2} a.u. (B3LYP) and 3.14×10^{-2} a.u. (PW91). We note that these values do not include zero-point vibrational energies and thermal corrections.

An inventory of intermolecular interactions in the four formic acid dimers studied here is provided in the rightmost column of Table 7.1. D_1 and D_3 are stabilized by primary hydrogen bonds only while D_2 and D_4 include one secondary hydrogen bond each. D_1 exhibits two equivalent primary hydrogen bonds where the hydroxyl group in one monomer donates a proton to the carbonyl group of the other (see Fig. 7.1). D_2 and D_4 have two types of contacts: a secondary C=O $\cdots$ H–C hydrogen bond and a C=O $\cdots$ H–O (D_2) and H–O $\cdots$ H–O (D_4) primary HB. D_3 has two non–equivalent primary hydrogen bonds, where R simultaneously acts as donor and acceptor in two different functional groups, the O–H bond in L acts as donor and acceptor of both HB's, freeing the carbonyl group in L of intermolecular interactions. We note that although secondary hydrogen bonds are typically considered weaker than primary hydrogen bonds [47], the overall stability of the dimers is not correlated with the primary or secondary nature of the HB's. For example, D_2 is lower in energy than D_3, even though D_2 has one primary and one secondary HB's and D_3 has two primary HB's. This lack of correlation extends to the number of hydrogen bonds, as seen in the case of two water dimers in Ref. [93].

Table 7.1 also lists preparation energies for each dimer and its components according to Eqs. 7.3 and 7.4. It is clear from the definition of E_{f} (Eq. 3.2) and from Eq. 7.3 that E_{prep} is always positive. We also expect larger values of E_{prep} for fragments that are more distorted relative to their isolated states. E_{prep} decreases in going from D_1 to D_4. Fig. 7.2, which shows the densities on the plane of two monomers, makes it obvious that this decrease corresponds to the decrease in the total density deformation.

There are characteristic deformation patterns for the primary and secondary bonds, as shown in Fig. 7.2. The O atom of the H-donating O–H group has a significant density

Table 7.1. Relevant energies (a.u.) from P-DFT calculations (B3LYP, PW91, $v_{\mathrm{P}}(\mathbf{r})$ with the aug–cc–pVTZ basis set) on the lowest energy formic acid dimers (Fig. 7.1). The energy for the isolated *anti* formic acid monomer is $E_{\mathrm{L}}^{0} = E_{\mathrm{R}}^{0} = -189.846$ a.u. All energies in kcal/mol.

System	BE	$E_{\mathrm{prep}}^{\mathrm{D_i}}$ (Eq. 7.3)	$E_{\mathrm{prep}}^{\mathrm{L}}$	$E_{\mathrm{prep}}^{\mathrm{R}}$	E_{P}	Intermolecular Interactions	
D_1 (B3LYP)	−18.19	7.14	3.57 (50%)	3.57 (50%)	−25.33	C=O ··· H–O	C=O ··· H–O
D_1 (PW91)	−19.70	6.99	3.49 (50%)	3.49 (50%)	−26.69	C=O ··· H–O	C=O ··· H–O
D_2 (B3LYP)	−9.61	4.67	2.56 (55%)	2.11 (45%)	−14.28	C=O ··· H–O	C=O ··· H–C
D_2 (PW91)	−10.55	4.76	2.76 (58%)	2.00 (42%)	−15.31	C=O ··· H–O	C=O ··· H–C
D_3 (B3LYP)	−6.87	2.08	1.14 (55%)	0.94 (45%)	−8.95	C=O ··· H–O	H–O ··· H–O
D_3 (PW91)	−7.84	2.08	1.11 (54%)	0.97 (46%)	−9.92	C=O ··· H–O	H–O ··· H–O
D_4 (B3LYP)	−5.01	1.71	1.06 (62%)	0.66 (38%)	−6.72	C=O ··· H–C	H–O ··· H–O
D_4 (PW91)	−5.62	1.75	1.13 (65%)	0.62 (35%)	−7.37	C=O ··· H–C	H–O ··· H–O

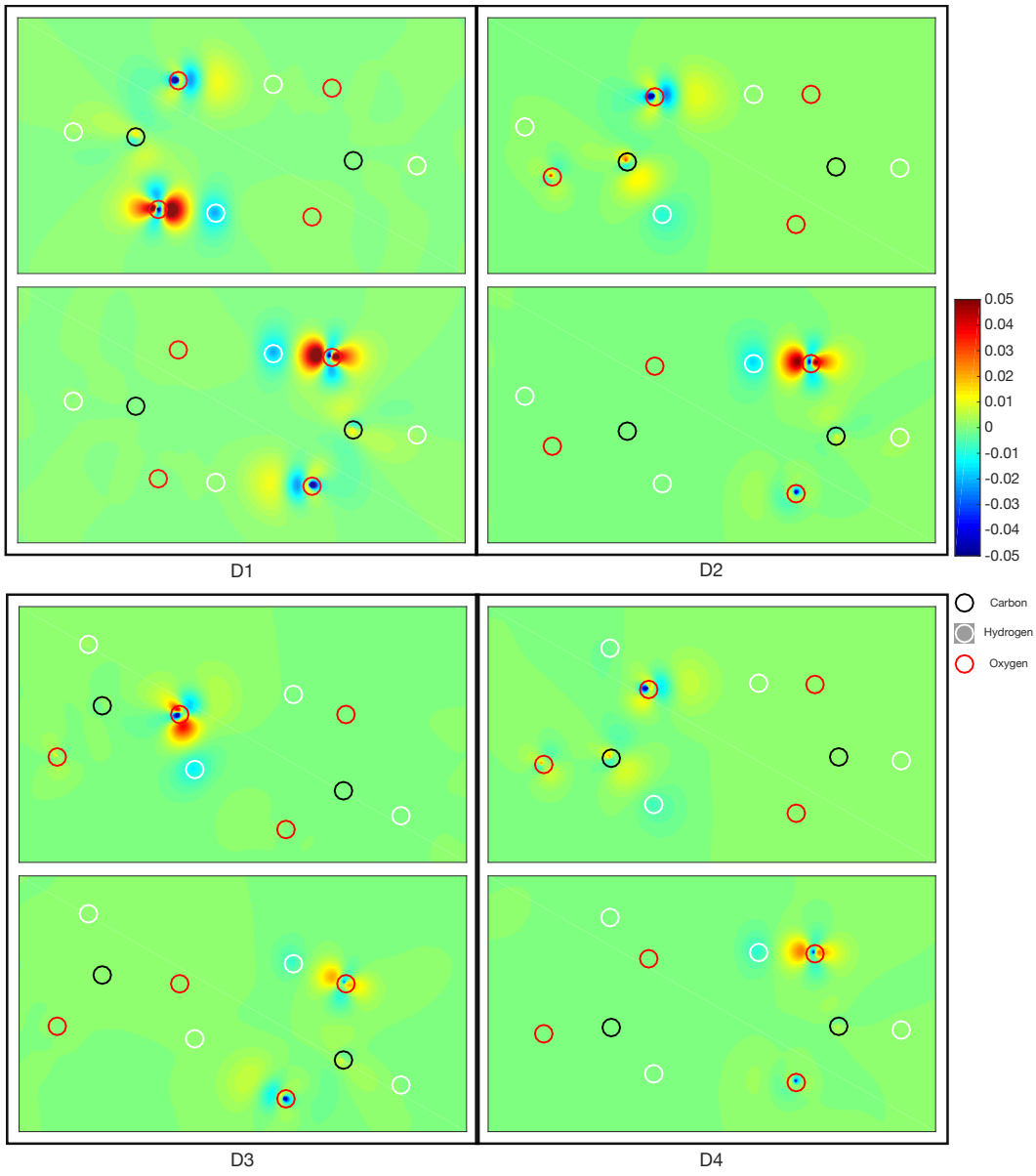

Figure 7.2. Density distortions, Eq. 7.2, On the molecular plane for various dimer configurations (in a.u.). For clarity, atom positions are indicated by hollow circles centered at atomic positions and bond lines are omitted. Upper panels correspond to the left monomer; lower panels correspond to the right monomers.

increase along the approximate direction of the HB in a dumbbell-like shape. The O atom of the acceptor has a density decrease of similar shape and direction. The H atom of the O–H group also has some density deficiency around it. The secondary bond pattern is very similar (note that the O–H donor is now replaced with C–H), but the deformation is smaller in magnitude and is more disperse. These observations suggest that the stronger intermolecular bonds require larger deformation of the original wavefunctions of the fragments, a result that may appear obvious to many chemists, but can not be quantified without a rigorous definition of fragments within a molecule. This is also consistent with the orbital interaction picture where it is generally thought that the gain of electron density in the $\sigma^{\star}_{\mathrm{O-H}}$ region of the donor and the simultaneous loss of charge in the region associated to the O atom of the acceptor is responsible for the formation of a hydrogen bond. [89], [90], [100] Although fragment occupation numbers remain constant in the present P-DFT implementation, fragment densities are indeed distorted; these distortions are linked to the charge transfer within fragments, provided by the orbital interactions.

The fragment preparation energies can be analyzed further. Since in D_1 both monomers are the same, their preparation energies are identical. In D_2 and D_4 the left monomer acts as a donor of a secondary hydrogen bond. In those cases, $E^{\mathrm{L}}_{\mathrm{prep}}$ is significantly larger than $E^{\mathrm{R}}_{\mathrm{prep}}$, even though the density deformation reaches higher values in the R-monomer. The L-monomer has a more delocalized density deformation. This imbalance can also be attributed to the fact that weaker secondary HB's require smaller preparation energies. In D_3, the energy needed to prepare L is larger than the energy needed to prepare R because of the double donor/acceptor function of the O–H group in L.

Partition energies, E_{P}, also shown in Table 7.1, are always negative and their magnitudes are correlated with the corresponding E_{prep}'s. That E_{P} is negative can be proven from the variational principle, but the observed correlation with E_{prep} (*i.e.* that E_{prep} decreases as E_{P} decreases) cannot. As predicted by the analysis of Fig. 7.2, larger preparation energies lead to larger partition energies, which is seen for all dimers in Table 7.1. This trend is followed not only by formic acid dimers but by all other systems we have studied so far. Whereas this observation seems obvious, a hard proof is missing.

Table 7.2. Total preparation energies for different systems. All P-DFT calculations using B3LYP/aug–cc–pVTZ with an expansion of $v_{\mathrm{P}}(\mathbf{r})$ in the same basis set. $R_{\text{O-O}}$ and $R_{\text{C-O}}$ are the distances between oxygen atoms in primary hydrogen bonds and between carbon and oxygen atoms in secondary hydrogen bonds, respectively.

System	Distance (Å)	E_{prep} (kcal/mol)[a]
LiH (neutral fragments)	1.59	34.76
LiH (ionic fragments)	1.59	23.59
H_2	0.74	12.76
D_1	$R_{\text{O-O}} = 2.67$	7.14
D_2	$R_{\text{O-O}} = 2.73$, $R_{\text{C-O}} = 3.13$	4.67
D_3	$R_{\text{O-O}} = 2.73$, 2.89	2.08
C_s Water Dimer	$R_{\text{O}} = 2.86$	1.86
D_4	$R_{\text{O-O}} = 2.90$, $R_{\text{C-O}} = 3.35$	1.71
C_{2h} Water Dimer	$R_{\text{O-O}} = 2.76$	0.42
He_2	1.60	0.53

[a]Our results for the diatomic molecules in this table differ slightly from those of the original work of Nafziger, Wu, and Wasserman [101] because we recalculated all energies using the aug–cc–pVTZ basis set.

It was noticed in previous work [93] that the character of chemical interactions (formal bonds, long range, van der Waals, etc.) appears to be related to the magnitude of the preparation energy. Thus, as expected, preparation energies in Table 7.1 suggest a direct correlation with binding energies. Table 7.2 lists recalculated total E_{prep} for a set of diatomic and polyatomic systems already available in the literature, as well as our results for the formic acid dimers. Nicely, the preparation energies for the formic acid dimers fall in the same range as that of the water dimer. They lead to interaction energies that are stronger than van der Waals contacts but weaker than ionic and covalent bonds. In hydrogen bonding, the distance separating the two moieties dictates the strength of the interaction. This tendency can be seen in Table 7.2.

7.2.2 Partition potentials

Hydrogen bonding is a complex interaction with various degrees of contribution from electrostatic, inductive, and dispersive forces depending on the nature of the individual

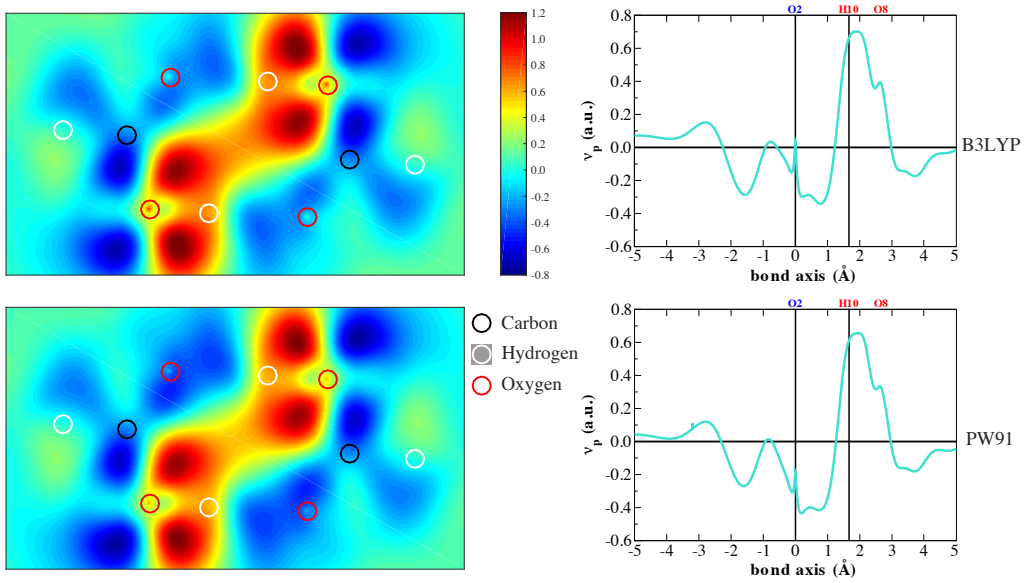

Figure 7.3. Partition potential, $v_P(\mathbf{r})$, for D_1 using B3LYP (top) and PW91 (bottom) functionals. The aug-cc-pVTZ basis set was used for all calculations. The left two plots show the $v_P(\mathbf{r})$ map on the molecular plane. The right two plots show $v_P(\mathbf{r})$ along the approximate HB line (through H atom of the donor and O atom of the acceptor).

molecules. In this work, we use the PW91 functional, which fortuitously yields accurate interaction energies and molecular geometries in weakly-bonded clusters such as the benzene and methane dimers among others [96]; and we also use the very popular B3LYP hybrid functional.

Fig. 7.3 shows that all features of the partition potential are largely insensitive to the choice of XC functional (we only show results for D_1, but the same is also true for D_2—D_4). Since $v_P(\mathbf{r})$ is obtained through the density-to-potential inversion of eq. 7.1, this is due to the *densities* being insensitive to the choice of XC functional. The question of whether the approximate XC functionals can accurately capture the exact features of $v_P(\mathbf{r})$ remains open. [24] For both functionals, we were able to achieve density convergence to the order of 10^{-8} a.u. in a reasonable number of iterations (on the order of 10^2).

Fig. 7.5 compares the B3LYP partition potentials for all four dimers. In contrast to the monomer density deformations, similar bonds are *not* characterized by similar features in $v_P(\mathbf{r})$. This is further highlighted in Figure 7.4, where the partition potentials are plotted

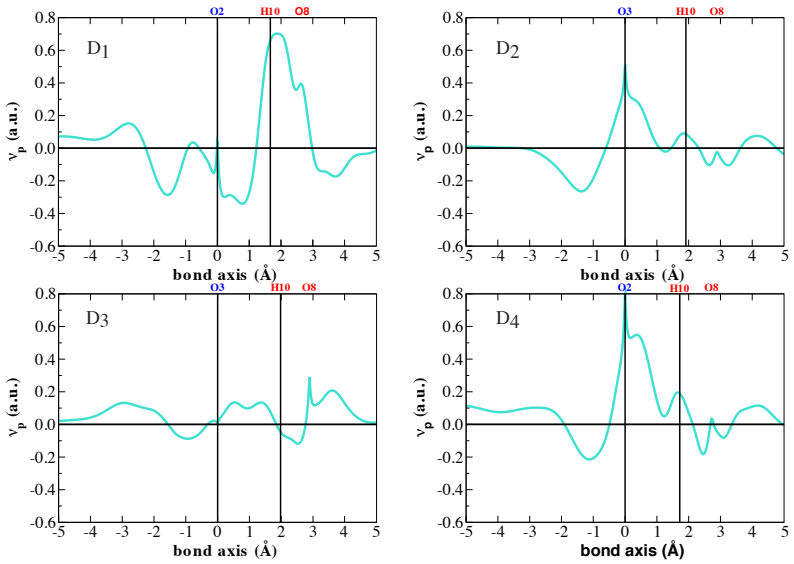

Figure 7.4. 1D plots of $v_{\mathrm{P}}(\mathbf{r})$ along the approximate bond axis. The B3LYP functional in conjunction with the aug-cc-pVTZ basis set was used for all calculations. Vertical lines in the 1D plots enclose the intermolecular bonding region.

along the following nearly-linear intramolecular bonds: C=O $\cdots$ O–H in D_1 and D_2; O–H $\cdots$ O–H in D_3; and O–H $\cdots$ O–H in D_4. Note that although the density deformations in the binding regions are qualitatively similar in all four dimers, $v_{\mathrm{P}}(\mathbf{r})$ is qualitatively different for the global minimum (D_1), where it is highly negative.

The non-transferability of $v_{\mathrm{P}}(\mathbf{r})$ or any of its features indicates its sensitivity to the density variations in regions that may be far from $\mathbf{r}$. In contrast, the density deformations are highly localized. Qualitatively, the 2D density deformations of Figure 7.2 show that, due to the formation of the hydrogen bond, charge is accumulated in the region occupied by the antibonding orbital in the R monomer and simultaneously withdrawn from the region occupied by the lone pair in the L monomer. Quantitatively, accumulation of charge in the antibonding region of R and depletion of charge in the lone pair region of L are larger for stronger bonds.

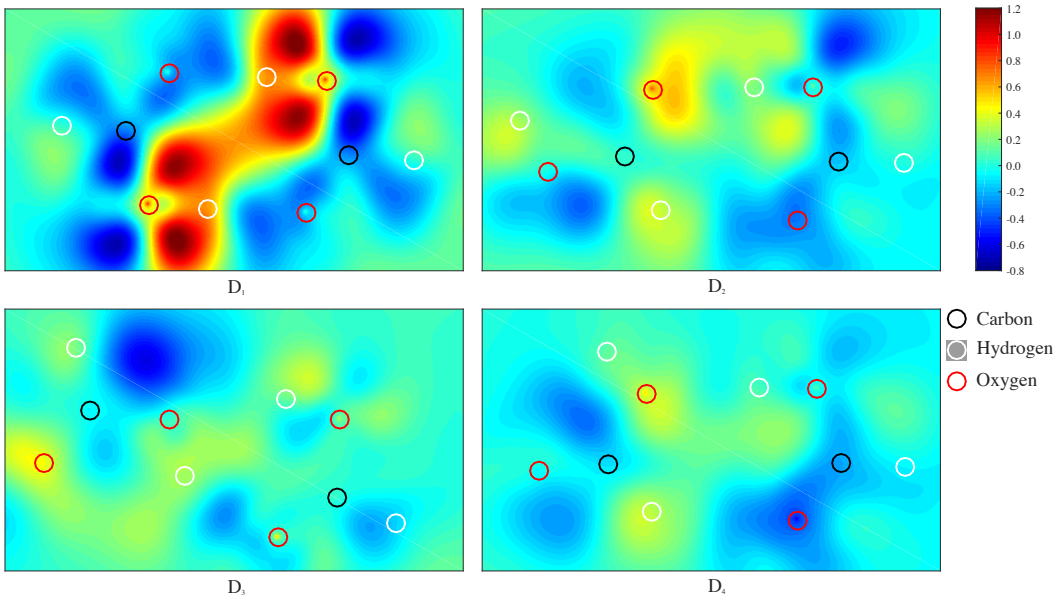

Figure 7.5. Partition potential, $v_{\mathrm{P}}(\mathbf{r})$, for dimers for D_1—D_4 (B3LYP/aug-cc-pVTZ).

7.3 Final Remarks

Contrary to our original expectation, we show that the partition potential is *not* transferable between systems with similar types of hydrogen-bonding. The result highlights the nonlocal character of $v_{\mathrm{P}}(\mathbf{r})$ in contrast to the local features of density deformations of the individual fragments, which *are* largely transferable. In practical calculations, we should take advantage of the fact that fragment calculations can be done locally while still preserving the global features of the partition potential. We also highlight the intuitive yet nontrivial observation that large binding energies correspond to large preparation energies, and that the strength of the partition potential is correlated with the overall stability of the dimer.

REFERENCES

[1] A. Szabo and N. S. Ostlund, *Modern Quantum Mechanics: Introduction to Advanced Electronic Structure Theory*, 2nd ed. New York, USA: Dover, 1996.

[2] R. Requist and E. Gross, "Exact factorization-based density functional theory of electrons and nuclei," *Phys. Rev. Lett.*, vol. 117, p. 193 001, 19 2016.

[3] L. D. Landau and E. M. Lifschitz, *Quantum mechanics: Non-relativistic theory*, 3rd ed., J. Menzies, Ed. Oxford, England: Butterworth-Heinemann, 1981.

[4] R. Pauncz, *The Symmetric Group in Quantum Chemistry*. Boca Raton, USA: CRC Press, 1995.

[5] P. Hohenberg and W. Kohn, "Inhomogeneous Electron Gas," *Phys. Rev.*, vol. 136, pp. 864–871, Nov. 1964.

[6] M. Levy, "Universal Variational Functionals of Electron Densities, First-Order Density Matrices, and Natural Spin-Orbitals and Solution of the v-Representability Problem," *Proc. Natl. Acad. Sci. U.S.A.*, vol. 76, pp. 6062–6065, 1979.

[7] V. L. Lignères and E. A. Carter, "An Introduction to Orbital-Free Density Functional Theory," in *Handbook of Materials Modeling*, S. Yip, Ed. Dordrecht, Netherlands: Springer, 2005, p. 137.

[8] W. Kohn and L. Sham, *Phys. Rev. A*, vol. 140, pp. 1133–1138, 1965.

[9] K. Burke and L. O. Wagner, "Dft in a nutshell," *Int. J. Quantum Chem.*, vol. 113, pp. 96–101, 2013.

[10] J. P. Perdew and K. Schmidt, "Jacob's ladder of density functional approximations for the exchange-correlation energy," in *AIP Conference Proceedings*, IOP Institute of Physics Publishing, 2001, pp. 1–20.

[11] J. P. Perdew, "Density-functional approximation for the correlation energy of the inhomogeneous electron gas," *Phys. Rev. B*, vol. 33, pp. 8822–8824, 1986.

[12] C. Lee, W. Yang, and R. G. Parr, "Development of the colle-salvetti correlation-energy formula into a functional of the electron density," *Phys. Rev. B*, vol. 37, pp. 785–789, 1988.

[13] J. P. Perdew, K. Burke, and M. Ernzerhof, "Generalized gradient approximation made simple," *Phys. Rev. Lett.*, vol. 77, pp. 3865–3868, 1996.

[14] J. P. Perdew and L. A. Constantin, "Laplacian-level density functionals for the kinetic energy density and exchange-correlation energy," *Phys. Rev. B*, vol. 75, p. 155 109, 2007.

[15] A. D. Becke, "Density-functional thermochemistry. iii. the role of exact exchange," *J. Chem. Phys.*, vol. 98, pp. 5648–5652, 1993.

[16] A. D. Becke, "A new mixing of hartree-fock and local density-functional theories," *J. Chem. Phys.*, vol. 98, pp. 1372–1377, 1993.

[17] J. P. Perdew, M. Ernzerhof, and K. Burke, "Rationale for mixing exact exchange with density functional approximations," *J. Chem. Phys.*, vol. 105, pp. 9982–9985, 1996.

[18] C. R. Jacob and M. Reiher, "Spin in density-functional theory," *Int. J. Quantum Chem.*, vol. 112, pp. 3661–3684, 2012.

[19] T. Gál and P. Geerlings, "Energy surface, chemical potentials, Kohn-Sham energies in spin-polarized density functional theory," *J. Chem. Phys.*, vol. 133, pp. 144 105–144 105, 2010.

[20] J. P. Perdew, R. G. Parr, M. Levy, and J. J. L. Balduz, "Density-functional theory for fractional particle number: Derivative discontinuities of the energy," *Phys. Rev. Lett.*, vol. 49, pp. 1691–1694, 1982.

[21] E. P. Gyftopoulos and G. N. Hatsopoulos, "Quantum-thermodynamic definition of electronegativity," *Proc. Nat. Acad. Sci. U.S.A.*, vol. 60, pp. 786–793, 1968.

[22] R. G. Parr and W. Yang, *Density-Functional Theory of Atoms and Molecules*. New York, USA: Oxford University Press, 1994.

[23] W. Yang, Y. Zhang, and P. W. Ayers, "Degenerate ground states and a fractional number of electrons in density and reduced density matrix functional theory," *Phys. Rev. Lett.*, vol. 84, pp. 5172–5175, 2000.

[24] Y. Oueis and A. Wasserman, "Exact partition potential for model systems of interacting electrons in 1-d," *Eur. Phys. J. B*, vol. 91, p. 247, 2018.

[25] M. H. Cohen and A. Wasserman, "On hardness and electronegativity equalization in chemical reactivity theory," *J. Stat. Phys.*, vol. 125, pp. 1121–1139, 2006.

[26] J. Nafziger and A. Wasserman, "Density-based partitioning methods for ground-state molecular calculations," *J. Phys. Chem. A*, vol. 118, pp. 7623–7639, 2014.

[27] M. A. Mosquera and A. Wasserman, "Partition density functional theory and its extension to the spin-polarized case," *Molecular Phys.*, vol. 111, pp. 505–515, 2013.

[28] B. Fornberg, "Generation of finite difference formulas on arbitrarily spaced grids," *Math. Comput.*, vol. 51, pp. 699–706, 1988.

[29] N. Helbig, J. I. Fuks, M. Casula, M. J. Verstraete, M. A. L. Marques, I. V. Tokatly, and A. Rubio, "Density functional theory beyond the linear regime: Validating an adiabatic local density approximation," *Phys. Rev. A*, vol. 83, p. 032 503, 2011.

[30] S. A. Shpilkin, E. A. Smolenskii, and N. S. Zefirov, "Topological structure of the configuration space and the separation of spin and spatial variables for n-electron systems," *J. Chem. Inf. Comput. Sci.*, vol. 36, pp. 409–412, 1996.

[31] C. G. Broyden, "A class of methods for solving nonlinear simultaneous equations," *Mathematics of Computation*, vol. 19, pp. 577–593, 1965.

[32] D. S. Jensen and A. Wasserman, "Numerical methods for the inverse problem of density functional theory," *Int. J. Quantum Chem.*, vol. 118, e25425, 2018.

[33] J. Nafziger, K. Jiang, and A. Wasserman, "Accurate reference data for the nonadditive, noninteracting kinetic energy in covalent bonds," *J. Chem. Theory Comput.*, vol. 13, pp. 577–586, 2017.

[34] K. Jiang, J. Nafziger, and A. Wasserman, "Non-additive non-interacting kinetic energy of rare gas dimers," *J. Chem. Phys.*, vol. 148, p. 104 113, 2018.

[35] T. A. Wesołowski and A. Warshel, "Frozen density functional approach for ab initio calculations of solvated molecules," *J. Phys. Chem. A*, vol. 97, pp. 8050–8053, 1993.

[36] C. R. Jacob and J. Neugebauer, "Subsystem density-functional theory," *Wiley Interdiscip. Rev. Comput. Mol. Sci.*, vol. 4, pp. 325–362, 2014.

[37] O. V. Gritsenko and E. J. Baerends, "Effect of molecular dissociation on the exchange-correlation kohn-sham potential," *Phys. Rev. A*, vol. 54, pp. 1957–1972, 1996.

[38] N. Helbig, I. V. Tokatly, and A. Rubio, "Exact kohn–sham potential of strongly correlated finite systems," *J. Chem. Phys.*, vol. 131, p. 224 105, 2009.

[39] D. G. Tempel, T. J. Martínez, and N. T. Maitra, "Revisiting molecular dissociation in density functional theory: A simple model," *J. Chem. Theory Comput.*, vol. 5, pp. 770–780, 2009.

[40] J. I. Fuks, S. E. B. Nielsen, M. Ruggenthalerbc, and N. T. Maitra, "Time-dependent density functional theory beyond kohn–sham slater determinants," *Phys. Chem. Chem. Phys.*, vol. 18, p. 20 976, 2016.

[41] M. Cohen, A. Wasserman, R. Car, and K. Burke, "Charge transfer in partition theory," *J. Phys. Chem. A*, vol. 113, pp. 2183–2192, 2009.

[42] R. Tang, J. Nafziger, and A. Wasserman, "Fragment occupations in partition density functional theory," *Phys. Chem. Chem. Phys.*, vol. 14, pp. 7780–7786, 2012.

[43] T. Gould and J. Toulouse, "Kohn-sham potentials in exact density-functional theory at noninteger electron numbers," *Phys. Rev. A*, vol. 90, 050502(R), 2014.

[44] D. M. Chipman, "Theoretical study of the properties of methyl radical," *J. Chem. Phys.*, vol. 78, pp. 3112–3132, 1983.

[45] D. M. Chipman, "The spin polarization model for hyperfine coupling constants," *Theor. Chem. Acc.*, vol. 82, pp. 93–115, 1992.

[46] J. A. Pople, P. M. W. Gill, and N. C. Handy, "Spin-unrestricted character of kohn-sham orbitals for open-shell systems," *Int. J. Quantum Chem.*, vol. 56, pp. 303–305, 1995.

[47] G. Gilli and P. Gilli, *The Nature of the Hydrogen Bond*. New York, USA: Oxford University Press, 2009.

[48] K. Niffenegger, Y. Oueis, J. Nafziger, and A. Wasserman, "Density embedding with constrained chemical potential," *Mol. Phys.*, vol. 117, pp. 2188–2194, 2019.

[49] M. H. Cohen and A. Wasserman, "On the foundations of chemical reactivity theory," *J. Phys. Chem. A*, vol. 111, pp. 2229–2242, 2007.

[50] P. Elliott, K. Burke, M. H. Cohen, and A. Wasserman, "Partition density-functional theory," *Phys. Rev. A*, vol. 82, p. 024 501, 2010.

[51] G. B. Arfken, H. J. Weber, and F. E. Harris, *Mathematical Methods for Physicists: A Comprehensive Guide*, 7th ed. Oxford: Elsevier, 2013.

[52] E. Prodan, "Nearsightedness of electronic matter in one dimension," *Phys. Rev. B*, vol. 73, p. 085 108, 2006.

[53] J. P. Perdew, "What do the kohn-sham orbital energies mean? how do atoms dissociate?" In *Density Functional Methods in Physics*, R. M. Dreizler and J. da Providência, Eds., Boston, USA: Springer, 1985, pp. 265–308.

[54] J. P. Perdew and M. Levy, "Density functional theory for open systems," in *Many-Body Phenomena at Surfaces*, D. Langreth and H. Suhl, Eds., Orlando, USA: Academic Press, pp. 71–89.

[55] T. A. Wesołowski and J. Weber, "Kohn-sham equations with constrained electron density: An iterative evaluation of the ground-state electron density of interacting molecules," *Chem. Phys. Lett.*, vol. 248, pp. 71–76, 1996.

[56] E. Fabiano, S. Laricchia, and F. Della Sala, "Frozen density embedding with non-integer subsystems' particle numbers," *J. Chem. Phys.*, vol. 140, p. 114 101, 2014.

[57] W. Lorenz, "Development in charge transfer theory," *J. Electroanal. Chem.*, vol. 191, pp. 31–58, 1985.

[58] Y. Lykhach, S. M. Kozlov, T. Skala, A. Tovt, V. Stetsovych, N. Tsud, F. Dvorak, V. Johanek, A. Neitzel, J. Myslivecek, S. Fabris, V. Matolin, K. M. Neyman, and J. Libuda, "Counting electrons on supported nanoparticles," *Nat. Mater.*, vol. 15, pp. 284–288, 2016.

[59] O. T. Hofmann, P. Rinke, M. Scheffler, and G. Heimel, "Charge transfer at metal(/insulator)/organic interfaces: Cu(/nacl)/tcne," *ACS Nano*, vol. 9, pp. 5391–5404. 2015.

[60] W. Liu, A. Tkatchenko, and M. Scheffler, "Modeling adsorption and reactions of organic molecules at metal surfaces," *Acc. Chem. Res.*, vol. 47, pp. 3369–3377, 2014.

[61] K. Jiang, M. A. Mosquera, Y. Oueis, and A. Wasserman, "Virial relations in density embedding," *Int. J. Quantum Chem.*, vol. 120, e26204, 2020.

[62] T. A. Wesolowski and Y. A. Wang, *Recent Progress in Orbital-free Density Functional Theory*. Singapore: World Scientific, 2013.

[63] S. Kümmel and L. Kronik, "Orbital-dependent density functionals: Theory and applications," *Rev. Mod. Phys.*, vol. 80, pp. 3–60, 2008.

[64] A. Genova, D. Ceresoli, and M. Pavanello, "Avoiding fractional electrons in subsystem dft based ab-initio molecular dynamics yields accurate models for liquid water and solvated oh radical," *J. Chem. Phys.*, vol. 144, p. 234 105, 2016.

[65] J. M. G. Lastra, J. W. Kaminski, and T. A. Wesołowski, "Orbital-free effective embedding potential at nuclear cusp," *J. Chem. Phys.*, vol. 129, p. 074 107, 2008.

[66] M. Levy and J. P. Perdew, "Hellmann-feynman, virial, and scaling requisites for the exact universal density functionals. shape of the correlation potential and diamagnetic susceptibility for atoms," *Phys. Rev. A*, vol. 32, pp. 2010–2021, 1985.

[67] S. Ghosh and V. A. Singh, "Energy theorems in constrained density-functional theory," *J. Phys. Condens. Matter*, vol. 1, pp. 1971–1981, 1989.

[68] J. I. Rodríguez, P. W. Ayers, A. W. Götz, and F. L. Castillo-Alvarado, "Virial theorem in the Kohn–Sham density-functional theory formalism: Accurate calculation of the atomic quantum theory of atoms in molecules energies," *J. Chem. Phys.*, vol. 131, p. 021 101, 2009.

[69] S. Srebrenik and R. F. W. Bader, "Towards development of quantum-mechanics of a subspace," *J. Chem. Phys.*, vol. 63, pp. 3945–3961, 1975.

[70] R. F. W. Bader, "Bader definition of an atom - reply," *J. Chem. Phys.*, vol. 85, pp. 3133–3134, 1986.

[71] L. M. Li and R. G. Parr, "The atom in a molecule - a density-matrix approach," *J. Chem. Phys.*, vol. 84, pp. 1704–1711, 1986.

[72] R. A. Harris and D. F. Heller, "Density functional theory of interacting closed shell systems .2. determination of charge-densities and hellman-feynman theorem," *J. Chem. Phys.*, vol. 62, pp. 3601–3604, 1975.

[73] R. G. Gordon and Y. S. Kim, "Theory for the forces between closed-shell atoms and molecules," *J. Chem. Phys.*, vol. 56, pp. 3122–3133, 1972.

[74] L. H. Thomas, "The calculation of atomic fields," *Math. Proc. Cambridge Philos. Soc.*, vol. 23, pp. 542–548, 1926.

[75] E. Fermi, "Un metodo statistico per la determinazione di alcune priorieta dell'atome," *Rendiconti. Accademia Nazionale dei Lincei*, vol. 6, pp. 602–607, 1927.

[76] C. F. v Weizsäcker, "Zur theorie der kernmassen," *Zeitschrift Für Physik a Hadrons and Nuclei*, vol. 96, pp. 431–458, 1935.

[77] A. S. Kompaneets and E. S. Pavlovsky, "Self-consistent equations for atoms," *J. Exp. Theor. Phys.*, vol. 31, p. 427, 1956.

[78] D. A. Kirzhnits, "Quantum corrections to the thomas-fermi equation," *Journal of Experimental and Theoretical Physics*, vol. 5, p. 64, 1957.

[79] F. Tran and T. A. Wesołowski, "Link between the kinetic- and exchange-energy functionals in the generalized gradient approximation," *Int. J. Quantum Chem.*, vol. 89, pp. 441–446, 2002.

[80] A. Lembarki and H. Chermette, "Obtaining a gradient-corrected kinetic-energy functional from the Perdew-Wang exchange functional," *Phys. Rev. A*, vol. 50, pp. 5328–5331, 1994.

[81] A. Krishtal, D. Sinha, A. Genova, and M. Pavanello, "Subsystem density-functional theory as an effective tool for modeling ground and excited states, their dynamics and many-body interactions," *J. Phys. Condens. Matter*, vol. 27, p. 183 202, 2015.

[82] A. Wasserman, J. Nafziger, K. L. Jiang, M. C. Kim, E. Sim, and K. Burke, "The importance of being inconsistent," *Annu. Rev. Phys. Chem.*, vol. 68, pp. 555–581, 2017.

[83] S. Gómez, Y. Oueis, and A. R. A. Wasserman, "Partition potential for hydrogen-bonding in formic acid dimers," *Int. J. Quantum Chem.*, vol. 119, e25814, 2019.

[84] J. F. Pérez, C. Z. Hadad, and A. Restrepo, "Structural studies of the water tetramer," *Int. J. Quantum Chem.*, vol. 108, pp. 1653–1659, 2008.

[85] F. Ramírez, C. Z. Hadad, D. Guerra, J. David, and A. Restrepo, "Structural studies of the water pentamer," *Chem. Phys. Lett.*, vol. 507, pp. 229–233, 2011.

[86] G. Hincapié, N. Acelas, M. Castano, J. David, and A. Restrepo, "Structural studies of the water hexamer," *J. Phys. Chem. A*, vol. 114, pp. 7809–7814, 2010.

[87] N. Acelas, G. Hincapié, D. Guerra, J. David, and A. Restrepo, "Structures, energies, and bonding in the water heptamer," *J. Chem. Phys.*, vol. 139, p. 044 310, 2013.

[88] D. L. Nelson and M. M. Cox, *Lehninger Principles of Biochemistry*, 7th ed. New York, USA: WH Freeman, 2017.

[89] A. E. Reed, L. A. Curtiss, and F. Weinhold, "Intermolecular interactions from a natural bond orbital, donor-acceptor viewpoint," *Chem. Rev.*, vol. 88, pp. 899–926, 1988.

[90] F. Weinhold and R. Klein, "Anti-electrostatic hydrogen bonds," *Angew. Chem. Int. Ed.*, vol. 53, pp. 11 214–11 217, 2014.

[91] J. Grabowski, "What is the covalency of hydrogen bonding?" *Chem. Rev.*, vol. 111, pp. 2597–2625, 2011.

[92] A. Buckingham, J. D. Bene, and S. McDowell, "The hydrogen bond," *Chem. Phys. Lett.*, vol. 463, pp. 1–10, 2008.

[93] S. Gómez, J. Nafziger, A. Restrepo, and A. Wasserman, "Partition-dft on the water dimer," *J. Chem. Phys.*, vol. 146, p. 074 106, 2017.

[94] Y. Zhang and A. Wasserman, "Transferability of atomic properties in molecular partitioning: A comparison," *Journal of Chemical Theory and Computation*, vol. 6, pp. 3312–3318, 2010.

[95] K. Marushkevich, L. Khriachtchev, M. Räsänen, M. Melavuori, and J. Lundell, "Dimers of the higher-energy conformer of formic acid: Experimental observation," *J. Phys. Chem. A*, vol. 116, pp. 2101–2108, 2012.

[96] S. Tsuzuki and H. P. Lüthi, "Interaction energies of van der waals and hydrogen bonded systems calculated using density functional theory: Assessing the pw91 model," *J. Chem. Phys.*, vol. 114, pp. 3949–3957, 2001.

[97] M. Valiev, E. J. Bylaska, N. Govind, K. Kowalski, H. J. J. v. D. T. P. Straatsma, D. Wang, J. Nieplocha, E. Apra, T. Windus, and W. de Jong, "Nwchem: A comprehensive and scalable open-source solution for large scale molecular simulations," *Comput. Phys. Commun.*, vol. 181, pp. 1477–1489, 2010.

[98] Q. Wu and W. Yang, "A direct optimization method for calculating density functionals and exchange–correlation potentials from electron densities," *J. Chem. Phys.*, vol. 118, pp. 2498–2509, 2003.

[99] F. Kollipost, R. W. Larsen, A. V. Domanskaya, M. Nörenberg, and M. A. Suhm, "Communication: The highest frequency hydrogen bond vibration and an experimental value for the dissociation energy of formic acid dimer," *J. Chem. Phys.*, vol. 136, p. 151 101, 2012.

[100] P. Farfán, A. Echeverri, E. Diaz, J. D. Tapia, S. Gómez, and A. Restrepo, "Dimers of formic acid: Structures, stability, and double proton transfer," *J. Chem. Phys.*, vol. 147, p. 044 312, 2017.

[101] J. Nafziger, Q. Wu, and A. Wasserman, "Molecular binding energies from partition density functional theory," *J. Chem. Phys.*, vol. 135, p. 234 101, 2011.

A. THREE ELECTRONS IN 1D: AN EXACT SOLUTION

The electronic-structure hamiltonian of Eq. 2.2 describes only electrostatic effects of the electronic motion. Spin in the non-relativistic quantum mechanics is introduced phenomenologically, i.e., it is postulated that the electronic wavefunction should be antisymmetric under particle interchange:

$$\Psi(\dots,\mathbf{x}_\mathrm{i},\dots,\mathbf{x}_\mathrm{j},\dots) = -\Psi(\dots,\mathbf{x}_\mathrm{j},\dots,\mathbf{x}_\mathrm{i},\dots)\ , \tag{A.1}$$

where $\mathbf{x}_\mathrm{i} = (\mathbf{r}_\mathrm{i}, s_\mathrm{i})$ is the particle coordinate consisting of spatial and spin coordinates. The ground state wavefunction of an electronic system in the form of Eq. A.1 should still be an eigenfunction of the hamiltonian of Eq. 2.2. We also expect this wavefunction to be an eigenfunction of $\hat{S}_{z,\mathrm{total}}$ operator and (in the absence of magnetic fields and vanishing spin-spin and spin-orbit interactions) an eigenfunction of $\hat{S}^2$ operator [3]. The spin part is naturally described with the help of $\hat{S}_{z,\mathrm{total}}$ eigenstates. For example, for 3 electrons: $|\uparrow,\uparrow,\uparrow\rangle, |\uparrow,\uparrow,\downarrow\rangle, |\uparrow,\downarrow,\uparrow\rangle \dots, |\downarrow,\downarrow,\downarrow\rangle$. The ground state wavefunction can then be written as the superposition of the $\hat{S}_{z,\mathrm{total}}$ eigenstates "weighted" by the eigenstates of 2.2 with the same eigenvalue:

$$\Psi(\mathbf{x}_1,\mathbf{x}_2,\dots,\mathbf{x}_N) = \sum_{s_1,s_2,\dots,s_N} \psi_{s_1,s_2,\dots,s_N}(\mathbf{r}_1,\mathbf{r}_2,\dots,\mathbf{r}_N)\,|s_1,s_2,\dots,s_N\rangle\ . \tag{A.2}$$

In the case of 1 or 2 electrons, the expansion simplifies to a product of the spatial ground state with an $\hat{S}_{z,\mathrm{total}}$ eigenstate: $\psi_0(\mathbf{r})\,|\uparrow\rangle$ or $\psi_0(\mathbf{r}_1,\mathbf{r}_2)(|\uparrow\downarrow\rangle - |\downarrow\uparrow\rangle$[1]. The solution is less trivial for 3 or more electrons. To keep this manuscript self-contained, we will discuss practical aspects of computing the 3-electron problem in Chap. 4. The generalization to an arbitrary number of electrons can be found in textbooks on Group Theory (e.g., Ref [4]).

We will now solve the problem of 3 electrons in 1D with $N_\mathrm{S} = 1$ (i.e., a doublet) that we expect to be the ground-state spin state. Recall that $\hat{S}_{z,\mathrm{total}}$ operator in the space of 3

[1] for brevity, normalization constants will be dropped throughout this appendix.

electrons has 8 eigenstates: 4 degenerate states corresponding to $N_S = 1$ and 4 degenerate states corresponding to $N_S = 3$. The degenerate states with $N_S = 1$ can be written as:

$$|1,-1\rangle_1 = |\downarrow\uparrow\downarrow\rangle - |\uparrow\downarrow\downarrow\rangle \ , \tag{A.3a}$$

$$|1,-1\rangle_2 = |\downarrow\downarrow\uparrow\rangle - |\uparrow\downarrow\downarrow\rangle \ , \tag{A.3b}$$

$$|1,+1\rangle_1 = |\uparrow\downarrow\uparrow\rangle - |\downarrow\uparrow\uparrow\rangle \ . \tag{A.3c}$$

$$|1,+1\rangle_2 = |\uparrow\uparrow\downarrow\rangle - |\downarrow\uparrow\uparrow\rangle \ , \tag{A.3d}$$

Of course, there are infinitely many ways these eigenstates can be represented, but the form of Eqs. A.3 turns out to be the most convenient one. The states of Eqs. A.3a and A.3b share the same $\hat{S}_{z,\text{total}}$ eigenvalue and will serve as our basis for constructing the full antisymmetric wavefunction (the same process can, of course, be repeated for states A.3c and A.3d). Observe that the state A.3a has a peculiar "mixed" symmetry. The first term in A.3a is symmetric with respect to the interchange of s_1 with s_3, and the second term is symmetric with respect to the interchange of s_2 with s_3. The entire state A.3a is antisymmetric with respect to the interchange of s_1 with s_2 (i.e., A.3a was constructed from $|\downarrow\uparrow\downarrow\rangle$ by antisymmetrizing it with respect to the interchange of s_1 with s_2). Analogously, A.3b is obtained from $|\downarrow\downarrow\uparrow\rangle$ by antisymmetrizing it with respect to the interchange of s_1 with s_3. We now need to construct eigenstates of 2.2 with spatial "mixed" symmetries that are transpose to those of states A.3a and A.3b.

Let us look at an arbitrary eigenstate of the spatial hamiltonian 2.2, $g(x_1, x_2, x_3)$. We can first symmetrize it with respect to the interchange of x_1 and x_3 and then antisymmetrize it with respect to the inerchange of x_1 with x_3:

$$f(x_1, x_2, x_3) = [g(x_1, x_2, x_3) + g(x_2, x_1, x_3)] - [g(x_3, x_2, x_1) + g(x_2, x_3, x_1)] \ . \tag{A.4}$$

The spatial symmetry of A.4 is transpose to the spin symmetry of A.3a. Similarly, we can construct a spatial function to "go along" the spin function A.3a:

$$h(x_1, x_2, x_3) = [g(x_1, x_3, x_2) + g(x_3, x_1, x_2)] - [g(x_2, x_3, x_1) + g(x_3, x_2, x_1)] \ . \tag{A.5}$$

It is not difficult to see that:

$$\Psi(\mathbf{x}_1, \mathbf{x}_2, \mathbf{x}_3) = f(x_1, x_2, x_3) \left|1, -1\right\rangle_1 - h(x_1, x_2, x_3) \left|1, -1\right\rangle_2 \tag{A.6}$$

is the fully antisymmetric wavefunction. One can also verify that A.5 is an eigenfunction of $\hat{S}^2$ (and obviously of $\hat{S}_{z,\text{total}}$). Observe that the (anti)symmetrization procedure of Eqs. A.4 and A.5 fails if $g(x_1, x_2, x_3)$ is either fully symmetric or fully antisymmeteric (i.e., the procedure returns the trivial eigenstate). Therefore, our procedure of finding $\Psi(\mathbf{x}_1, \mathbf{x}_2, \mathbf{x}_3)$ reduces to finding the lowest spatial eigenstate $g(x_1, x_2, x_3)$ that does not return zero when inserted into either of Eqs. A.4 or A.5.

VITA

YANAL OUEIS

EDUCATION

Ph.D. Chemistry. GPA: 3.97/4 2015–expected 2021

Purdue University, West Lafayette, Indiana USA

Advisor: Adam Wasserman

Research: Density-functional theory; quantum embedding methods

B.S. Chemistry *with distinction.* **GPA:** 3.75/4 2012–2015

University of Minnesota–Twin Cities, Minneapolis, Minnesota USA

Advisor: William Arnold

Research: Quantitative structure-activity relationships for organic contaminants in water

AWARDS AND HONORS

Andrews Fellowship 2015–2017

Purdue University

One of only two *two-year* fellowships offered by the Purdue Department of Chemistry for outstanding applicants to the PhD program

Maroon Global Excellence Scholarship 2012–2015

University of Minnesota

Scholarship for international students, awarded on the basis of academic merit

TEACHING EXPERIENCE

Purdue University 2015–2019

Teaching Assistant: Physical chemistry, CHM 374 (Spring 2019); General chemistry honors, CHM 136 (Fall 2018); General chemistry, CHM 115 and CHM 116 (2015–2018, 5 semesters total)

University of Minnesota 2012–2014

Teaching Assistant: Numerical methods in chemical engineering, CHEN 3201 (Summer–Fall 2014); Introduction to materials science, MATS 3011 (Fall 2014)

Undergraduate tutor: First-year courses in physics, chemistry and calculus (Fall 2012–Fall 2014)

PRESENTATIONS

- Oral: Y. Oueis and A. Wasserman. Partition density-functional theory: application to model systems. Physical Chemistry Seminar, Purdue University, West Lafayette, IN. December 2020.
- Oral: Y. Oueis and A. Wasserman. What we can learn from exact embedding potentials of model systems. ACS Spring 2019 National Meeting, Orlando, FL. March 2019.
- Poster: Y. Oueis and A. Wasserman. Exact partition potential for a model system of interacting electrons. The 50th Midwest Theoretical Chemistry Conference, Chicago, IL. June 2018.
- Poster: Y. Oueis and A. Wasserman. Partition Density Functional Theory. Summer school on time-dependent Density Functional Theory, Telluride, CO. July 2017.

PUBLICATIONS

- Y. Oueis and A. Wasserman. Chemical Reactivity. In *Putting the Theory Back in Density Functional Theory*. Springer. Lecture Notes in Physics, **In press**.
- K. Jiang, M.A. Mosquera, Y. Oueis and A. Wasserman. Virial relations in density embedding. *Int. J. Quantum Chem.*, vol. 120, p. e26204, **2020**.
- K. Niffenegger, Y. Oueis, J. Nafziger and A. Wasserman. Density embedding with constrained chemical potential. *Mol. Phys.*, vol. 117, pp. 2188-2194, **2019**.
- S. Gomez, Y. Oueis, A. Restrepo and A. Wasserman. Partition potential for hydrogen-bonding in formic acid dimers. *Int. J. Quantum Chem.*, vol. 119, p. e25814, **2019**.

- Y. Oueis and A. Wasserman. Exact partition potential for model systems of interacting electrons in 1-D. *Eur. Phys. J. B*, vol. 91, p. 247, **2018**.

- W.A. Arnold, Y. Oueis, M. O'Connor, J.E. Rinaman, M.G. Taggart, R.E. McCarthy, K.A. Foster and D.E. Latch. QSARs for phenols and phenolates: oxidation potential as a predictor of reaction rate constants with photochemically produced oxidants, *Environ. Sci.: Processes Impacts*, vol. 19, pp. 324-338, **2019**.